Journal of the Mechanical Behavior of Biomedical Materials 177 (2026) 107371

Contents lists available at ScienceDirect

Journal of the Mechanical Behavior of Biomedical Materials

journal homepage: www.elsevier.com/locate/jmbbm

A review on the identification of the mechanical properties of soft tissues and tissue-mimicking phantoms

Hasan Koruk [a,*], Srinath Rajagopal [a], Raphaela de Melo Baesso [a], Andre Victor Alvarenga [a], Stylianos Vasileios Kontomaris [b]

[a] Ultrasound and Underwater Acoustics, Department of Medical, Marine and Nuclear, National Physical Laboratory, Teddington, Middlesex, TW11 0LW, United Kingdom

[b] School of Sciences, European University Cyprus, 2404, Nicosia, Cyprus

ARTICLE INFO

Keywords:
Soft material
Tissue
Tissue-mimicking phantom
Mechanical properties
Shear modulus
Young's modulus
Viscosity
Limitations
Elastography

ABSTRACT

Characterising the mechanical properties of soft materials - such as gels and biological tissues - presents significant challenges compared to conventional, stiff engineering materials like ceramics, metals, and polymers. A major issue identified is the considerable variability in measured properties across different techniques, or even between different laboratories employing the same method. This comprehensive review addressed the need for a thorough examination of existing techniques, their limitations, and their drawbacks. Both laboratory-based and clinical methods were explored, including laboratory techniques such as tensile testing, compression test, indentation, atomic force microscopy, and rheometry, as well as clinical methods including ultrasound elastography and magnetic resonance elastography. The principles of operation and the theoretical foundations underlying the most widely employed modalities for material and tissue characterisation were presented. The limitations of these techniques were detailed, and numerous studies on the mechanical properties of soft tissues and tissue-mimicking phantoms were reported. The mechanical properties of various soft materials identified using these diverse techniques were compared and evaluated. The findings highlighted a clear need for the development of more reliable test apparatus and standardised procedures to accurately characterise these properties across nano, micro, and macro scales. These findings offer a valuable resource for researchers in the field, facilitating informed selection of characterisation methods and promoting greater accuracy and consistency in future work.

1. Introduction

The knowledge of the mechanical properties of soft materials is needed in various fields, including tissues in medical applications and soft phantoms in bioengineering applications (Li et al., 2018; Navarro-Lozoya et al., 2019; Krivega et al., 2024; Lemine et al., 2024). For example, their properties are needed for simulations in the design stage or robot-aided surgery (Famaey and Vander Sloten, 2008), regenerative medicine (Carton et al., 2024), disease assessment in elastography (Sigrist et al., 2017), and the validation of *in vivo* elastography results (Santos et al., 2025). In general, accurate knowledge of their mechanical properties is important to understand the mechanics of soft tissues (Alekya et al., 2019; Chavan et al., 2024). Unlike conventional engineering materials, whose mechanical properties typically include shear or Young's modulus, Poisson's ratio, yield strength, and ultimate strength, the mechanical profile of soft materials is typically defined by their shear or Young's modulus (stiffness), viscosity (damping), and Poisson's ratio (Koruk and Rajagopal, 2024; Singh and Chanda, 2021; Magazzù and Marcuello, 2023; Bisht et al., 2024). Although the shear or Young's modulus are used to describe the stiffness of materials, many parameters are used to describe the damping of materials, including loss angle, viscosity, loss factor, and viscous damping ratio (Koruk and Rajagopal, 2024). It is worth noting that the stiffness and damping of materials can be expressed in terms of the complex modulus (storage modulus and loss modulus), and some techniques provide the complex modulus as an output parameter representing these properties (Yengul et al., 2019). In addition to elastic and viscous properties, tear resistance is a relevant metric for soft materials, particularly when assessing their

* Corresponding author.
E-mail addresses: hasan.koruk@npl.co.uk (H. Koruk), srinath.rajagopal@npl.co.uk (S. Rajagopal), raphaela.baesso@npl.co.uk (R. de Melo Baesso), andre.alvarenga@npl.co.uk (A.V. Alvarenga), s.kontomaris@research.euc.ac.cy (S.V. Kontomaris).

https://doi.org/10.1016/j.jmbbm.2026.107371
Received 26 November 2025; Received in revised form 3 February 2026; Accepted 6 February 2026
Available online 10 February 2026

ability to withstand crack propagation and catastrophic failure under physiological or surgical loads (Yang et al., 2015; Kahle et al., 2025; Bircher et al., 2019). It is worth noting that materials generally described as soft typically have a Young's modulus in the range of 0.1 kPa to several MPa. This range encompasses many biological tissues and tissue-mimicking phantoms (McKee et al., 2011; Liu et al., 2015).

Characterisation of the mechanical properties of conventional stiff engineering materials, including ceramics, metals, and polymers, is relatively straightforward. Techniques, such as tensile testing, are commonly employed to quantify key mechanical properties, such as Young's modulus, yield strength and ultimate strength. Furthermore, the differences in the mechanical properties of these traditional engineering materials measured using different techniques across different laboratories can be quite low. However, identifying the mechanical properties of soft materials, such as gels and tissues, presents significant challenges. This complexity arises due to several factors: (i) Unlike traditional engineering materials that can be safely assumed to be elastic, soft materials exhibit both elastic and viscous properties, and they need to be considered as viscoelastic structures (Islam et al., 2020; Koruk et al., 2024). However, depending on the viscoelastic model used, different mechanical properties can be obtained for the same material. (ii) Low force levels for the deformation of soft materials are needed to extract their mechanical properties (Czerner et al., 2015; Wu et al., 2018). Therefore, other force sources, such as friction and intermolecular forces, must be considered in the mathematical model. However, these forces depend on numerous factors, such as the positioning and properties of the sample, making it difficult to model them accurately. (iii) Some techniques for characterising soft materials require the use of small samples (Nayar et al., 2012; Slouf et al., 2020). As a result, these fragile samples can be quite difficult to prepare, and their dimensional tolerances can cause significant errors in the defined mechanical properties. (iv) Unlike traditional stiff materials that are durable and easy to use under different conditions, the mechanical properties of soft materials depend on various environmental factors (e.g., temperature and humidity), excitation (e.g., frequency), and operator skill (Wu et al., 2018; Mishra and Cleveland, 2024; Shahmirzadi and Hsieh, 2010). Overall, the variability in the mechanical properties of soft materials identified using different techniques or the same technique across different laboratories can be significantly high (Wu et al., 2018; Nayar et al., 2012; Polio et al., 2018; Żmudzińska et al., 2018).

There are several conventional techniques for the identification of the mechanical properties of soft materials in the laboratory: tensile test, compression test, indentation, atomic force microscopy (AFM), and rheometry. Although the tensile test is a traditional mechanical test for conventional engineering materials, it has been used to determine the mechanical properties of soft materials as well (Chow and Zhang, 2011; Cooney et al., 2015; Sudres et al., 2021; Kriener et al., 2023; Illi et al., 2023). Compression testing is commonly used in various engineering applications to determine mechanical behaviours of materials under compressive loading and has found use in the mechanical characterisation of some soft materials (Cloyd et al., 2007; Lyshchik et al., 2005; Yu et al., 2020; Ledoux and Blevins, 2007; Song et al., 2007). Indentation has been used for the mechanical characterisation of all types of materials including metals and ceramics and later has been used for the mechanical characterisation of many soft materials (He et al., 2024; Yoo et al., 2011; van Hoorn et al., 2016; Herbert et al., 2008; Delaine-Smith et al., 2016). AFM has been used to measure mechanical behaviours of various materials at precise sample locations, in very small volumes and at shallow depths, including micro and nano structures such as living cells and cell organelles (Cohen and Kalfon-Cohen, 2013; Owen, 2023; Kuznetsova et al., 2007; Dufrêne et al., 2017; Efremov et al., 2020; Chang et al., 2021). In contrast to aforementioned techniques, viscometry/rheometry is used to identify the mechanical properties of only viscous fluids and soft materials (Mishra and Cleveland, 2024; Ghanbari et al., 2020; Jóźwiak and Boncel, 2020; Stojkov et al., 2021; Chen et al., 2010; Sander et al., 2017; Hou and Kassim, 2005). In addition to these techniques used in the laboratory, there are some techniques used in the clinic for the assessment of the mechanical properties of soft tissue, including ultrasound elastography (Sigrist et al., 2017; DeWall, 2013; Jeong et al., 2014) and magnetic resonance elastography (Zhang et al., 2020; Li et al., 2022; Kennedy et al., 2022). Beyond common methods, several specialised techniques have been used to identify the mechanical properties of soft materials and cells, including pipette aspiration, pressure myography, scanning acoustic microscopy, cavitation rheometry, optical coherence elastography (OCE), optical stretching, cellular shear wave elastography (cSWE), acoustic force spectroscopy (AFS), cell monolayer rheometry, magnetic twisting cytometry (MTC), and particle-tracking microrheometry.

It should be noted that each identification method has its own advantages and limitations. Existing literature on the mechanical characterisation of soft materials has largely offered only partial reviews of the experimental techniques used to determine the mechanical properties of soft materials (Alekya et al., 2019; Akhtar et al., 2011; Navindaran et al., 2023; Oyen, 2014). The prior studies often fail to explore the specific drawbacks and limitations of various techniques in detail, and a comprehensive comparison of the mechanical properties identified through these different methods has been notably absent. This study fills these gaps by (1) systematically reviewing a wide array of techniques for identifying soft material properties; (2) an explanation of their underlying theoretical foundations; (3) reporting a large number of studies that explored the mechanical properties of various soft tissues and tissue-mimicking phantoms; (4) exploring in detail their inherent limitations and practical drawbacks; and (5) comparing and evaluating the resulting mechanical properties obtained from different methods. In this comprehensive review, Sections 2.1 to 2.8 outline a brief overview of the operating principles and underlying theories of the most used laboratory techniques - such as tensile testing, compression testing, indentation, atomic force microscopy, and rheometry - as well as clinical methods, including ultrasound elastography and magnetic resonance elastography. Furthermore, these sections explore the specific drawbacks and practical limitations inherent to each technique. Section 2.9 provides a concise overview of additional characterisation techniques, while Section 2.10 discusses tissue nonlinearity and the requirement for advanced mathematical modelling. In addition to summarising the limitations of various techniques, Section 3 compares and evaluates the mechanical properties of various soft materials measured by different identification techniques and discusses a metrological roadmap for standardised soft tissue characterisation. The main conclusions are listed in Section 4. The findings presented in this study offer a valuable resource for researchers in the field, facilitating informed selection of characterisation methods and promoting greater accuracy and consistency in future work.

2. Identification methods

Sections 2.1 through 2.8 survey common laboratory and clinical techniques, including atomic force microscopy and ultrasound elastography. Section 2.9 details additional specialised methodologies, while Section 2.10 addresses broader mechanical considerations such as tissue nonlinearity. Schematics of various common techniques are presented in Fig. 1.

2.1. Tensile testing

The most common parameters measured in tensile or tension testing (Fig. 1a) for soft materials are the Young's modulus and Poisson's ratio. In this method, a sample is placed between two fixtures (grips) that clamp the sample. First, the sample's dimensions - length, thickness, and width (or diameter in the case of a circular cross-section) - are measured. Then an axial force F is applied to the sample at one end whereas the other end is fixed. The change in length of the sample is measured by increasing the force until a predetermined strain is reached or the sample breaks. The tensile stress is calculated using $\sigma = F/A_0$ where A_0

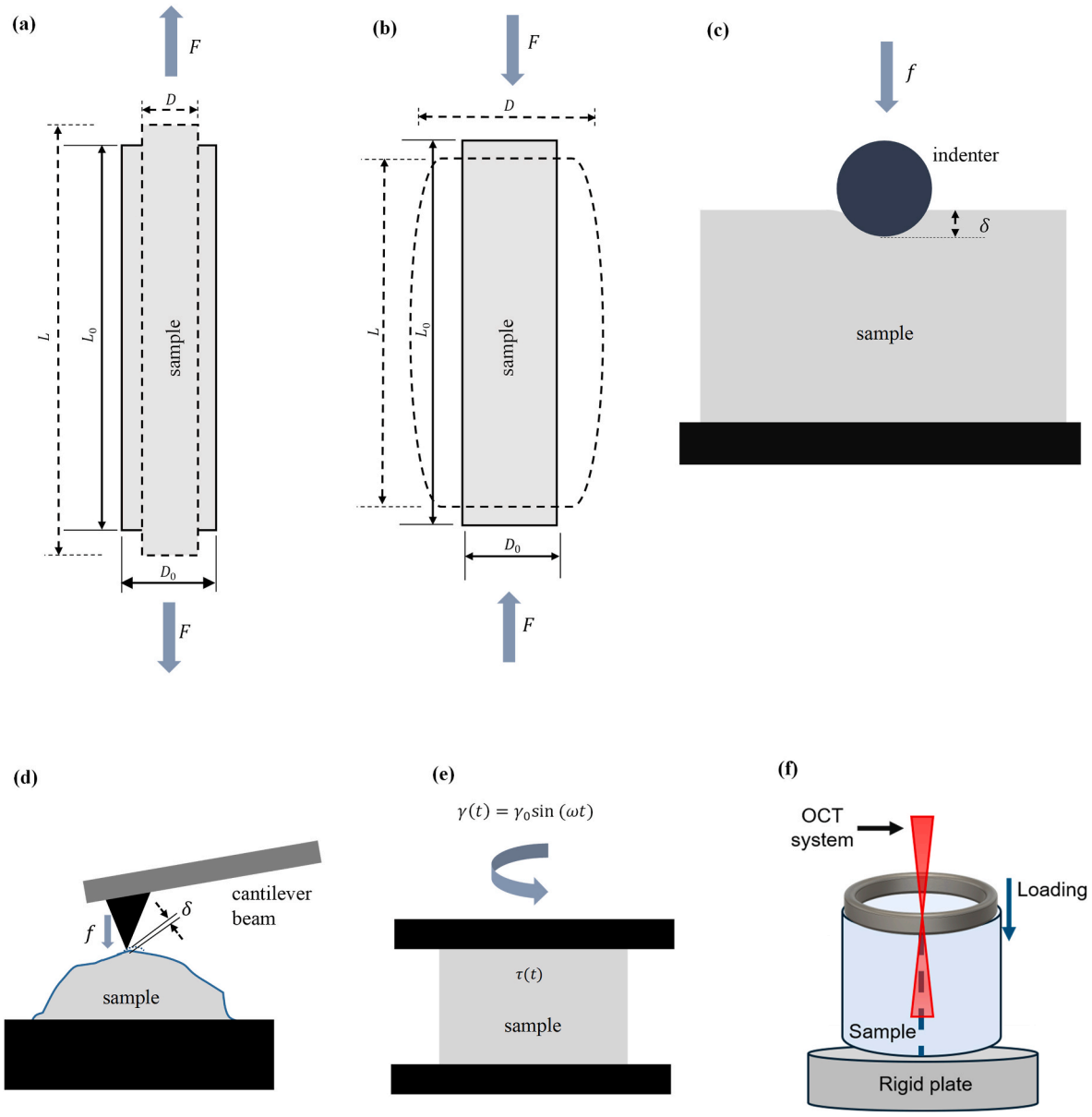

Fig. 1. Schematics for (a) tensile testing, (b) compression testing, (c) spherical indentation, (d) atomic force microscope, (e) torsional rheometer, and (f) optical coherence elastography.

is the cross-sectional area of the sample before the start of loading. The corresponding axial strain is determined using $\varepsilon = \Delta L/L_0$ where L_0 is the initial length of the sample and ΔL is the elongation of the sample. Overall, the Young's modulus (E) and Poisson's ratio (ν) of the material are determined from the linear part of the stress-strain curve using the following equations (Innocenti et al., 2018):

$$E = \frac{\sigma(\varepsilon)}{\varepsilon} \tag{1}$$

$$\nu = -\frac{\varepsilon_{\text{transverse}}}{\varepsilon} \tag{2}$$

where $\varepsilon_{\text{transverse}} = \Delta D/D_0$ is the transverse strain of the material, which is the change in the lateral dimension or width of the material (ΔD) divided by its original width (D_0). The shear modulus can be calculated using the equation $G = E/[2(1+\nu)]$ (Koruk, 2021). If needed, other parameters such as the yield strength (the maximum stress that can be applied before permanent shape change is achieved) and ultimate strength (the maximum stress a sample can withstand without breaking) can be calculated using the stress-strain curve. It is worth noting that there are no universal standard protocols specifically for soft tissues. Tensile testing often utilises dumbbell specimens - typically an overall length of 115 mm, a gauge length of 25 mm, and a thickness of 2-3 mm - following standards (ISO 37-2024, 2024; ASTM D412-16, 2021) to ensure valid failure occurs within a defined gauge length while minimising stress concentrations at the grips.

It should be noted that σ and ε are the engineering stress and strain that are referred to sample dimensions before the start of loading (i.e., A_0 and L_0). Especially for large deformations in the elastic region, the true stress and strain given by $\sigma_{\text{true}} = \sigma \cdot \ln(1+\varepsilon)$ and $\varepsilon_{\text{true}} = \ln(1+\varepsilon)$ can be used in Equations (1) and (2) for determining material properties (Duprey et al., 2010), where ln represents the natural logarithm. It should be noted that using an external extensometer to directly measure the strain on the sample is quite common (Lim et al., 2011); this eliminates measurement influences from other test components and increases accuracy. Although the uniaxial tensile test is commonly used in practical applications, the biaxial tensile test has been used to determine mechanical properties of some soft materials (Jiang et al., 2021;

Yohsuke et al., 2011). The biaxial tensile test involves applying forces to the sample in two perpendicular directions, making it more complex than the uniaxial tensile test. Similarly, static or quasi-static tensile testing is predominantly used for the characterisation of soft materials. However, dynamic tensile testing - which involves subjecting a specimen to rapidly varying loading rates rather than a constant force - has also been employed to investigate the dynamic behaviour of certain soft materials under high loading rates (Lim et al., 2011; Nie et al., 2009). Strain rate is typically less than 10^{-5} s^{-1} for static tests, ranges from 10^{-5} s^{-1} to 10^{-1} s^{-1} for quasi-static tests, and ranges from 10 s^{-1} to 10^{4} s^{-1} for dynamic tests (Nie et al., 2009; Su et al., 2022; Griffin et al., 2016).

Biaxial tensile tests are employed to characterise the mechanical properties of anisotropic biological tissues such as skin, heart valves, and blood vessels (Takada et al., 2023; Ross et al., 2026; Laurence et al., 2023). These tissues exhibit different mechanical responses depending on the direction of the applied force, and testing in multiple axes simultaneously captures this complex, directional behaviour more accurately than standard uniaxial tests (Ayyalasomayajula and Skallerud, 2022; Sacks and Sun, 2003). The deformation in each direction can be independently controlled, allowing the application of various loading protocols, such as equal biaxial, unequal biaxial, or off-axis stretches. This capability enables a more complete assessment of the tissue's directional mechanical response and provides the stress-strain data required to identify material parameters for anisotropic constitutive models (Fehervary et al., 2016). It is worth noting that various constitutive models for anisotropic materials have been established (Holzapfel and Ogden, 2010; Gasser et al., 2006; Holzapfel et al., 2000), while the adoption of non-contact extensometry has improved strain measurement precision in biaxial tensile testing. Integrating these theoretical models with advanced experimental methods has facilitated innovative characterisation of biological tissue properties. Specifically, digital image correlation (DIC) has emerged as a robust, full-field optical technique for quantifying surface deformation without specimen contact (Fagerholt et al., 2013; Alberini et al., 2024; Ashkenazi et al., 2026). DIC is particularly effective for soft, hydrated tissues because it captures heterogeneous strain fields and eliminates measurement errors caused by grip compliance or slippage (Ning et al., 2010; He et al., 2020).

Tensile testing of soft and collagen-rich tissues may exhibit apparent stiffening behaviour, particularly under cyclic or repeated loading. Experimental studies have shown that cyclic tensile deformation can lead to a progressive increase in the effective stiffness and strength of collagenous substrates, even in the absence of cellular activity (Chen et al., 2018). Such stiffening has been attributed primarily to changes in the mechanical properties of individual collagen fibrils rather than to alterations in the overall anisotropic structure of the fibril network. These findings indicate that mechanical loading can modify the stiffness and failure characteristics of collagen fibril networks through passive chemomechanical processes, complementing active biological remodelling mechanisms. Recognition of these stiffening effects is essential for the interpretation of tensile mechanical data and for understanding the history-dependent behaviour of soft connective tissues (Chen et al., 2018).

Tensile testing has been used to quantify the mechanical behaviours/properties of various soft materials, including bovine artery (Chow and Zhang, 2011), porcine linea alba (Cooney et al., 2015), porcine Achilles tendon and human patellar tendon (Innocenti et al., 2018), the cervical, thoracic and lumbar porcine spinal meninges (Sudres et al., 2021), porcine cardiovascular tissues, diseased arterial tissue (Walsh et al., 2014), porcine aorta (Famaey et al., 2026), tissue-mimicking silicone and 3D-printed phantoms (Illi et al., 2023), and human abdominal wall (Kriener et al., 2023). In addition, biaxial testing has been employed to determine the mechanical properties of a range of anisotropic tissues, including aortic walls (Niestrawska et al., 2016), and mitral valve leaflets (Sadeghinia et al., 2022; Laville et al., 2020). However, the tensile test has some drawbacks and limitations, especially for fragile soft samples. It is generally difficult to prepare proper samples with the desired shape and dimensions (Kang et al., 2023; Pei et al., 2021; O'Leary et al., 2013a); noting that the value of the cross-sectional area of the sample affects the calculated stress. The ends of the sample can be damaged (Kang et al., 2023; Jiang et al., 2020) because of the gripping force; this problem is obvious especially for substantially soft samples. On the other hand, a relatively low gripping force leads to sample slippage, which causes greater incorrect strain values (Jiang et al., 2020; Scholze et al., 2018, 2020). The misalignment of grips (Kang et al., 2023; Ahearne and Liu, 2008) can produce a complicated loading field that is not considered in the calculation of material properties. The applied forces at the loading clamps do not transmit fully to the region of interest and this can produce improper material properties in biaxial tensile test if they are not accounted for (Jacobs et al., 2013). Overall, errors and uncertainties in biaxial testing arise from stress concentrations at clamps or hooks, measurement mismatches between disparate regions, geometric sample variations, and localised strain field fluctuations (Slazansky et al., 2016). If not properly accounted for, axial and radial inertia effects frequently observed in dynamic tensile tests can result in inaccurate material property measurements (Nie et al., 2009).

2.2. Compression testing

The compression testing (Fig. 1b) follows the same basic principle as tensile testing, and the material properties are calculated using the same procedure presented in Section 2.1. However, in a compression test, the sample is not gripped, instead it is placed between two flat plates for compressive loading. The sample can be either between two impermeable platens (unconfined compression test) or within an impermeable chamber that involves the use of a porous indenter (or impermeable indenter with porous chamber) to allow for fluid flow out of the sample (confined compression test) (Patel et al., 2019). The compression test can be performed under static or quasi static and dynamic loading (Song et al., 2007). It is important to emphasise that no single international standard exists specifically for the compression of biological soft tissues. Compression testing typically employs cylindrical specimens with a diameter of 28.6 mm and a thickness of 12.5 mm (ASTM D575-91, 2024) to maintain a uniform stress state and prevent specimen buckling during deformation.

Compression testing has been used to measure the mechanical behaviours/properties of various soft materials, including human thyroid tissue (Lyshchik et al., 2005), human plantar soft tissue (Ledoux and Blevins, 2007), human nucleus pulposus, hydrogels and tissue engineering scaffolds (Cloyd et al., 2007), and porcine spinal cord grey and white matter (Yu et al., 2020). However, many factors influence the quality of the results of a compression test. The quality and integrity of the sample surface can cause error in strain measurements and the value of the cross-sectional area of the sample affects the calculated stress (Jokinen, 2017). The sample's cross-sectional surface should be flat and parallel to ensure uniform axial loading; a slight misalignment may cause initial non-uniform stress distribution, resulting in strain inaccuracy (Oroszlany et al., 2015). The surface of the sample can be damaged because of scratching, cutting, and punching (Carlsson et al., 2014). Friction generated at the specimen/platen interface due to the adhesive property and viscoelasticity of soft samples adversely affect the accuracy of the stress-strain recordings, resulting in an error in stress (Rashid et al., 2012; Wu et al., 2004; Yang et al., 2018). If the contact between plates and sample does not hold the sample still, the sample moves during testing (Jokinen, 2017). Although it is rare during the compression testing of soft materials, the sample can buckle if the ratio of the sample length to diameter is large (Torres et al., 2014). Inertia effects present in dynamic compression tests can lead to inaccurate material property measurements if they are not properly considered (Liu et al., 2024).

2.3. Indentation

Indentation tests have been used for the mechanical characterisation of all types of materials including metals and ceramics, and later for the mechanical characterisation of soft materials including biological tissues (Argatov and Mishuris, 2018). In an indentation test (Fig. 1c), a hard indenter of known mechanical properties is pushed into a flat surface of a sample, and the mechanical properties of the sample are inferred from the size of the imprint or the penetration depth measured as a function of loading force/time. There are two fundamental types of indentation testers: non-instrumented and instrumented, and three main types of indentation tests: static, quasi-static, and dynamic (Slouf et al., 2020). In a non-instrumented indentation test, the hardness of the sample is determined from the size of the imprint on the sample surface after unloading (static test). In an instrumented indentation test, the penetration depth is recorded as a function of loading force, such as a trapezoidal force input (quasi-static test) or a trapezoidal force input oscillating with a defined frequency (dynamic test). The mechanical properties of the sample are determined from the recorded load–displacement curves in quasi-static and dynamic tests. It is worth noting that strain rate typically is less that 10^{-4} s^{-1} (or held at constant strain for several minutes), ranges from 10^{-4} to 10^{-1} s^{-1}, and ranges from 1 to 100 s^{-1} for static, quasi-static, and dynamic tests, respectively (Su et al., 2022; Zhu et al., 2025; Antonovaite et al., 2018). The mechanical properties of materials can be determined across different scales -macroscale (macro-indentation), microscale (micro-indentation) and nanoscale (nano-indentation) - by using an indentation tester together with indenters of varying sizes and shapes, such as conical and spherical designs (Herbert et al., 2008).

Based on the nature of the force applied to the indenter, the mathematical model employed to simulate the sample and the shape of the indenter, various mathematical models are used to extract the mechanical properties in indentation tests (Slouf et al., 2020; van Hoorn et al., 2016; Herbert et al., 2008; Cohen and Kalfon-Cohen, 2013; Argatov and Mishuris, 2018; VanLandingham, 2003). Although the non-instrumented indentation is commonly used for conventional stiff engineering materials (Oliver and Pharr, 1992), the instrumented indentation has been mostly used to determine the viscoelastic properties of soft materials (van Hoorn et al., 2016; Herbert et al., 2008; Cohen and Kalfon-Cohen, 2013; Cao et al., 2011). This section presents common mathematical approaches used to identify the elastic and viscoelastic properties of soft materials.

The equation used to fit the force–indentation data depends on the shape of the indenter. For spherical indenters and small indentation depths (δ) compared to the indenter's radius (R) - typically $\delta/R < 0.1$ (Holzapfel et al., 2000) - the applied force f on the sample surface is given by the Hertz equation (Koruk, 2021):

$$f = \frac{4}{3} E_{\text{reduced}} R^{1/2} \delta^{3/2} \tag{3}$$

where $E_{\text{reduced}} = \left(\frac{1-\nu_{\text{sample}}^2}{E_{\text{sample}}} + \frac{1-\nu_{\text{tip}}^2}{E_{\text{tip}}} \right)^{-1}$ is the reduced Young's modulus; E_{sample} and ν_{sample}, E_{tip} and ν_{tip} being the Young's moduli and Poisson's ratios of the sample and tip, respectively. When testing soft materials, the tip is several orders of magnitude stiffer than the sample, hence the reduced Young's modulus becomes $E_{\text{reduced}} = \frac{E_{\text{sample}}}{1-\nu_{\text{sample}}^2}$ (Wenger et al., 2007). In addition, the accurate equation for deep spherical indentations was derived by Sneddon (Sneddon, 1965; Maghsoudy-Louyeh et al., 2018) and is provided below:

$$f = \frac{E_{\text{sample}}}{2\left(1-\nu_{\text{sample}}^2\right)} \left[(a^2 + R^2) \ln\left(\frac{R+a}{R-a}\right) - 2aR \right] \tag{4}$$

$$\delta = \frac{1}{2} a \ln\left(\frac{R+a}{R-a}\right) \tag{5}$$

where a is the contact radius between the indenter and the sample. Equations (4) and (5) are accurate for any indentation depth; however, their use for data processing is challenging since they do not directly relate the applied force to the indentation depth. A simple alternative to the Sneddon model has been recently developed to streamline the data processing (V Kontomaris and Malamou, 2021). Force–indentation data obtained using conventional pyramidal indenters are usually processed using Sneddon's equation for conical indenters (Santos et al., 2012).

The Young's modulus of a viscoelastic material can be represented by a complex (or dynamic) quantity, having both the storage and dissipative energy components. The stress and strain as complex quantities can be written as follows:

$$\sigma(t) = \sigma_0 e^{j\omega t} = \sigma_0 [\cos(\omega t) + j \sin(\omega t)] \tag{6}$$

$$\varepsilon(t) = \varepsilon_0 e^{j(\omega t - \phi)} = \varepsilon_0 [\cos(\omega t - \phi) + j \sin(\omega t - \phi)] \tag{7}$$

where σ_0 and ε_0 are the stress and strain amplitudes, respectively. Hence, the complex Young's modulus E^* of the material can be written as follows:

$$E^* = \frac{\sigma_0 e^{j\omega t}}{\varepsilon_0 e^{j(\omega t - \phi)}} = \frac{\sigma_0}{\varepsilon_0} \cos(\phi) + j \frac{\sigma_0}{\varepsilon_0} \sin(\phi) = E' + jE'' \tag{8}$$

where E' is the storage Young's modulus, and E'' is the loss Young's modulus. The storage Young's modulus is related to the elastic behavior of the material, and the loss Young's modulus is related to the viscous behaviour of the material.

A modulated force $f(t) = f_0 \sin(\omega t)$ results in a displacement oscillation at the same frequency, given by $\delta(t) = \delta_0 \sin(\omega t - \Delta)$. Hence, the dynamic in-phase and out-of-phase equations can be re-written in terms of experimental observables as follows (Herbert et al., 2008; Cohen and Kalfon-Cohen, 2013):

$$E' = \frac{f_0}{\delta_0} \frac{\sqrt{\pi}}{2\beta\sqrt{A}} (1-\nu^2) \cos(\Delta) \tag{9}$$

$$E'' = \frac{f_0}{\delta_0} \frac{\sqrt{\pi}}{2\beta\sqrt{A}} (1-\nu^2) \sin(\Delta) \tag{10}$$

where f_0 is the steady-state modulated force amplitude, δ_0 is the resulting modulated displacement amplitude, Δ is the angular phase shift between the applied force and the measured displacement, ν is the Poisson's ratio, A is the projected contact area, and β is a constant related to the geometry of the contact; $\beta = 1$ for circular flat punch, sphere and cone and $\beta = 1.034$ for a Berkovich indenter. The contact area A is not an observable; however, it can be derived by calibrating the indenter (Cohen and Kalfon-Cohen, 2013). The Poisson's ratio ν is assumed to be known. The inertial contribution of the sample is assumed to be negligible compared to that of the testing system (Herbert et al., 2008). It should be noted that when $E'' = 0$, then E' takes the place of the ordinary Young's modulus E.

In the mechanical characterisation of soft materials including biological tissues, relaxation phenomena are an inherent part of the observed response. Under compressive loading and during rheological testing, time-dependent effects such as stress relaxation and creep arise from the viscoelastic nature of the material, resulting in changes in the measured stress or deformation over time. These effects influence the apparent stiffness and must be considered when interpreting mechanical parameters, particularly as a function of loading rate or hold duration. In this context, ramp-hold indentation is commonly employed, in which the indenter is driven at a constant velocity to a prescribed depth and subsequently held at constant displacement. The hold phase permits direct observation of stress relaxation, enabling assessment of the time-

dependent viscoelastic response that cannot be captured through purely dynamic or oscillatory indentation methods. In the ramp-hold indentation protocol, the indentation depth $\delta(t)$ is defined as a piecewise function of time t (Qiu et al., 2018):

$$\delta(t)=\begin{cases} v_i t & (0 \le t \le t_R) \\ \delta_{max} & (t_R \le t) \end{cases} \tag{11}$$

where v_i is the indentation velocity, $\delta_{max}=v_i t_R$ is the maximum indentation depth, and t_R is the indentation ramp time. Applying the correspondence principle for viscoelastic materials, a two-term Prony series $G(t)$ is employed to describe the time-dependent shear modulus in place of the shear modulus G (Qiu et al., 2018, 2020; Chen et al., 2021):

$$G(t)=C_0+\sum_{i=1}^{2} C_i e^{-\frac{t}{\tau_i}} \tag{12}$$

The coefficients C_0, C_i, and τ_i represent the model's parameters, from which the instantaneous (G_0) and long-term shear moduli (G_∞) are obtained:

$$G_0=G(0)=C_0+\sum_{i=1}^{2} C_i, G_\infty=C_0 \tag{13}$$

The applied force when using a flat punch indenter with radius R is determined as follows (Qiu et al., 2018, 2020):

$$f=\begin{cases} 8RXv_i\left[C_0 t-\sum_{i=1}^{2}\tau_i C_i\left(e^{-\frac{t}{\tau_i}}-1\right)\right], 0 \le t \le t_R \\ 8RXv_i\left[C_0 t_R+\sum_{i=1}^{2}\tau_i C_i e^{-\frac{t}{\tau_i}}\left(e^{\frac{t_R}{\tau_i}}-1\right)\right], t_R \le t \end{cases} \tag{14}$$

where X denotes a polynomial correction factor that compensates for the effects of finite substrate thickness.

In addition to analytical contact models, inverse finite element (FE) analysis (Ayyalasomayajula et al., 2024) has emerged as a powerful and flexible approach for extracting material parameters from indentation experiments, particularly in the case of ultra-soft and hyperelastic biological materials where closed-form solutions are often unavailable. In this context, inverse finite element analysis is formulated as an iterative procedure in which a numerical model of the indentation experiment is constructed using the same indenter geometry, boundary conditions, and loading protocol as those employed experimentally. The material response could be described through a selected hyperelastic constitutive model (e.g., neo-Hookean or Ogden) (Bonet, 2001), and an initial set of material parameters is assumed. The indentation process is then simulated numerically to generate a force-displacement curve, which is compared with the corresponding experimental response. The material parameters are subsequently adjusted in an automated manner to minimise the discrepancy between the simulated and experimental force-displacement curves, until optimal agreement is achieved, thereby allowing the effective material properties to be identified.

Indentation techniques have been used to determine the mechanical properties of various soft materials in macro, micro or nano scales, including bovine ocular tissues (Yoo et al., 2011), hydrogels (Toohey et al., 2016), rodent kidney, liver, spleen and uterus (Wu et al., 2020), porcine brain tissue (Li et al., 2020), and brain phantom (Yakovenko et al., 2021). Although indentation tests are less invasive and can provide localised material properties – unlike tensile and compression tests – they also have inherent limitations and shortcomings. The mathematical model used to simulate the sample is based on various assumptions and hence those assumptions will result in some kind of uncertainties in the identified mechanical properties (Wu et al., 2020). The reliability of the indentation technique is worse in relatively small and thin samples (Wu et al., 2016, 2020; Rubiano et al., 2019). A misalignment of the indenter tip can result in a change in the measured reaction force, and this can lead to an error in the identified material properties (Marinopoulos et al., 2023). The effect of friction on the identified mechanical properties can be significant, especially for a large aspect ratio (i.e., ratio of the indenter radius to the sample thickness) and a large Poisson's ratio (Lyashenko et al., 2024; Zhang et al., 1997). The roughness of sample surface and/or non-flat sample surface can introduce an error in determining the contact area and thus in the identified material properties (Kim et al., 2006; Chandran et al., 2018). Samples can get damaged, especially if the size and type of the indenter is not suitable for the sample (Lyashenko and Borysiuk, 2022). In addition, the inertia of the system components and the sample involved in motion could affect the identified material properties in case of dynamic loading (Koruk, 2022; Mijailovic et al., 2018; Esteki et al., 2020).

2.4. Atomic force microscopy

Atomic force microscopy (AFM) is a powerful tool that combines nanoscale imaging with the determination of mechanical properties through the nanoindentation method. However, an atomic force microscope contains additional components, such as a laser, making it more complicated due to its various operational modes, and the size of the indenter is smaller compared to conventional indentation (Liu et al., 2020; Radmacher, 2007). In the AFM, a micro- or nano-sized tip attached to a cantilever beam is used to probe the mechanical properties of a sample (Fig. 1d). The cantilever beam behaves as a spring during interactions with the surface of the sample and its bending deflections are measured by a laser beam. It is important to note that AFM is more suitable for indentation experiments of soft materials (Wenger et al., 2007; Lekka et al., 1999; Plodinec et al., 2012; Krieg et al., 2018). Various mathematical models including Hertz, Sneddon, Derjaguin-Muller-Toporov, and Johnson-Kendall-Roberts are used in the AFM to identify the mechanical properties of the sample (Owen, 2023; Maghsoudy-Louyeh et al., 2018). Although the Hertz (Denisin and Pruitt, 2016) and Sneddon (Smolyakov et al., 2016) models presented in Section 2.3 are commonly used in practice, they do not consider the adhesive contribution (Krieg et al., 2018).

An important issue when dealing with AFM nanoindentation of soft samples is related to the validity of Sneddon's equation (Equations (4) and (5)) due to the round tip apex of the indenter. Typical AFM tips have a tip radius in the range of 20 nm to 60 nm. To account for the rounded apex of the tip for shallow indentations, accurate equations for data processing have already been developed. For example, the following equations are used for a sphero-conical indenter (Briscoe et al., 1994):

$$f=\frac{2E_{sample}}{\left(1-\nu_{sample}^2\right)}\left\{a\delta-\frac{a^2}{2\tan(\theta)}\left[\frac{\pi}{2}-\arcsin\left(\frac{b}{a}\right)\right]-\frac{a^3}{3R} + \left(a^2-b^2\right)^{1/2}\left(\frac{b}{2\tan(\theta)}+\frac{a^2-b^2}{3R}\right)\right\} \tag{15}$$

$$\delta+\frac{a}{R}\left[\left(a^2-b^2\right)^{1/2}-a\right]-\frac{a}{\tan(\theta)}\left[\frac{\pi}{2}-\arcsin\left(\frac{b}{a}\right)\right]=0 \tag{16}$$

where θ is the cone's semi angle and $b=R\cos(\theta)$ is the transition radius between the spherical and the conical parts of the indenter. In addition, a is the contact radius and R denotes the radius of the spherical apex of the indenter. Equations (15) and (16) are valid for $a>b$. Similar equations have been proposed for pyramidal tips (Rico et al., 2005). In practice, Equations (15) and (16) do not provide a direct relationship between the applied force and the indentation depth to streamline the data processing. Simplified alternatives to these models have been developed to facilitate more efficient data processing (Kontomaris et al., 2022, 2024). Equations (15) and (16) consider the sample as an elastic half-space; it is assumed that the sample's thickness is significantly larger than the indentation depth, so the rigid substrate does not influence the

results. According to Buckle's rule, the indentation depth should not exceed 5–10% of the sample's thickness to avoid the influence of the substrate (Stolz et al., 2004; Persch et al., 1994; Baldwin et al., 2020). For large indentation depths or thin samples, appropriate corrections in terms of polynomial functions have been derived in the literature. These functions depend on the indenter's geometry, the indentation depth, the sample's thickness, the Poisson's ratio and whether the sample is bonded to the substrate or not (Santos et al., 2012; Garcia and Garcia, 2018; Gavara and Chadwick, 2012; Dimitriadis et al., 2002). Another key challenge in AFM nanoindentation is the heterogeneity of the tested samples at the nanoscale. Biological materials are highly heterogeneous at this scale; however, the equations presented above are valid for homogeneous materials. The heterogeneity of the tested material in the horizontal $(x-y)$ plane can be easily evaluated using conventional Young's modulus maps (Kontomaris et al., 2023a). However, the limitation of this approach is that it does not account for the depth-dependent mechanical properties of the material. To account for the depth-dependent mechanical properties of the material, 'average Young's modulus functions' have been introduced (Kontomaris et al., 2021).

The amount of force applied to the sample can be calculated using $f = k_e z_e$ where k_e is the equivalent spring constant of the cantilever beam and z_e is the equivalent deflection of the beam producing the deformation δ. Overall, the mechanical properties (e.g., the Young's modulus) of the sample are determined by fitting the force-displacement curve to the mathematical model (e.g., Equations (15) and (16)). AFM has been used to investigate numerous soft materials, including epithelial cells (Shigemura et al., 2023), agarose gels, fibroblasts, and breast cancer cells (Kontomaris et al., 2023b), single yest cells (Chang et al., 2021), and lipid membranes (Eid et al., 2021), producing results of major significance.

Although both macro- and nano-indentation often rely on Hertzian contact mechanics, they differ fundamentally in application. Macroscale indentation assumes material homogeneity and isotropy to measure averaged bulk behaviour. Conversely, nanoscale testing - especially of biological samples - reveals significant spatial and depth-dependent heterogeneity. This requires generating spatially resolved Young's modulus maps and utilising specialised data-processing models (Kontomaris et al., 2023a) to characterise mechanical properties as a function of indentation depth (Kontomaris et al., 2021, 2023b; Ding et al., 2018).

In AFM measurements, the elastic modulus derived from fitting represents an apparent or average value (Kontomaris et al., 2021, 2023b; Ding et al., 2018). This occurs because the inherent heterogeneity of biological materials causes mechanical properties to vary with indentation depth. For soft samples like cells and tissues, indentation typically ranges from 100 nm to 2 μm (Ding et al., 2018; Wong et al., 2023; Pogoda et al., 2012). Therefore, the resulting analysis is highly sensitive to the specific depth applied in indentation-based methods including AFM. While traditional AFM indentation is time-intensive, the force scanning method introduced by Darling (2011) offers a high-throughput alternative for mechanical mapping. In this approach, a series of topographical images are captured at varying setpoint forces, representing progressive sample indentations. The force range is calibrated through preliminary tests to ensure valid deformation. By reconstructing force-indentation curves from specific spatial locations across the image stack, the Young's modulus can be derived from the slope of the linearised Hertz relationship, eliminating the need for explicit contact point determination and drastically reducing total scanning time.

In nanoindentation experiments on soft samples, particularly biological materials, the sample preparation and measurement protocol play a critical role in the reliability of the extracted mechanical parameters (Kim et al., 2025). Biological samples are ideally measured in a liquid environment, where their native hydrated state is preserved and their response is inherently viscoelastic. Despite this, in many AFM-based nanoindentation studies, data processing relies on classical contact mechanics models derived for linear elastic materials, such as the Hertz model. This apparent inconsistency is commonly addressed by performing measurements under conditions that minimise viscoelastic contributions. In particular, the use of low ramp frequencies (typically in the range of 1-2 Hz) has been shown to significantly reduce time-dependent effects, allowing the mechanical response to be approximated as quasi-elastic (Yang et al., 2009; Guz et al., 2014; Gavara, 2017). Under such conditions, viscoelastic dissipation is minimised, which can be experimentally verified by the reduction of hysteresis between the loading and unloading force-indentation curves. Therefore, when classical elastic models are employed for data analysis, it is necessary to perform preliminary tests to determine an appropriate ramp frequency at which the force-indentation response exhibits minimal hysteresis. This procedure effectively acts as a preconditioning and validation step, ensuring that the subsequent analysis reflects a stabilised, approximately linear mechanical behaviour of the sample.

Fig. 2 presents representative force-indentation curves for a human fibroblast, utilising open-access data from (Hermanowicz et al., 2014). These measurements were conducted at 37 °C under humidified conditions (5% CO_2) using a Veeco probes AFM cantilever featuring a 20 nm nominal tip radius, a 25° half-opening angle, and a spring constant of 0.01 N/m (calibrated via the thermal tune method). A Poisson's ratio of 0.5 was assumed for all calculations. In Fig. 2a, data from the central region of the cell were fit using Sneddon's model, resulting in a Young's modulus of 8.2 kPa. Conversely, Fig. 2b illustrates the substrate effect on data acquired at the cell edge. While a standard Sneddon fit (curve 1) yielded an inflated modulus of 23.7 kPa, applying the Garcia and Garcia model (Garcia and Garcia, 2018) (curve 2) accounted for the underlying substrate influence to provide a more accurate modulus of 13.1 kPa.

Although the AFM can be used to investigate the structural and nanomechanical properties of structures at high spatial resolution in physiologically relevant conditions (Yurtsever et al., 2021), it has its own disadvantages and limitations. Like the conventional indentation, the mathematical model used to simulate the sample is based on various assumptions and hence those assumptions could produce an error in the identified mechanical properties (Efremov et al., 2020). Additionally, as a small structure of micro-scale, interaction forces like van der Waals force, surface stress, electrostatic force and residual stress can have significant influence on the AFM deflection and thus on the identified material properties (Marrese et al., 2017; Variola, 2015; Zhang et al., 2010). Like conventional indentation, the identified material properties will not be accurate if the sample surface is not flat (Liu and Tschumperlin, 2011). The cantilever beam slippage or moving cells produce jumps in the response curve (Cartagena-Rivera et al., 2016). A sharper tip can damage the surface of the delicate samples during measurements (Norman et al., 2021; Cho et al., 2023). Inertia effects can produce an error in the material properties if they are not accounted for (Abbasi and Karami Mohammadi, 2010). However, the most significant sources of error related to the AFM nanoindentation method arise from uncertainties in the cantilever's spring constant, the determination of deflection sensitivity (Schillers et al., 2017) and the contact point determination (Crick and Yin, 2007). For example, Matei et al. (2006) reported that the precision and accuracy of the thermal noise method are 5% and 10%, respectively. Furthermore, Schillers et al. (2017) observed that the error in deflection sensitivity for cell samples can vary between 5% and 20%. To reduce errors related to the spring constant and the cantilever's sensitivity when testing soft materials like cells, a reliable technique known as the standardized nanomechanical AFM procedure (SNAP) has been developed (Schillers et al., 2017). SNAP enables precise calibration of the AFM optical lever system, which is essential for all force spectroscopy methods, resulting in reliable values that are consistent across various instruments, laboratories, and operators.

As mentioned earlier, another source of error - primarily related to soft biological samples - is the determination of the contact point. When the contact point is missed by less than 50 nm, the material properties

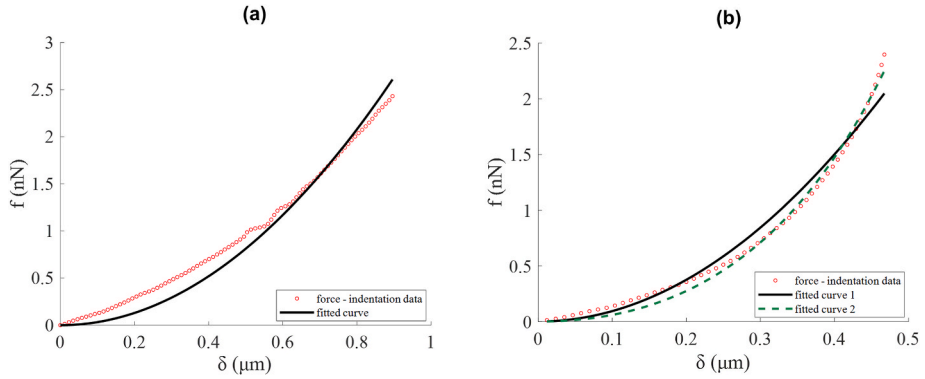

Fig. 2. Representative force-indentation curves for a human fibroblast measured with a conical AFM probe. Panel (a) displays data from the central region fitted with Sneddon's model, yielding a Young's modulus of 8.2 kPa. Panel (b) highlights the substrate effect at the cell edge; while the standard Sneddon fit (curve 1) yields an inflated apparent modulus of 23.7 kPa, the Garcia and Garcia corrected model (curve 2) provides a refined value of 13.1 kPa. The original datasets are accessible via the AtomicJ Repository (Hermanowicz et al., 2014).

for small indentations are inaccurate; however, the error diminishes asymptotically beyond 200 nm of indentation, resulting in an accurate estimate of material stiffness (Crick and Yin, 2007). On the other hand, if the contact point is missed by more than 100 nm, it becomes impossible to accurately estimate the true material properties. Although noise introduces additional uncertainty in material properties at small indentations, the effect of missing the contact point is the dominant factor. Estimating the contact point when testing soft materials is challenging, as the cantilever's deflection does not change abruptly from one point to another (A-Hassan et al., 1998). An additional factor to consider is the choice of a suitable cantilever for the experiments. The cantilever's spring constant should be similar to the stiffness of the tested material (Krieg et al., 2018). In addition, it is also important to note that the applied strains should not exceed 20% (Krieg et al., 2018). Another critical issue is related to the changes in the indenter's shape during experiments. In particular, the radius of a sharp pyramidal tip may increase due to wear during contact scanning, which affects the calculations of the elastic modulus (Fu et al., 2024).

2.5. Rheometry

It is important to note that the rheology is the study of flow and deformation of matter. Rheometers are probably the most used systems to determine the viscoelastic properties of soft materials. Rheometers can be categorised into three main groups: rotational, extensional, and capillary (Krishnan et al., 2017). Amongst rheometers, rotational (or shear) rheometers are commonly used for the determination of the viscoelastic properties of soft materials. For example, a sinusoidal small amplitude oscillatory shear of amplitude γ_0 is imposed to the sample at a certain frequency ($\omega = 2\pi f$) and the shear strain deformation of the sample to this shear stress is measured (dynamic oscillatory test) in a shear-controlled rheometer (Fig. 1e). The resulting shear stress oscillates at the same frequency and is proportional to the shear amplitude in the linear viscoelastic regime. However, there will be a phase shift (Δ) between the input strain and resulting stress for a viscoelastic sample (Fig. 3a), and the relation between stress and strain can be written using the sum of the sine and cosine contributions. Hence, the input shear strain and resulting shear stress can be expressed as follows (Laun et al., 2014):

$$\gamma(t) = \gamma_0 \sin(\omega t) \tag{17}$$

$$\tau(t) = \gamma_0[G' \sin(\omega t) + G'' \cos(\omega t)] \tag{18}$$

where G' is the storage shear modulus and G'' is the loss shear modulus; $G^* = G' + jG''$ being the complex shear modulus. The resulting shear stress as a phase-shifted signal of stress amplitude τ_0 and phase angle Δ can be expressed as $\tau(t) = \tau_0 \sin(\omega t + \Delta)$ where $\tau_0 = \gamma_0\sqrt{G'^2 + G''^2}$ and $\tan(\Delta) = G''/G'$; $|G^*| = \sqrt{G'^2 + G''^2}$ being the magnitude of the complex modulus. Overall, the storage and shear modulus can be determined from the input γ_0 and measured τ_0 and Δ as follows:

$$G' = |G^*|\cos(\Delta) \tag{19}$$

$$G'' = |G^*|\sin(\Delta) \tag{20}$$

The shear viscosity is defined as:

$$\eta = \frac{G''}{\omega} \tag{21}$$

where ω is the circular frequency in rad/s. Fig. 3b displays an example of the frequency-dependent storage (G') and loss (G'') moduli for a collagen

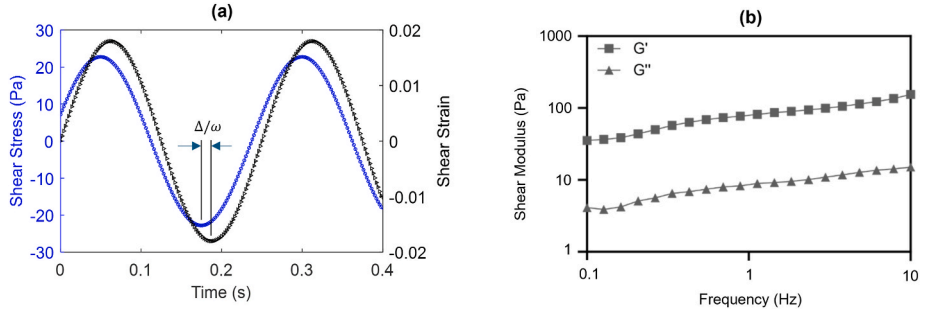

Fig. 3. (a) Representative sinusoidal stress and strain curves ($f = 4$ Hz) of a viscoelastic material with a storage modulus of $G' = 1200$ Pa, loss modulus of $G'' = 400$ Pa, and phase shift of $\Delta = 0.32$ rad. (b) Frequency-dependent storage (G') and loss (G'') moduli for a collagen hydrogel substrate characterised via rheometry (reprinted from (Cho and Lee, 2023)).

hydrogel substrate (Cho and Lee, 2023). To comprehensively characterise a material's rheological profile, experiments must integrate measurement modes, frequency selection, and geometry options to mitigate errors and capture both linear and nonlinear behaviours. Transient tests, such as stress relaxation and creep recovery, identify time-dependent behaviours, while frequency sweeps measure viscoelastic properties under oscillatory deformation to generate a rheological "fingerprint" (Singh et al., 2018). This fingerprint quantifies solid-like behaviour (G'), liquid-like behaviour (G''), and structural indicators like $\tan(\Delta) = G''/G'$, which are critical for analysing polymer entanglement and formulation stability. In contrast, strain sweeps vary deformation at a constant frequency to identify the linear viscoelastic region and the structural breakdown point (Singh et al., 2018; Tunick, 2011). The choice of geometry further influences accuracy; cone-plate fixtures provide the uniform shear rate essential for precise viscosity measurements, whereas parallel-plate fixtures allow for adjustable gaps suitable for particulate samples but introduce non-homogeneous shear (Song et al., 2017). While results from these geometries typically coincide during small-amplitude oscillatory shear, discrepancies often arise at high frequencies or in the nonlinear regime. For highly shear-thinning materials, proper corrections - such as horizontal or vertical shift factors - are frequently required to align data across different geometries and frequencies to ensure accurate characterisation (Song et al., 2017). Crucially, while these standard geometries apply simple shear, real biological tissues often experience complex, multi-directional shear forces *in vivo* (Patteson and Janmey, 2024). This simplification can introduce errors when translating rheological data to physiological loading, necessitating awareness of this limitation and the potential use

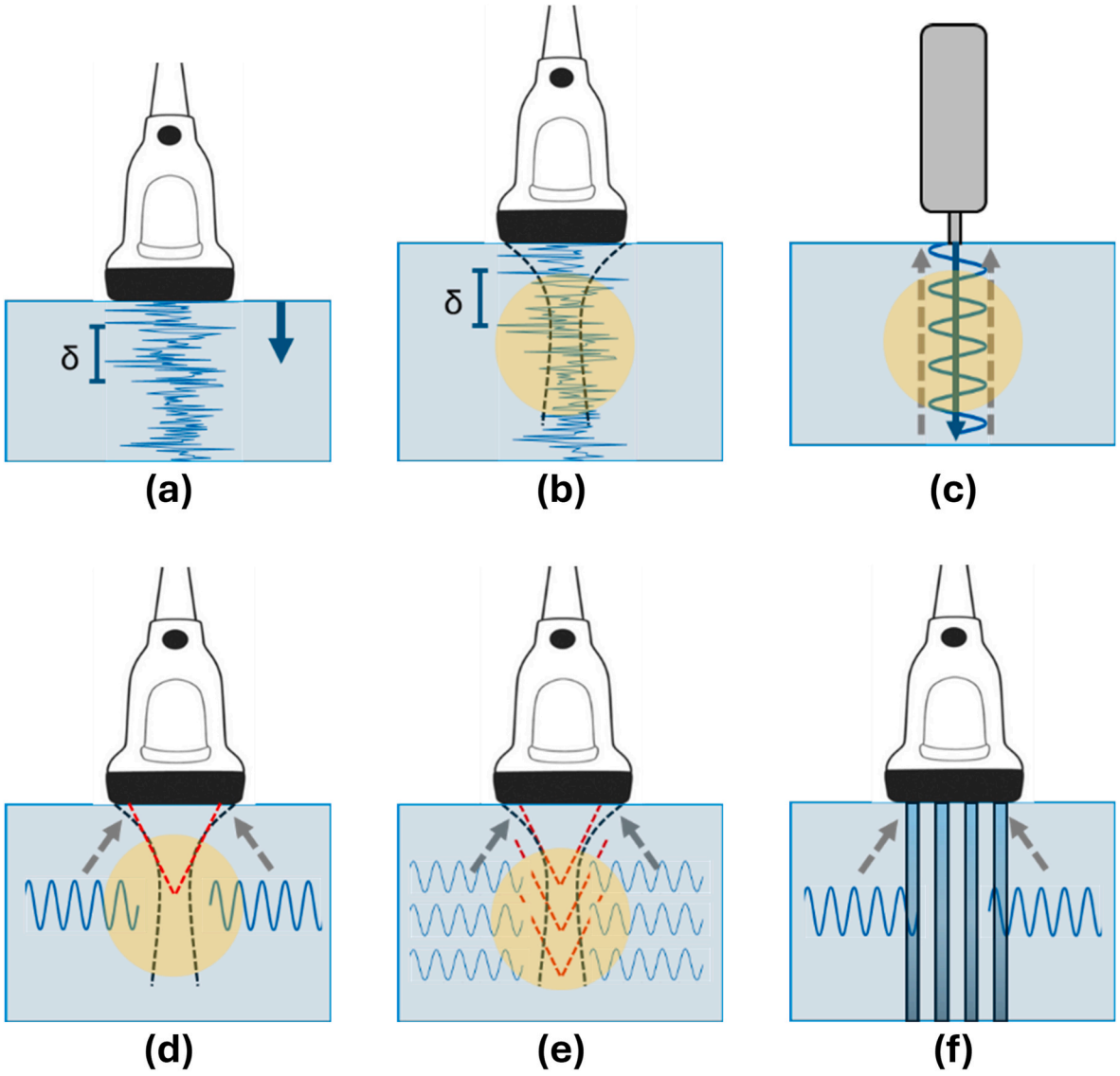

Fig. 4. Schematics of ultrasound elastography techniques. (a) Strain elastography: Manual compression is applied to the tissue; the blue waveform represents the radiofrequency (RF) signals used to track axial displacement and strain (indicated by the arrow). (b) ARFI strain imaging: A focused RF push pulse (blue) generates a localized internal force, where δ represents the resulting axial tissue displacement tracked by RF pulses. (c) One-dimensional transient elastography (1D-TE): A mechanical vibrator generates shear waves (arrows) that propagate through the tissue, monitored by an ultrasound tracking beam (blue waveform). (d) Point shear wave elastography (pSWE): A single focused ARFI push (red lines) generates a diverging shear wave. Blue waveforms show the propagation direction perpendicular to the push axis, with grey arrows indicating the tracked RF displacement. (e) Two-dimensional shear wave elastography (2D-SWE): Multiple ARFI pushes at varying lateral positions (red lines) create a 2D shear wave front; blue waveforms denote multi-directional propagation across the imaging plane, tracked via RF displacement (grey arrows). (f) Comb-push ultrasound shear elastography (CUSE): Several simultaneous, unfocused ARFI beams (blue stripes) produce overlapping shear waves. Blue waveforms highlight the resulting interference patterns, with grey arrows representing the tracked displacement. (For interpretation of the references to colour in this figure legend, the reader is referred to the Web version of this article.)

of complementary modelling or specialised tests to better approximate complex shear environments.

Rheometry has been used to investigate many soft materials, including porcine kidney (Nasseri et al., 2002), bovine liver (Klatt et al., 2010), human skin (Lamers et al., 2013), rodent liver (Lin et al., 2017), fibroblasts (Sander et al., 2017), hydrogels (Yengul et al., 2019), and various porcine organs such as heart, kidney, liver, and brain (Mishra and Cleveland, 2024). While rheometry is widely used in practice, rheometers still have many practical limitations. Simplified deformation fields for stress, strain, and strain rate components are used in rheological material functions. However, in practice, forces and displacements are often measured at the boundaries of a specimen, hence the calculation of true stress and strain can be hampered by different parameters, including instrument inertia, specimen inertia, boundary effects, and volumetric effects (Ewoldt et al., 2015). Therefore, system inertia (e.g., rotor), sample inertia, boundary effects, the friction of bearings, the residual torque of bearings, and volumetric effects could adversely affect the determined material properties (Ewoldt et al., 2015; Gabriel and Kaschta, 1998; Klemuk and Titze, 2009). Pre-compression is necessary to ensure proper coupling between the sample and the plates, and the rate of the pre-compression force can influence the identified viscoelastic properties (Mishra and Cleveland, 2024; Engstrom et al., 2019; Hrapko et al., 2008; Ayyildiz et al., 2015). However, these forces may not be present in the material (e.g., the liver) during normal operation, and pre-compression may lead to material properties that differ from those observed under normal physiological conditions. In addition to compression stiffening of the material with the increase of pre-stress, the increase of the contact force between the sample and plates may contribute to the increase of material properties with the increase of pre-stress. On the other hand, if the pre-compression force is low, the sample will slip between the plates, and this would lead to obtaining incorrect material properties (Walter et al., 2017). Furthermore, soft samples can break, especially upon applying sufficiently large shear oscillations (Saint-Michel et al., 2017).

2.6. Ultrasound elastography

Ultrasound elastography (Fig. 4) provides complementary information on tissue stiffness to conventional ultrasound imaging (Zhang et al., 2023). Ultrasonic elastography has been developed as an alternative to manual palpation. It has two significant advantages over manual palpation: results are objective and can be quantitative, rather than subjective and qualitative, and observations can be made in almost all parts of the body. The two principal methods of measuring mechanical properties using ultrasound are: measuring the movement of the tissue (strain) for a given applied force (stress) and measuring the velocity of shear waves through the region of interest (Schrenk et al., 2020). Strain elastography is a qualitative technique in which relative stiffness differences in the insonified region are displayed (Dietrich et al., 2017). In this technique, the resulting normal strain is measured after applying a normal stress to the tissue. This stress can be generated either by manually compressing the probe (Fig. 4a) or by utilising an acoustic radiation force impulse (ARFI) (Fig. 4b). In shear wave elastography (SWE), acoustic impulses generate shear waves that propagate at much lower speeds - typically between 1 m/s and 10 m/s in soft tissues - compared to longitudinal (compressional) waves, which travel at significantly higher velocities, typically between 1450 and 1700 m/s in soft biological media. Specific examples include speeds of 1450-1570 m/s in breast tissue, 1522-1623 m/s in the liver, 1500-1610 m/s in skeletal muscle, and 1460-1580 m/s in the brain, all falling within the standard soft-tissue range (Sigrist et al., 2017; Sarvazyan et al., 2013). The scanning system can measure the shear wave speeds. The shear modulus G can be determined from the measured shear wave speed v_s using the following equation (Nakaoka et al., 2022):

$$G = \rho v_s^2 \tag{22}$$

where ρ is the tissue density. It should be remembered that the Young's modulus can be calculated using the simple equation $E = 2G(1 + \nu)$.

SWE refers to techniques based on mechanical stress, generated either externally, using external actuators, or internally, using acoustic radiation force impulse (ARFI) to produce a push pulse within the tissue (Oglat and Abukhalil, 2024; Ferraioli et al., 2024). The one-dimensional transient elastography (1D-TE) (Fig. 4c) is a technique embedded in the FibroScan™ system (Echosens, Paris, France), which utilises a main probe containing both an ultrasound transducer and a mechanical vibrating device that generates shear waves through an external vibration source, thereby propagating through the tissue (DeWall, 2013; Oglat and Abukhalil, 2024). In the ARFI-SWE, localised tissue displacements are generated using focused ultrasound beams, and the resulting shear wave propagation is then detected (Oglat and Abukhalil, 2024). This technique can be divided into point SWE (pSWE) (Fig. 4d), in which a push-pulse is focused on a single focal location, and two-dimensional SWE (2D-SWE) (Fig. 4e), in which several ARFI push-pulses are generated at multiple focal locations. Another approach is the comb-push ultrasound shear elastography (CUSE) (Fig. 4f), in which sub-apertures are used to simultaneously transmit unfocused push beams at different spatial locations (Song et al., 2012, 2013; Racedo and Urban, 2019). It is important to highlight that, in SWE, tissue motion is captured using ultrafast ultrasound imaging - achieving frame rates of several thousand frames per second - to track the shear wave propagation and derive mechanical properties. Shear wave dispersion ultrasound vibrometry (SDUV) is another ultrasound-based technique that quantifies tissue elasticity and viscosity by analysing the frequency-dependent propagation speed of shear waves in soft tissue (Urban et al., 2012). A focused ultrasound “push” beam generates harmonic shear waves, while a separate “detect” beam monitors their propagation using pulse-echo ultrasound. Shear wave speed at different frequencies (typically 100-400 Hz) is calculated from phase differences measured at two locations along the propagation path, and these measurements are fitted to a viscoelastic model to estimate shear elasticity and viscosity (Urban et al., 2012; Chen et al., 2009).

Notably, at low frequencies - typically below 200-300 Hz in soft-tissue applications - the shear wavelength is much larger than tissue thickness, leading to guided wave behaviour and strong dispersion, which can bias stiffness measurements if not properly corrected (Bernal et al., 2011; Gennisson et al., 2013). As frequency increases and the shear wavelength becomes comparable to or smaller than the tissue thickness, the wave propagation approaches the bulk shear wave regime, reducing dispersion and improving accuracy in estimating intrinsic tissue elasticity (Bercoff et al., 2004; Palmeri and Nightingale, 2011). This consideration is especially important in thin organs or layers (e.g., arterial walls or skin), where inappropriate frequency selection can lead to overestimation or underestimation of stiffness due to boundary-induced artifact (Bernal et al., 2011; Gennisson et al., 2013).

Ultrasound elastography is used in the clinic to image the mechanical properties of various soft tissues (Sigrist et al., 2017; Gennisson et al., 2013; Bamber et al., 2013; Cosgrove et al., 2013). Its applications include the evaluation of the liver (Bernal et al., 2011; Ferraioli et al., 2018), breast (Barr et al., 2015), thyroid (Swan et al., 2021), prostate (Barr et al., 2017), kidney (Cè et al., 2023), and musculoskeletal tissue (Albano et al., 2023). In addition to the clinic, ultrasound elastography can be used in the laboratory to determine the mechanical properties of soft tissue-mimicking materials for development and validation purposes (Yengul et al., 2019; Nguyen et al., 2014). Alongside measuring the shear moduli of tissues, there have been some attempts to exploit the damping (or viscosity) in quantitative ultrasound elastography (Li et al., 2021a; Tecse et al., 2023).

Although ultrasound elastography offers non-invasive imaging of the mechanical properties of organs deep within the body, it presents some drawbacks (Kimondo et al., 2025). Shear wave propagation in some regions violates the assumed relationship between shear modulus and

shear wave speed, especially near boundaries and within thin layers, and this can produce an error in the calculated material properties (Patra and Grover, 2022). Similarly, disregarding viscosity may bias the estimation of the true shear modulus (Zhu et al., 2015). The external pre-compression results in stiffening, hence different shear moduli are measured based on the initial resting pressure (Lam et al., 2016). Partial volume averaging artifacts can lead to image degradation (Patra and Grover, 2022). Different shear moduli can be mapped based on the selected anatomical area (Zelesco et al., 2018). In strain imaging, the attenuation of longitudinal waves as they travel deeper into the tissue reduces the signal-to-noise ratio, resulting in decreased accuracy in deep regions compared to superficial ones (Cui et al., 2022). Superimposed compressional and shear waves reflecting at the interfaces can reduce the accuracy of the measured shear moduli (Gennisson et al., 2013). Respiration, patient position, and operator skill can affect the identified shear modulus of tissues (Zelesco et al., 2018).

2.7. Magnetic resonance elastography

Magnetic resonance elastography (MRE) (Fig. 5) is a phase-contrast–based technique that images propagating mechanical waves, from which material properties, such as shear modulus, are determined (Manduca et al., 2021). In this technique, mechanical waves are generated and delivered to the patient's deeper tissues. An MRI acquisition sequence measures the propagation and velocity of the waves, and mechanical parameters are recovered from this information. In isotropic, nearly incompressible tissue, shear waves propagate at speeds that depend on the shear modulus, while longitudinal waves are much faster and typically filtered out. As mentioned before, for viscoelastic materials, the shear modulus is complex: $G^* = G' + jG''$, where G' denotes storage modulus and G'' denotes loss modulus. A common direct inversion uses the Helmholtz equation: $G^* = -\rho\omega^2\mathbf{u}/(\nabla^2\mathbf{u})$, where $\mathbf{u}$ is the harmonic displacement, ρ is density, ω is angular frequency, and ∇^2 denotes the Laplacian operator (Manduca et al., 2021; Ma et al., 2023, 2025). This framework demonstrates how wave equations and inversion techniques connect measured wave fields to intrinsic tissue properties, allowing for the quantitative characterisation of stiffness and damping *in vivo*.

The applications of MRE include the evaluation of the liver (Venkatesh et al., 2013; Akkaya et al., 2018), kidney (Low et al., 2015), and prostate (Sahebjavaher et al., 2014). In addition to measuring the shear moduli of tissues, there have been attempts to exploit the viscosity in MRE (Wang et al., 2024; Reiter et al., 2021; Majumdar and Klatt, 2021). Despite MRE provides non-invasive imaging of the mechanical properties of organs deep in the body, it has some shortcomings. The drawbacks listed in Section 2.6 for ultrasound elastography are also encountered in MRE. A partial volume effect occurs when different materials are encompassed within the same voxel in elastography techniques. However, the partial volume effect is encountered even if the voxel is filled with the same material in magnetic resonance elastography, since wave displacements due to vibrations are spatially distributed (Ito et al., 2017).

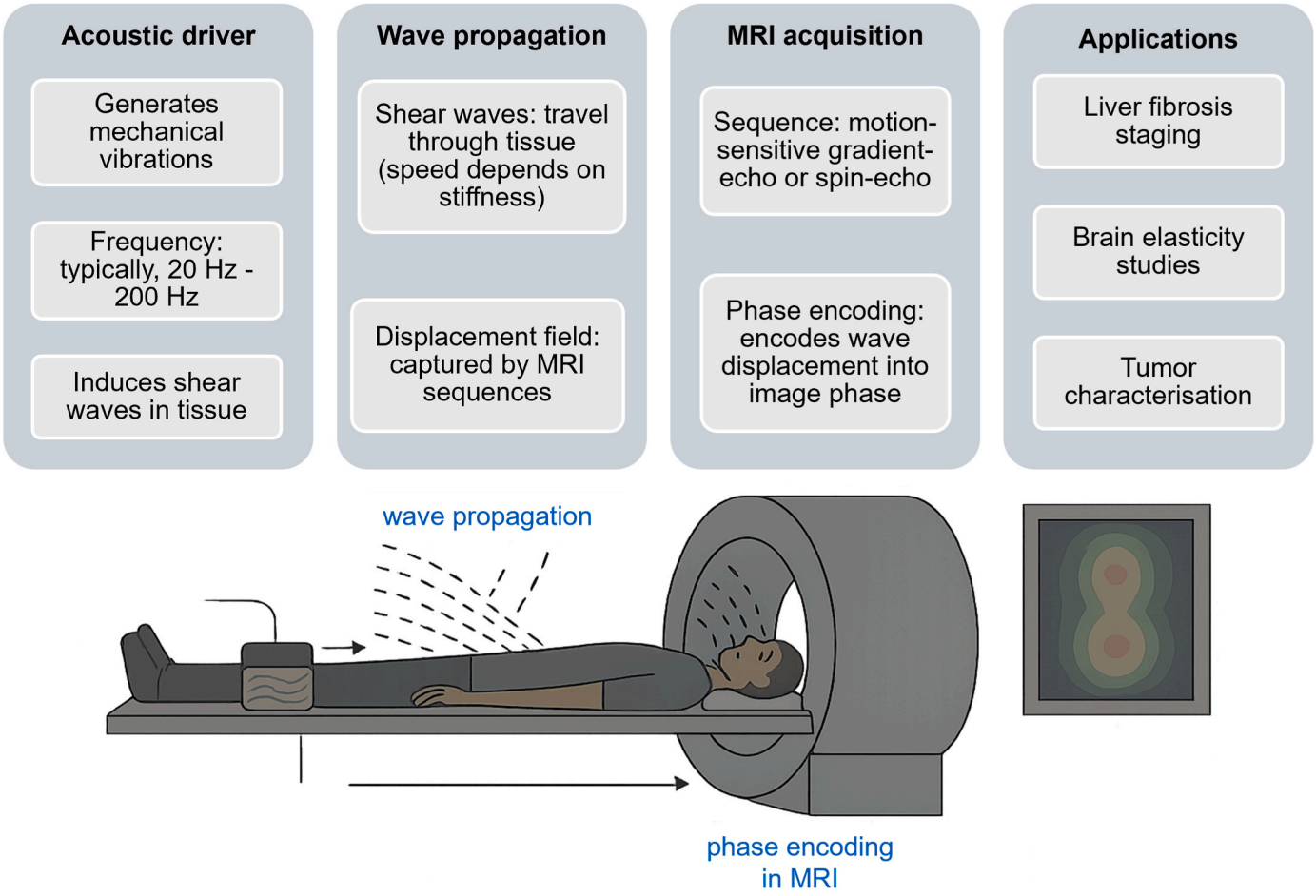

Fig. 5. The working principle of magnetic resonance elastography (MRE), illustrating the mechanical driver, wave propagation through tissue, and subsequent MRI acquisition.

2.8. Optical coherence elastography

Optical coherence elastography (OCE) is an advanced imaging modality that extends optical coherence tomography (OCT) by incorporating mechanical property assessment. First introduced by Schmitt (1998), OCE applies controlled mechanical stimuli - such as compression, shear, or wave-based excitation - to biological tissues and uses OCT (Fig. 1f) to capture high-resolution displacement fields and strain maps (Schmitt, 1998; Liang et al., 2010). These elastograms provide insight into tissue stiffness and elasticity, offering contrast beyond conventional optical imaging. Recent improvements in phase-sensitive OCT have enabled sub-nanometre displacement detection, facilitating quantitative reconstruction of biomechanical parameters such as Young's modulus (Sun et al., 2011; Singh et al., 2025). This combination of structural and mechanical imaging makes OCE particularly valuable for studying tissue microarchitecture and mechanobiology.

OCE has demonstrated significant potential in various biomedical applications. In ophthalmology, it is used to assess corneal and retinal biomechanics, aiding in the diagnosis of keratoconus and glaucoma (Kirby et al., 2017). Oncology leverages OCE to detect tumours based on stiffness differences, while cardiovascular research employs it to evaluate arterial wall compliance and plaque vulnerability (Sun et al., 2011; Zvietcovich and V Larin, 2022). Dermatology and tissue engineering also benefit from OCE for monitoring skin elasticity and scaffold mechanics (Wang et al., 2023a). As technology advances with faster volumetric imaging and improved mechanical modelling, OCE is poised to become a key tool for clinical diagnostics and mechanobiological research (Singh et al., 2025).

Despite its promise, OCE faces several limitations that hinder widespread clinical adoption. First, imaging depth is restricted to superficial tissues due to OCT's penetration limits, limiting its applications in deeper organs (Schmitt, 1998; Liang et al., 2010). Quantitative accuracy is highly dependent on mechanical models and assumptions, which often neglect anisotropy, viscoelasticity, tissue heterogeneity, and boundary effects, leading to variability in reconstructed parameters such as Young's modulus (Sun et al., 2011; Singh et al., 2025; Wang et al., 2023a). In wave-based approaches, mode contamination from non-shear components (e.g., Rayleigh/Lamb/longitudinal) complicates dispersion analysis and inversion (Singh et al., 2025; Zvietcovich and V Larin, 2022). Phase-sensitive displacement measurements, while enabling sub-nanometre resolution, remain vulnerable to noise, phase jitter, timing jitter, and laser frequency nonlinearity, and are further impacted by imperfect synchronisation between excitation/trigger and acquisition (Liang et al., 2010; Singh et al., 2025; Kirby et al., 2017; Zvietcovich and V Larin, 2022). Rapid physiological motions (breathing, cardiac, ocular) and structural changes between scans introduce motion artifacts and decorrelation, degrading strain and wavefield estimates (Liang et al., 2010; Singh et al., 2025; Kirby et al., 2017). Moreover, optical reflections and interference from tissue interfaces or sample edges can bias phase and amplitude, causing reconstruction errors (Schmitt, 1998; Liang et al., 2010; Sun et al., 2011). Additionally, strain estimation algorithms introduce errors through phase unwrapping and dynamic range constraints (Schmitt, 1998; Liang et al., 2010). Finally, the lack of standardised frameworks for data sharing and reproducibility complicates cross-platform validation and clinical translation (Singh et al., 2025; Wang et al., 2023a). These challenges underscore the need for improved modelling, robust phase and timing stabilisation, precise synchronisation, artifact-aware inversion, and harmonised methodologies to fully realise OCE's potential.

2.9. Other techniques

Some other techniques have been used for the identification of the mechanical properties of soft materials, including the pipette aspiration (Buffinton et al., 2015), pressure myography (Bloksgaard et al., 2017), scanning acoustic microscopy (Liu et al., 2023; Jensen et al., 2006), cavitation rheometry (Cui et al., 2011), acoustic particle palpation or the use of spherical objects located within the soft material and at the soft material interface (Koruk and Pouliopoulos, 2023), and vibration tests, such as experimental modal analysis (Wang et al., 2020) and logarithmic decrement (Rosicka et al., 2021). Other methods include optical stretching, cellular shear wave elastography (cSWE), acoustic force spectroscopy (AFS), cell monolayer rheometry, magnetic twisting cytometry (MTC), and particle-tracking microrheometry, which can be used to identify the mechanical properties of single cells or organelles (Wu et al., 2018; Hao et al., 2020). For example, the pipette aspiration technique is a simple method of identifying the initial slope of the stress-strain curve (or the Young's modulus) of the soft material by using a pipette to partially aspirate a sample into its tip (Buffinton et al., 2015; Aoki et al., 1997). However, this technique has various drawbacks. For example, surface irregularities on the sample and the gap between the pipette tip and the sample can have a dramatic effect on the accuracy of the identified mechanical properties (Ohashi et al., 2005; Maghzinajafabadi et al., 2019).

cSWE is an optical elastography technique for assessing mechanical properties of single cells and small clusters by generating high-frequency shear waves with a vibrating micropipette and tracking propagation via high-speed optical microscopy (Grasland-Mongrain et al., 2018). Using speckle tracking and passive elastography methods inspired by seismology, cSWE achieves microsecond temporal and micrometre spatial resolution, enabling studies of dynamic processes and mechanical heterogeneity in regions like the nucleus and cytoplasm (Grasland-Mongrain et al., 2018; Li et al., 2021b). However, challenges include limited viscosity assessment, lower spatial resolution compared to AFM, lack of standardised validation at kilohertz frequencies, and low throughput (Grasland-Mongrain et al., 2018; Li et al., 2021b). In contrast, AFS uses ultrasonic standing waves in microfluidic chambers to apply controlled piconewton-scale forces on tethered microspheres, enabling high-throughput measurement of material properties such as stiffness and viscoelasticity (Sitters et al., 2015). By tracking bead displacement optically, AFS provides force-extension data for polymers and biomolecular complexes, offering advantages over optical tweezers in scalability and integration with lab-on-chip systems, though spatial resolution and calibration remain challenges (Sitters et al., 2015). On the other hand, MTC applies controlled torque to ligand-coated magnetic beads attached to cell-surface receptors using rotating magnetic fields, enabling measurement of cellular viscoelastic properties (Zhang et al., 2017; Laurent et al., 2002). By tracking bead rotation, MTC quantifies complex shear modulus and dynamic stiffening across frequencies from Hz to kHz, supporting studies of mechanotransduction and cytoskeletal remodelling. While non-invasive and compatible with live-cell imaging, limitations include lower spatial resolution than AFM and sensitivity to bead adhesion geometry and torque calibration (Zhang et al., 2017).

The resonant vibration test or experimental modal analysis (Wang et al., 2020) can be used to identify the mechanical properties of a structure. In this case, the frequency response functions of the structure are measured using a response sensor (e.g., an accelerometer or a laser vibrometer) and an exciter (e.g., a hammer or shaker). By analysing the measured frequency response functions, the Young's modulus and damping of the structure are identified. Similarly, the logarithmic decrement method (Rosicka et al., 2021), which does not require the measurement of the input, can be used to determine the mechanical properties of a structure when a single mode of vibration can be isolated from the others. However, these techniques require relatively large durable samples such as beams and plates, which are not feasible for relatively soft samples. Some sources of error and uncertainty for vibration-based methods include the boundary conditions, the effect of contact-type response and excitation sensors, and assumptions related to modelling the structure among others (Koruk, 2014; Koruk and Sanliturk, 2012).

Small spherical particles located within the tissue (Cebrecos et al.,

2021; Levy and Oldenburg, 2021), and at the tissue interface (Koruk et al., 2015; Bezer et al., 2020) exposed to static and dynamic external forces have been used to identify the mechanical properties of soft materials. However, for techniques based on a spherical object located within a soft material sample, there are several practical issues. For example, in these techniques, there is a need to locate a bubble (or a non-deformable sphere) within the soft material sample, which can alter the material properties (Koruk and Pouliopoulos, 2023). A more practical technique is the use of particles located at the material interface. Although the use of a bubble has many practical issues (Bezer et al., 2020; Koruk and Choi, 2018, 2019), the use of a non-deformable sphere eliminates many disadvantages of other techniques and is quite promising for characterising the viscoelastic properties of soft materials (Koruk et al., 2024; Koruk, 2022; Koruk and Pouliopoulos, 2024).

2.10. Further considerations

Biological tissues exhibit complex, non-linear mechanical behaviours that deviate from the linear elasticity assumed in traditional engineering models, creating significant challenges for accurate disease modelling and diagnosis (Johnston and Callanan, 2023; Chen et al., 2013). This non-linear behaviour arises from the hierarchical arrangement of extracellular matrix components, where the softer elastin network dominates at low strains while wavy collagen fibres offer minimal resistance (Ionescu and Chirita, 2009; Sanz-Herrera et al., 2025). As strain increases, these collagen fibres straighten and align with the load, becoming the primary load-bearing elements and causing a dramatic increase in stiffness known as strain stiffening (Fontenele and Bouklas, 2023; Marieswaran et al., 2018). Furthermore, directionally dependent fibre orientation results in anisotropic properties, where the mechanical response varies according to the direction of applied force. Because diseases like fibrosis and solid tumours cause significant mechanical alterations detectable via elastography, characterising the specific degree of non-linearity - rather than relying on a single linear stiffness value - may offer more reliable diagnostic biomarkers for distinguishing healthy from diseased tissue (Oberai et al., 2009).

While simple phenomenological models are suitable for small strains, they often yield significant errors during large deformations, necessitating the use of hyper-elastic frameworks like the Mooney-Rivlin or Ogden models to account for reversible nonlinearity (Bonet, 2001; Lohr et al., 2022; Panda and Buist, 2018; Ahsanizadeh and Li, 2015). The Mooney-Rivlin model is frequently favoured for its balance of simplicity and accuracy in moderate strain ranges up to 200%, whereas the Ogden model offers superior descriptive power across the entire deformation range despite requiring additional parameters (Holzapfel and Ogden, 2025; Gomez-Jimenez et al., 2024). To fully capture the mechanical complexity of soft tissues, advanced finite element implementations often integrate these hyper-elastic models with viscoelastic frameworks, such as the generalized Maxwell model using Prony series, to simultaneously address large-strain behaviour and time-dependent phenomena like creep and stress relaxation (Panda and Buist, 2018). However, implementing these coupled frameworks remains difficult for practical applications due to the high computational cost and the extensive experimental data required to accurately calibrate the numerous material parameters, a complexity which often makes such models impractical for clinical applications (Nguyen et al., 2020; Farajpour and Ingman, 2024).

There are significant challenges in reconciling mechanical measurements taken under *in vivo* (perfused, warm), in situ, and *ex vivo* conditions, primarily due to variations in tissue conformation and physiological state (Bertalan et al., 2023; Guertler et al., 2018; Zhang, 2005; Ottensmeyer et al., 2004). *In vivo* testing preserves native perfusion, temperature, and intrinsic stretch - elements proven to affect stiffness, viscoelasticity, and stress–strain behaviour - whereas *ex vivo* tissue, lacking blood flow and active pre-strain, often displays reduced stiffness and altered hysteresis (Zhang, 2005; Ottensmeyer et al., 2004). Even in situ approaches, which preserve perfusion temporarily, cannot maintain full physiological conditions of warm, pressurised circulation, leading to relaxation-mediated conformational changes. Additionally, advances in elastography reveal that viscoelastic properties are highly environment-dependent, with *in vivo* measurements offering distinct insights unavailable *ex vivo* (Zhang et al., 2021).

3. Comparison and evaluation

Identifying the mechanical properties of soft materials is considerably more challenging than those of conventional engineering materials. Although various techniques exist to characterise these properties, each has its own drawbacks and limitations. The sources of error and uncertainty associated with the techniques discussed in Section 2 are summarised in Table 1. Due to the different sources of error and uncertainty, the mechanical properties of the same soft material, when measured using different techniques, can vary significantly.

The mechanical properties of various soft materials measured using different identification techniques are listed and compared in Table 2. For example, Amador et al. (2011) measured the shear moduli of gelatine phantoms using an ultrasound elastography method (SDUV) and macro-indentation; the shear modulus measured by the ultrasound elastography method was 1.4 times the value measured by macro-indentation for the 7% gelatine phantom. Czerner et al. (2015) measured the Young's modulus of gelatine (20%) gels using different methods; the Young's modulus measured by macro-indentation was 1.6-1.7 times the values measured using compression test, nano-indentation and oscillatory rheometry. Buffinton et al. (2015) measured the Young's moduli of polyacrylamide gels using tensile testing, nano-indentation, and pipette aspiration; the Young's moduli measured by compression test and pipette aspiration were 1.3 and 2 times the value measured by nano-indentation for the gel with the acrylamide to bis-acrylamide ratio of 30:0.5. Symons et al. (2022) measured the Young's modulus of soft gels using micro-indentation and compression test; the Young's moduli measured by compression test was 1.5 times the value measured by micro-indentation for 2% agarose hydrogel.

The storage and loss Young's moduli of the porcine sclera tissue measured by Nayar et al. (2012) using macro compression and nano-indentation tests differed by 1-2 orders of magnitude. The shear moduli of liver tissue of 50 patients measured by ultrasound shear wave elastography was approximately twice the values measured by MRE (Zhao et al., 2014). Żmudzińska et al. (2018) measured the Young's modulus of 12 porcine liver using the ultrasound shear wave elastography and macro-indentation; the Young's moduli measured by macro-indentation was 1.1-1.6 times the value measured by ultrasound elastography. Yengul et al. (2019) eliminated possible variation caused by batch-to-batch gel variation, sample geometry differences, boundary artifacts and environmental effects in a controlled experimental study. Even in this controlled study, the difference between the storage and shear moduli of the gel (12%) phantom measured by shear wave ultrasound elastography and torsional vibration rheometry were around 7 and 40%, respectively. In another study, it is observed that the shear modulus determined by SDUV, and acoustic radiation force impulse (ARFI) is 1.2 and 5.6 times the result determined by rotary rheometer, respectively, whereas the viscosity determined by rheometry is 1.7 times the result determined by SDUV (Zhu et al., 2015). Interested readers may refer to some other previous comparative studies between MRE and ultrasound transient elastography (Oudry et al., 2009), rheometry and ARFI shear wave elastography (Amador et al., 2016), the quantification of shear wave speed bias across ultrasound and MRE platforms (Palmeri et al., 2021), and the stress-strain curves obtained via ultrasound elastography and traditional compression tests (Wang et al., 2022).

It is seen that different techniques can produce quite different mechanical properties, even for the same homogenous soft samples (Amador et al., 2011; Symons et al., 2022). The situation can become

Table 1
Sources of error and uncertainty in the identified mechanical properties of soft materials for different techniques.

Technique	Source of Error and Uncertainty
Tensile testing	- Improper tailored shape of the sample - Imprecise measure of the cross-sectional area of the sample - Misalignment from the loading axis - Material slippage due to improper clamping - Sample damage due to improper gripping - Insufficient transmission of forces at loading clamps to the ROI (in biaxial tensile test) - Inertia effects (in dynamic tensile test)
Compression testing	- Improper quality and integrity of the sample surface - Imprecise measure of the cross-sectional area of the sample - Misalignment from the loading axis - Material slippage due to insufficient contact force - Damage of the sample surface - Friction generated at the specimen/platen interface - Sample buckling - Inertia effects (in dynamic compression test)
Indentation	- Assumptions used in models to simulate the sample - Effect of adhesion/friction between the sample and indenter - Imprecise determination of the contact point - Misalignment of the indenter tip - Effect of a small and/or thin sample - Effect of roughness/non-flat sample surface - Damage of the sample - Inertia of the system and sample
Atomic force microscopy	- Assumptions used in models to simulate the sample - Effect of interaction forces - Effect of roughness/non-flat sample surface - Effect of cantilever beam slippage - Damage of the sample surface - Inertia effects - Spring's constant calibration - Cantilever's sensitivity
Rheometry	- Assumptions regarding material deformation - Effect of pre-compression - Material slippage - System and sample inertia effects - Boundary effects - Friction of bearings - Residual torque of bearings - Volumetric effects - Sample rupture
Ultrasound elastography (and Magnetic resonance elastography)	- Assumptions regarding tissue deformation and/or shear wave propagation - Effect of viscosity - Effect of external precompression - Partial volume averaging artifacts - Effect of attenuation of vibration energy during propagation - Selected region of interest for analysis - Effect of superimposed compressional and shear waves - Effect of respiration - Effect of patient position - Operator skill
Optical coherence elastography	- Assumptions used in models - Contributions from non-shear modes - Timing jitter and frequency nonlinearity in lasers - Rapid tissue motion or structural changes between scans - Imperfect synchronisation between the trigger signal and data acquisition - Reflections and interference from tissue interfaces or sample edges - Effect of physiological movements - Effect of anisotropy and viscoelasticity

more complicated for heterogeneous, layered, and/or highly viscous soft structures (Wu et al., 2018; Zhu et al., 2015; Zhao et al., 2014). Furthermore, the variability of the material properties identified by a particular technique can be quite high (e.g., more than 50%) (Wu et al., 2018; Nayar et al., 2012; Żmudzińska et al., 2018). As known, the mechanical properties of soft materials depend on many factors, including precompression load, loading rate, frequency, and temperature (Wu et al., 2018; Mishra and Cleveland, 2024; Żmudzińska et al., 2018). Therefore, one should ensure that same or similar test parameters are used when comparing the mechanical properties of soft materials identified using different techniques. Furthermore, the mechanical properties of materials, especially heterogenous ones, can be different based on the scale (nano, micro or macro) measured (Nayar et al., 2012; Polio et al., 2018; Richbourg et al., 2022). While it may not be possible to eliminate all sources of error and uncertainty, minimising the artifacts discussed in Section 2 - and the sources summarised in Tables 1–is essential for improving the accuracy in identifying the mechanical properties of soft materials. Findings from this study underscore the necessity of reliable test rigs and procedures for characterising these properties across multiple scales. Measuring soft tissue mechanics across spatial scales provides a hierarchical view of biological function: nanoscale measurements reveal molecular foundations and protein interactions; microscale analysis captures cellular mechanobiology and regional variations, identifying early pathological markers; and macroscale testing defines bulk organ behaviour for clinical diagnostics and biomimetic design (Guo et al., 2022; Lam and Park, 2025; Holzapfel et al., 2025). Together, these scales bridge the gap between individual molecular triggers and the collective mechanical performance of human systems (Guo et al., 2022; Li and Xu, 2023).

Characterising soft materials such as elastomers, gels, and hydrogels is challenging under traditional American Society for Testing and Materials (ASTM) standards designed for stiff materials, as these standards often fail to account for the unique behaviours of soft tissues and phantoms. For instance, using ASTM D412 (ASTM D412-16, 2021) for tensile testing and using ASTM D575 (ASTM D575-91, 2024) for compression test frequently result in grip slippage or specimen barrelling, respectively, while using ASTM D945 (ASTM D945-16, 2016) for shear testing is hindered by non-uniform stress distributions and thickness sensitivity.

The accurate characterisation of biological tissue geometry - specifically thickness - remains a fundamental challenge in soft material mechanics (Famaey et al., 2026; O'Leary et al., 2013b; Schwarz et al., 2023). Precise geometric data is essential for converting raw force-displacement measurements into constitutive material properties; even minor inaccuracies in thickness measurement can lead to tensile stress calculation errors exceeding 25% (O'Leary et al., 2013b). The inherent nature of soft tissues, which are highly compliant, hydrated, and often spatially heterogeneous, complicates traditional measurement. Conventional contact tools like vernier callipers or micrometres frequently induce localised compression, which can lead to significant variations in obtained stresses. To mitigate this, non-contact techniques such as OCT, laser profilometry, and ultrasound-based measurements have gained prominence for providing non-destructive 3D mapping (O'Leary et al., 2013b; Lin et al., 2023).

Graphical representations, such as stress-strain or force-indentation curves, play a critical role in interpreting the mechanical response of

Table 2
Mechanical properties of various soft materials measured using different identification techniques.

Material	Parameters	Techniques	Identified Values	Comparison
Gelatine (7%) phantom (Amador et al., 2011)	Shear modulus, G	Macro-indentation Ultrasound elastography (SDUV)	$G_A = 1.16$ kPa $G_B = 1.61$ kPa	$G_B \cong 1.4 \cdot G_A$
Gelatine (20%) phantom (Czerner et al., 2015)	Young's modulus, G	Compression test Rheometry (oscillatory) Nano-indentation Macro-indentation	$E_A = 43$ kPa $E_B = 39$ kPa $E_C = 42$ kPa $E_D = 67$ kPa	$E_B \cong 0.9 \cdot E_A$ $E_C \cong E_A$ $E_D \cong 1.6 \cdot E_A$
Polyacrylamide (30:0.5d) gel (Buffinton et al., 2015)	Young's modulus, E	Nano-indentation Compression test Pipette aspiration	$E_A = 11.9 \pm 0.2$ kPa $E_B = 15.9 \pm 1.0$ kPa $E_C = 24.2 \pm 6.9$ kPa	$E_B \cong 1.3 \cdot E_A$ $E_C \cong 2 \cdot E_A$
Porcine sclera tissue (Nayar et al., 2012)	Storage & loss Young's moduli, E' & E''	Compression test Nano-indentation	$E'_A = 405.4 \pm 205.0$ kPa $E''_A = 280.4 \pm 172.4$ kPa $E'_B = 53.4 \pm 39.1$ kPa $E''_B = 6.1 \pm 1.9$ kPa	$E'_B \cong \frac{1}{8} E'_A$ $E''_B \cong \frac{1}{50} E''_A$
Human liver tissue (Zhao et al., 2014)	Shear modulus, G	Magnetic resonance elastography Ultrasound elastography (shear wave)	$G_A = 1.5 - 11.3$ kPa $G_B = 1.2 - 26.1$ kPa	$G_B \cong 2 \cdot G_A$
Porcine (lobe II) liver (Żmudzińska et al., 2018)	Young's modulus, E	Ultrasound elastography (shear wave) Macro-indentation	$E_A = 14.9 \pm 2.7$ kPa $E_B = 17.0 \pm 12.1$ kPa (for $\varepsilon = 2.5 - 7.5\%$) $E_B = 23.6 \pm 18.4$ kPa (for $\varepsilon = 5 - 10\%$)	$E_B \cong 1.1 \cdot E_A$ ($\varepsilon = 2.5 - 7.5\%$) $E_B \cong 1.6 \cdot E_A$ ($\varepsilon = 5 - 10\%$)
Porcine lung (Polio et al., 2018)	Young's modulus, E	Micro-indentation Rheometry (oscillatory) Tensile testing Cavitation rheometry	$E_A = 1.4 \pm 0.4$ kPa $E_B = 3.3 \pm 0.5$ kPa $E_C = 3.4 \pm 0.4$ kPa $E_D = 6.1 \pm 1.6$ kPa	$E_B \cong 2.4 \cdot E_A$ $E_C \cong 2.4 \cdot E_A$ $E_D \cong 4.4 \cdot E_A$
Human cells (Wu et al., 2018)	Young's modulus, E	Atomic force microscopy Rheometry (oscillatory) Magnetic twisting cytometry	$E_A = 13.5 \pm 7.0$ kPa $E_B = 0.95 \pm 0.15$ kPa $E_C = 1.62 \pm 0.11$ kPa	$E_B \cong \frac{1}{15} E_A$ $E_C \cong \frac{1}{8} E_A$
Agarose (2%) hydrogel (Symons et al., 2022)	Young's modulus, E	Micro-indentation Compression test	$E_A = 27 \pm 3$ kPa $E_B = 40 \pm 5$ kPa	$E_B \cong 1.5 \cdot E_A$
Gelatine (12%) phantom (Yengul et al., 2019)	Storage & loss shear moduli, G' & G''	Ultrasound elastography (shear wave) Rheometer (torsional vibration)	$G'_A \cong 2.8 \pm 0.1$ kPa $G''_A \cong 0.6 \pm 0.1$ kPa $G'_B \cong 2.6 \pm 0.3$ kPa $G''_B \cong 1.0 \pm 0.3$ kPa	$G'_B \cong 0.9 \cdot G'_A$ $G''_B \cong 1.7 \cdot G''_A$
Oil-in-gelatine (40%) phantom (Zhu et al., 2015)	Shear modulus & viscosity, G & η	Rheometry (rotary) Ultrasound elastography (SDUV) Ultrasound elastography (ARFI – shear wave)	$G_A = 1.06 \pm 0.18$ kPa $\eta_A = 4.90 \pm 0.20$ Pa $\cdot s$ $G_B = 1.31 \pm 0.09$ kPa $\eta_B = 2.89 \pm 0.14$ Pa $\cdot s$ $G_C = 5.90 \pm 0.36$ kPa	$G_B \cong 1.2 \cdot G_A$ $\eta_B \cong 0.6 \cdot \eta_A$ $G_C \cong 5.6 \cdot G_A$
Poly(vinyl alcohol) hydrogel ($\varphi_0 = 0.075$; $N_j = 20$) (Richbourg et al., 2022)	Shear modulus, G	Tensile test Compression test Rheometry Macro-indentation Nano-indentation	$G_A \cong 65$ kPa $G_B \cong 60$ kPa $G_C \cong 45$ kPa $G_D \cong 70$ kPa $G_E \cong 105$ kPa	$G_B \cong 0.9 \cdot G_A$ $G_C \cong 0.7 \cdot G_A$ $G_D \cong 1.1 \cdot G_A$ $G_E \cong 1.6 \cdot G_A$

materials. The loading curve is often used to extract the elastic modulus for purely elastic contact (e.g., using Hertzian theory (Pogoda et al., 2012)), while the upper part of the unloading curve is used in the Oliver-Pharr method for elastic-plastic contacts (Oliver and Pharr, 1992; Andriotis et al., 2023). Nonlinear regions can additionally be analysed using energy-based or polynomial fitting approaches (Kontomaris et al., 2021; Ding et al., 2018). Shear and loss moduli are commonly determined from oscillatory or dynamic measurements, where the amplitude and phase shift of the response provide information on the material's elastic and viscous behaviour (Koruk and Rajagopal, 2024). These methods allow a comprehensive characterisation of material properties, even when the experimental response is nonlinear, highlighting the importance of graphical data in both understanding and comparing mechanical behaviour. Graphical representations have been shown to be important in determining the viscoelastic properties of materials by measuring the area differences between the loading and unloading curves in a nanoindentation experiment (Ciasca et al., 2016).

Characterising the mechanical properties of soft materials is highly sensitive to the specific strain state and loading regime employed during analysis. While uniaxial testing is the conventional method for evaluating longitudinal stiffness, it often fails to capture the anisotropic complexities revealed by biaxial loading, which more accurately mimics the multi-axial stress states found in physiological tissues (Cooney et al., 2015; Takada et al., 2023). Furthermore, the distinction between quasi-static and dynamic testing is vital, as the inherent frequency-dependent viscoelasticity of soft materials means that equilibrium responses can differ substantially from those measured under physiological loading rates (Wang and Liu, 2014; Boyer et al., 2009). Consequently, selecting a technique requires aligning the experimental strain state and rate with the intended application to ensure the resulting data is both representative and predictive.

Mechanical characterisation techniques for soft tissues and phantoms rely on models that often assume pure elasticity, linearity, isotropy, homogeneity, and near-incompressibility to convert raw data - such as force-displacement or shear wave speed - into material properties (Mulk et al., 2023; Fung, 1993). However, when these assumptions are violated, results represent “apparent properties” rather than true material properties, leading to significant inaccuracies. For instance, assuming pure elasticity in viscoelastic tissues causes static tests to overestimate stiffness and creates frequency-dependent discrepancies due to phase lag (Ormachea and Parker, 2020), while applying linear models to large deformations fails to account for physiological

"strain-stiffening" common in biological tissues (Wang et al., 2023b). Furthermore, assuming isotropy in fibrous tissues like muscle or tendon ignores the directional dependence of mechanical response (Pirri et al., 2025; Guertler et al., 2020), and neglecting heterogeneity or compressibility can result in "averaging" errors and incorrect Young's Moduli calculations (Saccomandi et al., 2022). These discrepancies are particularly critical in clinical applications like ultrasound elastography, where shear wave speeds may vary with probe orientation or excitation frequency, potentially leading to diagnostic errors (Gennisson et al., 2013; Kimondo et al., 2025; Qiu et al., 2026).

The relative expense and operational effort of soft tissue characterisation are primarily dictated by instrumentation complexity and the rigor of specimen preparation. Laboratory techniques such as indentation, tensile, and compression testing are generally the most cost-effective and accessible, yet they demand significant manual effort for precise specimen dissection, standardised gripping, and extensive preconditioning cycles required to ensure data repeatability (Griffin et al., 2016). In contrast, AFM and rheometry involve higher costs and intensive operational labour due to specialised nanoscale calibration requirements and complex analytical post-processing to fit data to mechanical models (Galluzzi et al., 2018). Clinically, ultrasound elastography provides a low-cost, portable, and real-time solution with minimal operational overhead, often serving as a frontline diagnostic tool (Gennisson et al., 2013). Conversely, MRE remains the most expensive and effort-intensive modality, restricted by the high overhead of MRI facilities and the technical coordination of external mechanical vibration drivers (Ehman, 2022).

The key procedures and guidelines for various techniques used to characterise the mechanical properties of soft tissues and phantoms are outlined in Table 3. The contribution of specific parameters to the overall error or uncertainty of the identified properties is variable and context-dependent, relying on factors such as the sample's inherent stiffness and the applied loading conditions, such as the rate in rheometry or the force/depth in indentation. For instance, the precise contact point position in indentation testing can introduce a huge effect at low indentation depths ($\delta/R \ll 0.1$), where initial data points disproportionately influence fitting results, while at higher indentation depths ($\delta/R > 0.1$), the assumptions inherent in the contact model itself may produce a larger source of error (Lin et al., 2009). Therefore, a complete analysis absolutely requires pinpointing these diverse sources of uncertainty and conducting a thorough uncertainty analysis (Famaey et al., 2026), systematically adhering to established international guidelines like the Guide to the Expression of Uncertainty in Measurement (ISO/IEC Guide 98-1, 2024). This rigorous process mandates considering two distinct types of uncertainty for each identified source: type An uncertainty, which is derived directly from the statistical analysis of repeated observations and experimental data, and type B uncertainty, which is determined using prior external information such as manufacturer specifications, available calibration data, or established reference handbooks (Alvarenga et al., 2026). The overall, combined uncertainty of the identified material properties must then be meticulously determined by consolidating all these sources, for example, by utilising the well-established propagation of uncertainty method (ISO/IEC Guide 98-1, 2024). Consequently, researchers are strongly encouraged to systematically determine and report these corresponding uncertainties alongside the calculated mean mechanical properties, which ultimately helps clinicians and other researchers to more accurately explore potential outcomes, their inherent variability, and their associated likelihoods within practical applications.

Recognising that measurement systems possess unique characteristics, any proposed framework must serve as a contextual guide for establishing uncertainty, particularly when dealing with "black box" experimental or clinical systems. To ensure reliability in real-world scenarios, a structured validation approach is recommended, encompassing inter-laboratory comparisons with standardised materials to assess reproducibility, cross-platform evaluations using phantoms to

Table 3
Key procedures and guidelines for various techniques to characterise the mechanical properties of soft tissues and phantoms.

Technique	Key Procedures	Guidelines
Tensile testing	- Prepare dog-bone or dumbbell-shaped specimens to ensure failure in the narrow centre, not at the grips. - Mount the sample in the testing machine with appropriate grips to avoid cutting or slippage (e.g., using specialised soft-material fixtures or encasing ends). - Apply a controlled, continuous tensile (pulling) force at a constant speed, stretching the specimen until it breaks or desired deformation is reached. - Measure the applied force and the corresponding change in length (elongation) continuously, often using an extensometer.	- Obtain a precise measurement of the sample's cross-sectional area. - Ensure proper alignment of the specimen in the machine to avoid bending stresses. - Maintain consistent environmental conditions (temperature, humidity), as they can affect material properties. - Use extensometers (contact or noncontact) for accurate strain measurement, isolated from machine. - Use consistent strain rates across comparative samples, as soft materials are often strain-rate sensitive.
Compression testing	- Prepare short, squat cylindrical or cubical samples to prevent buckling. - Place the specimen between parallel plates (platens) of the machine. - Ensure the platens are parallel and aligned correctly to avoid eccentric loading. - Apply a compressive load to the specimen at a constant, uniform rate of speed. - Continuously measure and record the applied force and the corresponding displacement (deformation) data.	- Measure the cross-sectional area of the sample precisely. - Ensure platens are flat and parallel to within strict tolerances to ensure uniform load transfer and prevent bending. - Use lubrication on contact surfaces to minimise friction and prevent barrelling of the sample. - Environmental stability is paramount; maintain consistent temperature and humidity levels to preserve material integrity. - Use a non-contact extensometer or a deflectometer for more accurate strain measurements, free from machine compliance errors.
Indentation	- Place sample on a flat, rigid substrate. - Lower an indenter of a defined geometry (e.g., sphere, cone, pyramid) onto the sample surface. - Perform the test using a depth-control mode, which is more reliable for very compliant materials than force control. - Measure the load (force) required for a specific indentation depth.	- Choose appropriate indenter size and shape for the sample's heterogeneity and desired length scale (macro, micro, nano). - Ensure a flat, even sample surface for accurate results. - Control the indentation depth to remain within the limits of the chosen model and minimise substrate effects if testing thin samples. - Determine the contact point accurately in the force curves. - Select the correct contact mechanics model based on the material's properties (adhesion, elasticity).
Atomic force microscopy	- Select an appropriate AFM mode (e.g., force spectroscopy, nanomechanical imaging) and a cantilever with a stiffness that broadly	- Ensure the sample surface is clean and relatively free of contaminants. - Use blunt or colloidal probes for more reproducible results and to

(*continued on next page*)

Table 3 (*continued*)

Technique	Key Procedures	Guidelines
	matches the sample's stiffness. - Calibrate the cantilever spring constant and tip radius/geometry carefully. - Perform indentation/force mapping, collecting multiple force curves across the sample surface.	prevent sample damage, though this sacrifices spatial resolution. - Determine the contact point accurately in the force curves, especially in liquid environments where noise/adhesion can be a problem. - Analyse force-indentation curves with appropriate contact mechanics models to produce spatially resolved mechanical property maps.
Rheometry	- Carefully place the material into the gap between the rheometer's measuring plates. - Lower the upper plate to a preset height and remove any excess sample from the edges. - Apply a controlled force (stress) or deformation (strain/shear rate) to the sample using either rotational or oscillatory modes. - Measure the material's response (deformation or force).	- Ensure proper sample loading to avoid air bubbles or sample drying during the test. - Ensure the sample is adequately loaded between the plates to prevent slippage during the test. - Conduct preliminary tests, for example, to ensure measurements are within the linear viscoelastic range. - Control temperature precisely, as the viscosity and mechanical properties of soft materials are highly temperature dependent.
Ultrasound elastography	- Apply a clear, water-based gel to the skin over the target organ or surface of the sample. - Apply a mechanical force to the tissue (external compression or acoustic radiation force pulse). - Use ultrasound to track the resulting tissue displacement or shear wave propagation. - Map the deformation or wave speed across a region of interest.	- Use standardised protocols (e.g., specific to liver, breast, etc.) for reliable results. - Ensure good probe contact and consistent pressure application. - Acknowledge that simple models may be insufficient for complex, non-linear, or anisotropic tissues, which can affect reproducibility. - Account for wave attenuation and scattering properties of the specific soft material for accurate data interpretation.
Magnetic resonance elastography	- Place the subject/phantom in the MRI scanner with a device for applying mechanical waves. - Apply controlled mechanical waves into the subject. - Acquire MR images that are sensitive to the resulting tissue motion or displacement (wave fields). - Process the wave field data using specialised software to generate quantitative stiffness maps.	- Adhere to standardised MRE terminology and guidelines to ensure comparability of results - Ensure proper mechanical wave generation and coupling to the sample within the MRE apparatus. - Apply a precise, consistent mechanical vibration frequency to induce measurable shear waves in the tissue. - Ensure motion synchronisation between the driver and MRI sequence. - Utilise appropriate models and inversion algorithms to convert displacement data into quantitative mechanical property maps.

identify systematic differences, and prospective studies on representative cohorts to validate practical performance. In addition, discrepancies should be minimised through regular instrument calibration, multimodal measurement strategies, and strict environmental controls, while potential biases can be quantified by benchmarking results against independent mechanical testing and diverse estimation techniques.

4. Conclusion

In contrast to conventional stiff engineering materials, soft materials (e.g., gels and tissues) are fragile, require low force levels for deformation, exhibit both elastic and viscous behaviour, and their mechanical properties are influenced by multiple factors such as loading rate, frequency, and temperature. As a result, identifying their mechanical properties poses significant challenges. Common laboratory techniques include tensile testing, compression testing, indentation, atomic force microscopy and rheometry, while clinical methods comprise ultrasound elastography and magnetic resonance elastography. Each technique involves specific limitations and drawbacks. Considerable variability can arise in the identified mechanical properties of soft materials when different techniques are used, or when the same technique is applied across different laboratories. Although it may not be feasible to eliminate all sources of error and uncertainty, reducing the influence of those identified in this study is essential in improving the accuracy and reliability of mechanical properties characterisation. Systematically determined and reported uncertainties should accompany mean mechanical properties to help clinicians and researchers accurately assess outcomes, variability, and likelihoods in practical applications. This comprehensive review highlights the need to develop more reliable test rigs and procedures for accurately determining the mechanical properties of soft materials across nano-, micro- and macro-scales. The findings presented in this paper are intended to serve as a valuable resource for researchers working to characterise these properties using a range of techniques.

CRediT authorship contribution statement

Hasan Koruk: Writing – review & editing, Writing – original draft, Supervision, Project administration, Methodology, Investigation, Funding acquisition, Formal analysis, Conceptualization. **Srinath Rajagopal:** Writing – review & editing, Investigation, Funding acquisition. **Raphaela de Melo Baesso:** Writing – review & editing, Investigation. **Andre Victor Alvarenga:** Writing – review & editing, Investigation. **Stylianos Vasileios Kontomaris:** Writing – review & editing, Writing – original draft, Investigation.

Declaration of competing interest

The authors declare that they have no known competing financial interests or personal relationships that could have appeared to influence the work reported in this paper.

Acknowledgments

This study was supported by the UK Department for Science, Innovation & Technology through the funding of the National Measurement System.

Data availability

No data was used for the research described in the article.

References

A-Hassan, E., Heinz, W.F., Antonik, M.D., D'Costa, N.P., Nageswaran, S., Schoenenberger, C.-A., Hoh, J.H., 1998. Relative microelastic mapping of living cells by atomic force microscopy. Biophys. J. 74, 1564–1578. https://doi.org/10.1016/S0006-3495(98)77868-3.

Abbasi, M., Karami Mohammadi, A., 2010. A new model for investigating the flexural vibration of an atomic force microscope cantilever. Ultramicroscopy 110, 1374–1379. https://doi.org/10.1016/j.ultramic.2010.07.005.
Ahearne, M., Liu, I.K.-K., 2008. Mechanical characterisation of hydrogels for tissue engineering applications. Topics Tissue Eng. 4.
Ahsanizadeh, S., Li, L., 2015. Visco-hyperelastic constitutive modeling of soft tissues based on short and long-term internal variables. Biomed. Eng. Online 14, 29. https://doi.org/10.1186/s12938-015-0023-7.
Akhtar, R., Sherratt, M.J., Cruickshank, J.K., Derby, B., 2011. Characterizing the elastic properties of tissues. Mater. Today 14, 96–105. https://doi.org/10.1016/S1369-7021(11)70059-1.
Akkaya, H.E., Erden, A., Kuru Öz, D., Ünal, S., Erden, İ., 2018. Magnetic resonance elastography: basic principles, technique, and clinical applications in the liver. Diagn. Interv. Radiol. 24, 328–335. https://doi.org/10.5152/dir.2018.18186.
Albano, D., Basile, M., Gitto, S., Messina, C., Longo, S., Fusco, S., Snoj, Z., Gianola, S., Bargeri, S., Castellini, G., Sconfienza, L.M., 2023. Shear-wave elastography for the evaluation of tendinopathies: a systematic review and meta-analysis, radiol. Med. 129, 107–117. https://doi.org/10.1007/s11547-023-01732-4.
Alberini, R., Spagnoli, A., Sadeghinia, M.J., Skallerud, B., Terzano, M., Holzapfel, G.A., 2024. Second harmonic generation microscopy, biaxial mechanical tests and fiber dispersion models in human skin biomechanics. Acta Biomater. 185, 266–280. https://doi.org/10.1016/j.actbio.2024.07.026.
Alekya, B., Rao, S., Pandya, H.J., 2019. Engineering approaches for characterizing soft tissue mechanical properties: a review. Clin. BioMech. 69, 127–140. https://doi.org/10.1016/j.clinbiomech.2019.07.016.
Alvarenga, A.V., Ramnarine, K.V., Koruk, H., Rajagopal, S., 2026. Assessment of the uncertainty of shear wave speed measurements in ultrasound elastography. Ultrasonics 160, 107891. https://doi.org/10.1016/j.ultras.2025.107891.
Amador, C., Urban, M.W., Chen, S., Chen, Q., An, K.-N., Greenleaf, J.F., 2011. Shear elastic modulus estimation from indentation and SDUV on gelatin phantoms. IEEE Trans. Biomed. Eng. 58, 1706–1714. https://doi.org/10.1109/TBME.2011.2111419.
Amador, C., Otilio, B.L., Kinnick, R.R., Urban, M.W., 2016. Ultrasonic method to characterize shear wave propagation in micellar fluids. J. Acoust. Soc. Am. 140, 1719–1726. https://doi.org/10.1121/1.4962531.
Andriotis, O.G., Nalbach, M., Thurner, P.J., 2023. Mechanics of isolated individual collagen fibrils. Acta Biomater. 163, 35–49. https://doi.org/10.1016/j.actbio.2022.12.008.
Antonovaite, N., Beekmans, S.V., Hol, E.M., Wadman, W.J., Iannuzzi, D., 2018. Regional variations in stiffness in live mouse brain tissue determined by depth-controlled indentation mapping. Sci. Rep. 8, 12517. https://doi.org/10.1038/s41598-018-31035-y.
Aoki, T., Ohashi, T., Matsumoto, T., Sato, M., 1997. The pipette aspiration applied to the local stiffness measurement of soft tissues. Ann. Biomed. Eng. 25, 581–587. https://doi.org/10.1007/BF02684197.
Argatov, I., Mishuris, G., 2018. Indentation Testing of Biological Materials. Springer, Cham. https://doi.org/10.1007/978-3-319-78533-2.
Ashkenazi, A., Shultz, A., Jordan, L., Solav, D., 2026. Indentation-based anisotropic material parameter identifiability: validation on a synthetic soft tissue phantom. J. Mech. Phys. Solid. 208, 106417. https://doi.org/10.1016/j.jmps.2025.106417.
ASTM D412-16, 2021. Standard Test Methods for Vulcanized Rubber and Thermoplastic Elastomers - Tension.
ASTM D575-91, 2024. Standard Test Methods for Rubber Properties in Compression.
ASTM D945-16, 2016. Standard Test Methods for Rubber Properties in Compression or Shear (Mechanical Oscillograph).
Ayyalasomayajula, V., Skallerud, B., 2022. Microstructure and mechanics of the bovine trachea: layer specific investigations through SHG imaging and biaxial testing. J. Mech. Behav. Biomed. Mater. 134, 105371. https://doi.org/10.1016/j.jmbbm.2022.105371.
Ayyalasomayajula, V., Ervik, Ø., Sorger, H., Skallerud, B., 2024. Macro-indentation testing of soft biological materials and assessment of hyper-elastic material models from inverse finite element analysis. J. Mech. Behav. Biomed. Mater. 151, 106389. https://doi.org/10.1016/j.jmbbm.2024.106389.
Ayyildiz, M., Cinoglu, S., Basdogan, C., 2015. Effect of normal compression on the shear modulus of soft tissue in rheological measurements. J. Mech. Behav. Biomed. Mater. 49, 235–243. https://doi.org/10.1016/j.jmbbm.2015.05.011.
Baldwin, SamuelJ., Sampson, J., Peacock, ChristopherJ., Martin, M.L., Veres, S.P., Lee, J. Michael, Kreplak, L., 2020. A new longitudinal variation in the structure of collagen fibrils and its relationship to locations of mechanical damage susceptibility. J. Mech. Behav. Biomed. Mater. 110, 103849. https://doi.org/10.1016/j.jmbbm.2020.103849.
Bamber, J., Cosgrove, D., Dietrich, C., Fromageau, J., Bojunga, J., Calliada, F., Cantisani, V., Correas, J.-M., D'Onofrio, M., Drakonaki, E., Fink, M., Friedrich-Rust, M., Gilja, O., Havre, R., Jenssen, C., Klauser, A., Ohlinger, R., Saftoiu, A., Schaefer, F., Sporea, I., Piscaglia, F., 2013. EFSUMB guidelines and recommendations on the clinical use of ultrasound elastography. Part 1: Basic Principle Tech. Ultraschall in Der Medizin - European J. Ultrasound. 34, 169–184. https://doi.org/10.1055/s-0033-1335205.
Barr, R.G., Nakashima, K., Amy, D., Cosgrove, D., Farrokh, A., Schafer, F., Bamber, J.C., Castera, L., Choi, B.I., Chou, Y.-H., Dietrich, C.F., Ding, H., Ferraioli, G., Filice, C., Friedrich-Rust, M., Hall, T.J., Nightingale, K.R., Palmeri, M.L., Shiina, T., Suzuki, S., Sporea, I., Wilson, S., Kudo, M., 2015. WFUMB guidelines and recommendations for clinical use of ultrasound elastography: part 2: breast. Ultrasound Med. Biol. 41, 1148–1160. https://doi.org/10.1016/j.ultrasmedbio.2015.03.008.
Barr, R.G., Cosgrove, D., Brock, M., Cantisani, V., Correas, J.M., Postema, A.W., Salomon, G., Tsutsumi, M., Xu, H.-X., Dietrich, C.F., 2017. WFUMB guidelines and recommendations on the clinical use of ultrasound elastography: part 5. Prostate. Ultrasound Med. Biol. 43, 27–48. https://doi.org/10.1016/j.ultrasmedbio.2016.06.020.
Bercoff, J., Tanter, M., Fink, M., 2004. Supersonic shear imaging: a new technique for soft tissue elasticity mapping. IEEE Trans. Ultrason. Ferroelectrics Freq. Control 51, 396–409. https://doi.org/10.1109/TUFFC.2004.1295425.
Bernal, M., Nenadic, I., Urban, M.W., Greenleaf, J.F., 2011. Material property estimation for tubes and arteries using ultrasound radiation force and analysis of propagating modes. J. Acoust. Soc. Am. 129, 1344–1354. https://doi.org/10.1121/1.3533735.
Bertalan, G., Becker, J., Tzschätzsch, H., Morr, A., Herthum, H., Shahryari, M., Greenhalgh, R.D., Guo, J., Schröder, L., Alzheimer, C., Budday, S., Franze, K., Braun, J., Sack, I., 2023. Mechanical behavior of the hippocampus and corpus callosum: an attempt to reconcile ex vivo with in vivo and micro with macro properties. J. Mech. Behav. Biomed. Mater. 138, 105613. https://doi.org/10.1016/j.jmbbm.2022.105613.
Bezer, J.H., Koruk, H., Rowlands, C.J., Choi, J.J., 2020. Elastic deformation of soft tissue-mimicking materials using a single microbubble and acoustic radiation force. Ultrasound Med. Biol. 46, 3327–3338. https://doi.org/10.1016/j.ultrasmedbio.2020.08.012.
Bircher, K., Zündel, M., Pensalfini, M., Ehret, A.E., Mazza, E., 2019. Tear resistance of soft collagenous tissues. Nat. Commun. 10, 792. https://doi.org/10.1038/s41467-019-08723-y.
Bisht, S.R., Marri, B.P., Karmakar, J., Mercado Shekhar, K.P., 2024. Viscoelastic characterization of phantoms for ultrasound elastography created using Low- and high-viscosity poly(vinyl alcohol) with ethylene glycol as the cryoprotectant. ACS Omega. https://doi.org/10.1021/acsomega.3c09224.
Bloksgaard, M., Leurgans, T.M., Spronck, B., Heusinkveld, M.H.G., Thorsted, B., Rosenstand, K., Nissen, I., Hansen, U.M., Brewer, J.R., Bagatolli, L.A., Rasmussen, L. M., Irmukhamedov, A., Reesink, K.D., De Mey, J.G.R., 2017. Imaging and modeling of acute pressure-induced changes of collagen and elastin microarchitectures in pig and human resistance arteries. Am. J. Physiol. Heart Circ. Physiol. 313, H164–H178. https://doi.org/10.1152/ajpheart.00110.2017.
Bonet, J., 2001. Large strain viscoelastic constitutive models. Int. J. Solid Struct. 38, 2953–2968. https://doi.org/10.1016/S0020-7683(00)00215-8.
Boyer, G., Laquièze, L., Le Bot, A., Laquièze, S., Zahouani, H., 2009. Dynamic indentation on human skin in vivo: ageing effects. Skin Res. Technol. 15, 55–67. https://doi.org/10.1111/j.1600-0846.2008.00324.x.
Briscoe, B.J., Sebastian, K.S., Adams, M.J., 1994. The effect of indenter geometry on the elastic response to indentation. J. Phys. D Appl. Phys. 27, 1156–1162. https://doi.org/10.1088/0022-3727/27/6/013.
Buffinton, C.M., Tong, K.J., Blaho, R.A., Buffinton, E.M., Ebenstein, D.M., 2015. Comparison of mechanical testing methods for biomaterials: pipette aspiration, nanoindentation, and macroscale testing. J. Mech. Behav. Biomed. Mater. 51, 367–379. https://doi.org/10.1016/j.jmbbm.2015.07.022.
Cao, Y., Ji, X., Feng, X., 2011. On determination of the damping factor of linear viscoelastic materials using dynamic indentation: a theoretical study. Sci. China Phys. Mech. Astron. 54, 598–605. https://doi.org/10.1007/s11433-011-4279-z.
Carlsson, L.A., Adams, D.F., Pipes, R.B., 2014. Test specimen preparation, strain and deformation measurement devices, and testing machines. In: Experimental Characterization of Advanced Composite Materials, fourth ed. Taylor & Francis, pp. 73–86.
Cartagena-Rivera, A.X., Logue, J.S., Waterman, C.M., Chadwick, R.S., 2016. Actomyosin cortical mechanical properties in nonadherent cells determined by atomic force microscopy. Biophys. J. 110, 2528–2539. https://doi.org/10.1016/j.bpj.2016.04.034.
Carton, F., Rizzi, M., Canciani, E., Sieve, G., Di Francesco, D., Casarella, S., Di Nunno, L., Boccafoschi, F., 2024. Use of hydrogels in regenerative medicine: focus on mechanical properties. Int. J. Mol. Sci. 25, 11426. https://doi.org/10.3390/ijms252111426.
Cè, M., Felisaz, P.F., Alì, M., Re Sartò, G.V., Cellina, M., 2023. Ultrasound elastography in chronic kidney disease: a systematic review and meta-analysis. J. Med. Ultrason. 50, 381–415. https://doi.org/10.1007/s10396-023-01304-z.
Cebrecos, A., Jiménez, N., Tarazona, R., Company, M., Benlloch, J.M., Camarena, F., 2021. Characterization of viscoelastic media combining ultrasound and magnetic-force induced vibrations on an embedded soft magnetic sphere. IEEE Trans. Ultrason. Ferroelectrics Freq. Control 68, 3540–3548. https://doi.org/10.1109/TUFFC.2021.3097883.
Chandran, P.L., Dimitriadis, E.K., Mertz, E.L., Horkay, F., 2018. Microscale mapping of extracellular matrix elasticity of mouse joint cartilage: an approach to extracting bulk elasticity of soft matter with surface roughness. Soft Matter 14, 2879–2892. https://doi.org/10.1039/C7SM02045G.
Chang, D., Hirate, T., Uehara, C., Maruyama, H., Uozumi, N., Arai, F., 2021. Evaluating young's modulus of single yeast cells based on compression using an atomic force microscope with a flat tip. Microsc. Microanal. 27, 392–399. https://doi.org/10.1017/S1431927620024903.
Chavan, R., Kamble, N., Kuthe, C., Sarnobat, S., 2024. On mechanical behavior and characterization of soft tissues. Biomed. Eng. Comput. Biol. 15. https://doi.org/10.1177/11795972241294115.
Chen, S., Urban, M.W., Pislaru, C., Kinnick, R., Zheng, Y., Yao, A., Greenleaf, J.F., 2009. Shearwave dispersion ultrasound vibrometry (SDUV) for measuring tissue elasticity and viscosity. IEEE Trans. Ultrason. Ferroelectrics Freq. Control 56, 55–62. https://doi.org/10.1109/TUFFC.2009.1005.
Chen, D.T.N., Wen, Q., Janmey, P.A., Crocker, J.C., Yodh, A.G., 2010. Rheology of soft materials. Annu. Rev. Condens. Matter Phys. 1, 301–322. https://doi.org/10.1146/annurev-conmatphys-070909-104120.

Chen, H., Zhao, X., Lu, X., Kassab, G., 2013. Non-linear micromechanics of soft tissues. Int. J. Non Lin. Mech. 56, 79–85. https://doi.org/10.1016/j.ijnonlinmec.2013.03.002.

Chen, M.L., Ruberti, J.W., Nguyen, T.D., 2018. Increased stiffness of collagen fibrils following cyclic tensile loading. J. Mech. Behav. Biomed. Mater. 82, 345–354. https://doi.org/10.1016/j.jmbbm.2018.03.027.

Chen, Y., Qiu, S., He, Z., Yan, F., Li, R., Feng, Y., 2021. Comparative analysis of indentation and magnetic resonance elastography for measuring viscoelastic properties. Acta Mech. Sin. 37, 527–536. https://doi.org/10.1007/s10409-020-01042-2.

Cho, A.Y., Lee, H.J., 2023. Investigating the impact of mechanical properties and cell-collagen interaction on NIH3T3 function: a comparative study on different substrates and culture environments. Gels 9, 922. https://doi.org/10.3390/gels9120922.

Cho, D.H., Aguayo, S., Cartagena-Rivera, A.X., 2023. Atomic force microscopy-mediated mechanobiological profiling of complex human tissues. Biomaterials 303, 122389. https://doi.org/10.1016/j.biomaterials.2023.122389.

Chow, M.-J., Zhang, Y., 2011. Changes in the mechanical and biochemical properties of aortic tissue due to cold storage. J. Surg. Res. 171, 434–442. https://doi.org/10.1016/j.jss.2010.04.007.

Ciasca, G., Sassun, T.E., Minelli, E., Antonelli, M., Papi, M., Santoro, A., Giangaspero, F., Delfini, R., De Spirito, M., 2016. Nano-mechanical signature of brain tumours. Nanoscale 8, 19629–19643. https://doi.org/10.1039/C6NR06840E.

Cloyd, J.M., Malhotra, N.R., Weng, L., Chen, W., Mauck, R.L., Elliott, D.M., 2007. Material properties in unconfined compression of human nucleus pulposus, injectable hyaluronic acid-based hydrogels and tissue engineering scaffolds. Eur. Spine J. 16, 1892–1898. https://doi.org/10.1007/s00586-007-0443-6.

Cohen, S.R., Kalfon-Cohen, E., 2013. Dynamic nanoindentation by instrumented nanoindentation and force microscopy: a comparative review. Beilstein J. Nanotechnol. 4, 815–833. https://doi.org/10.3762/bjnano.4.93.

Cooney, G.M., Moerman, K.M., Takaza, M., Winter, D.C., Simms, C.K., 2015. Uniaxial and biaxial mechanical properties of Porcine linea alba. J. Mech. Behav. Biomed. Mater. 41, 68–82. https://doi.org/10.1016/j.jmbbm.2014.09.026.

Cosgrove, D., Piscaglia, F., Bamber, J., Bojunga, J., Correas, J.-M., Gilja, O., Klauser, A., Sporea, I., Calliada, F., Cantisani, V., D'Onofrio, M., Drakonaki, E., Fink, M., Friedrich-Rust, M., Fromageau, J., Havre, R., Jenssen, C., Ohlinger, R., Săftoiu, A., Schaefer, F., Dietrich, C., 2013. EFSUMB guidelines and recommendations on the clinical use of ultrasound elastography. Part 2: Clin. Appl. Ultraschall iDer Medizin - European J. Ultrasound 34, 238–253. https://doi.org/10.1055/s-0033-1335375.

Crick, S.L., Yin, F.C.-P., 2007. Assessing micromechanical properties of cells with atomic force microscopy: importance of the contact point. Biomech. Model. Mechanobiol. 6, 199–210. https://doi.org/10.1007/s10237-006-0046-x.

Cui, J., Lee, C.H., Delbos, A., McManus, J.J., Crosby, A.J., 2011. Cavitation rheology of the eye lens. Soft Matter 7, 7827–7831. https://doi.org/10.1039/C1SM05340J.

Cui, X.-W., Li, K.-N., Yi, A.-J., Wang, B., Wei, Q., Wu, G.-G., Dietrich, C., 2022. Ultrasound elastography, endosc. Ultrasound 11, 252. https://doi.org/10.4103/EUS-D-21-00151.

Czerner, M., Fellay, L.S., Suárez, M.P., Frontini, P.M., Fasce, L.A., 2015. Determination of elastic modulus of gelatin gels by indentation experiments. Procedia Mater. Sci. 8, 287–296. https://doi.org/10.1016/j.mspro.2015.04.075.

Darling, E.M., 2011. Force scanning: a rapid, high-resolution approach for spatial mechanical property mapping. Nanotechnology 22, 175707. https://doi.org/10.1088/0957-4484/22/17/175707.

Delaine-Smith, R.M., Burney, S., Balkwill, F.R., Knight, M.M., 2016. Experimental validation of a flat punch indentation methodology calibrated against unconfined compression tests for determination of soft tissue biomechanics. J. Mech. Behav. Biomed. Mater. 60, 401–415. https://doi.org/10.1016/j.jmbbm.2016.02.019.

Denisin, A.K., Pruitt, B.L., 2016. Tuning the range of polyacrylamide gel stiffness for mechanobiology applications. ACS Appl. Mater. Interfaces 8, 21893–21902. https://doi.org/10.1021/acsami.5b09344.

DeWall, R.J., 2013. Ultrasound elastography: principles, techniques, and clinical applications. Crit. Rev. Biomed. Eng. 41, 1–19. https://doi.org/10.1615/CritRevBiomedEng.2013006991.

Dietrich, C., Barr, R., Farrokh, A., Dighe, M., Hocke, M., Jenssen, C., Dong, Y., Saftoiu, A., Havre, R., 2017. Strain elastography - how to Do it? Ultrasound Int. Open 3, E137–E149. https://doi.org/10.1055/s-0043-119412.

Dimitriadis, E.K., Horkay, F., Maresca, J., Kachar, B., Chadwick, R.S., 2002. Determination of elastic moduli of thin layers of soft material using the atomic force microscope. Biophys. J. 82, 2798–2810. https://doi.org/10.1016/S0006-3495(02)75620-8.

Ding, Y., Wang, J., Xu, G.-K., Wang, G.-F., 2018. Are elastic moduli of biological cells depth dependent or not? Another explanation using a contact mechanics model with surface tension. Soft Matter 14, 7534–7541. https://doi.org/10.1039/C8SM01216D.

Dufrêne, Y.F., Ando, T., Garcia, R., Alsteens, D., Martinez-Martin, D., Engel, A., Gerber, C., Müller, D.J., 2017. Imaging modes of atomic force microscopy for application in molecular and cell biology. Nat. Nanotechnol. 12, 295–307. https://doi.org/10.1038/nnano.2017.45.

Duprey, A., Khanafer, K., Schlicht, M., Avril, S., Williams, D., Berguer, R., 2010. In vitro characterisation of physiological and maximum elastic modulus of ascending thoracic aortic aneurysms using uniaxial tensile testing. Eur. J. Vasc. Endovasc. Surg. 39, 700–707. https://doi.org/10.1016/j.ejvs.2010.02.015.

Efremov, Y.M., Okajima, T., Raman, A., 2020. Measuring viscoelasticity of soft biological samples using atomic force microscopy. Soft Matter 16, 64–81. https://doi.org/10.1039/C9SM01020C.

Ehman, R.L., 2022. Magnetic resonance elastography: from invention to standard of care. Abdom. Radiol. 47, 3028–3036. https://doi.org/10.1007/s00261-022-03597-z.

Eid, J., Greige-Gerges, H., Monticelli, L., Jraij, A., 2021. Elastic moduli of lipid membranes: reproducibility of AFM measures. Chem. Phys. Lipids 234, 105011. https://doi.org/10.1016/j.chemphyslip.2020.105011.

Engstrom, T.A., Pogoda, K., Cruz, K., Janmey, P.A., Schwarz, J.M., 2019. Compression stiffening in biological tissues: on the possibility of classic elasticity origins. Phys. Rev. E 99, 52413. https://doi.org/10.1103/PhysRevE.99.052413.

Esteki, M.H., Alemrajabi, A.A., Hall, C.M., Sheridan, G.K., Azadi, M., Moeendarbary, E., 2020. A new framework for characterization of poroelastic materials using indentation. Acta Biomater. 102, 138–148. https://doi.org/10.1016/j.actbio.2019.11.010.

Ewoldt, R.H., Johnston, M.T., Caretta, L.M., 2015. Experimental challenges of shear rheology: how to avoid bad data. In: Spagnolie, S.E. (Ed.), Complex Fluids in Biological Systems: Experiment, Theory, and Computation. Springer New York, New York, NY, pp. 207–241. https://doi.org/10.1007/978-1-4939-2065-5_6.

Fagerholt, E., Børvik, T., Hopperstad, O.S., 2013. Measuring discontinuous displacement fields in cracked specimens using digital image correlation with mesh adaptation and crack-path optimization. Opt Laser. Eng. 51, 299–310. https://doi.org/10.1016/j.optlaseng.2012.09.010.

Famaey, N., Vander Sloten, J., 2008. Soft tissue modelling for applications in virtual surgery and surgical robotics. Comput. Methods Biomech. Biomed. Eng. 11, 351–366. https://doi.org/10.1080/10255840802020412.

Famaey, N., Fehervary, H., Lafon, Y., Akyildiz, A., Dreesen, S., Bruyère-Garnier, K., Allain, J.-M., Alloisio, M., Aparici-Gil, A., Catalano, C., Chassagne, F., Chokhandre, S., Crevits, K., Crielaard, H., Cunnane, E., Cunnane, C., De Leener, K., Desai, A., Driessen, R., Erdemir, A., Eskandari, M., Evans, S., Gasser, C., Gebhardt, M., Glasmacher, B., Holzapfel, G.A., Isasi, M., Jennings, L., Kurz, S., Leal-Marin, S., Lecomte, P., Morch, A., Mulvihill, J., Nemavhola, F., Pandelani, T., Pasta, S., Peña, E., Pierrat, B., Ploeg, H.-L., Polzer, S., Rausch, M., Schwarz, D., Screen, H., Sherifova, S., Sommer, G., Wang, S., Walsh, D., Yadav, D., Marchal, T., Geris, L., 2026. Community challenge towards consensus on characterization of biological tissue: c4Bio's first findings. J. Biomech. 194, 113021. https://doi.org/10.1016/j.jbiomech.2025.113021.

Farajpour, A., Ingman, W.V., 2024. Mathematical models for ultrasound elastography: recent advances to improve accuracy and clinical utility. Bioengineering 11, 991. https://doi.org/10.3390/bioengineering11100991.

Fehervary, H., Smoljkić, M., Vander Sloten, J., Famaey, N., 2016. Planar biaxial testing of soft biological tissue using rakes: a critical analysis of protocol and fitting process. J. Mech. Behav. Biomed. Mater. 61, 135–151. https://doi.org/10.1016/j.jmbbm.2016.01.011.

Ferraioli, G., Wong, V.W.-S., Castera, L., Berzigotti, A., Sporea, I., Dietrich, C.F., Choi, B. I., Wilson, S.R., Kudo, M., Barr, R.G., 2018. Liver ultrasound elastography: an update to the world Federation for ultrasound in medicine and biology guidelines and recommendations. Ultrasound Med. Biol. 44, 2419–2440. https://doi.org/10.1016/j.ultrasmedbio.2018.07.008.

Ferraioli, G., Barr, R.G., Berzigotti, A., Sporea, I., Wong, V.W., Reiberger, T., Karlas, T., Thiele, M., Cardoso, A.C., Ayonrinde, O.T., Castera, L., Dietrich, C.F., Iijima, H., Lee, D.H., Kemp, W., Oliveira, C.P., Sarin, S.K., 2024. WFUMB guideline/guidance on liver multiparametric ultrasound: part 1. Update to 2018 guidelines on liver ultrasound elastography. Ultrasound Med. Biol. 50, 1071–1087. https://doi.org/10.1016/j.ultrasmedbio.2024.03.013.

Fontenele, F.F., Bouklas, N., 2023. Understanding the inelastic response of collagen fibrils: a viscoelastic-plastic constitutive model. Acta Biomater. 163, 78–90. https://doi.org/10.1016/j.actbio.2022.07.011.

Fu, T., Uzoma, P.C., Ding, X., Wu, P., Penkov, O., Hu, H., 2024. A novel nano-spherical tip for improving precision in elastic modulus measurements of polymer materials via atomic force microscopy. Micromachines 15, 1175. https://doi.org/10.3390/mi15091175.

Fung, Y.-C., 1993. Biomechanics: Mechanical Properties of Living Tissues. Springer New York, New York, NY. https://doi.org/10.1007/978-1-4757-2257-4.

Gabriel, C., Kaschta, J., 1998. Comparison of different shear rheometers with regard to creep and creep recovery measurements, rheol. Acta 37, 358–364. https://doi.org/10.1007/s003970050122.

Galluzzi, M., Tang, G., Biswas, C.S., Zhao, J., Chen, S., Stadler, F.J., 2018. Atomic force microscopy methodology and AFMech suite software for nanomechanics on heterogeneous soft materials. Nat. Commun. 9, 3584. https://doi.org/10.1038/s41467-018-05902-1.

Garcia, P.D., Garcia, R., 2018. Determination of the elastic moduli of a single cell cultured on a rigid support by force microscopy. Biophys. J. 114, 2923–2932. https://doi.org/10.1016/j.bpj.2018.05.012.

Gasser, T.C., Ogden, R.W., Holzapfel, G.A., 2006. Hyperelastic modelling of arterial layers with distributed collagen fibre orientations. J. R. Soc. Interface 3, 15–35. https://doi.org/10.1098/rsif.2005.0073.

Gavara, N., 2017. A beginner's guide to atomic force microscopy probing for cell mechanics. Microsc. Res. Tech. 80, 75–84. https://doi.org/10.1002/jemt.22776.

Gavara, N., Chadwick, R.S., 2012. Determination of the elastic moduli of thin samples and adherent cells using conical atomic force microscope tips. Nat. Nanotechnol. 7, 733–736. https://doi.org/10.1038/nnano.2012.163.

Gennisson, J.-L., Deffieux, T., Fink, M., Tanter, M., 2013. Ultrasound elastography: principles and techniques. Diagn. Interv. Imaging 94, 487–495. https://doi.org/10.1016/j.diii.2013.01.022.

Ghanbari, A., Mousavi, Z., Heuzey, M., Patience, G.S., Carreau, P.J., 2020. Experimental methods in chemical engineering: Rheometry. Can. J. Chem. Eng. 98, 1456–1470. https://doi.org/10.1002/cjce.23749.

Gomez-Jimenez, S., Saucedo-Anaya, T., Guerrero-Mendez, C., Robles-Guerrero, A., Silva-Acosta, L., Navarro-Solis, D., Lopez-Betancur, D., Contreras Rodríguez, A.R., 2024. Mooney–rivlin parameter determination model as a function of temperature in

vulcanized rubber based on molecular dynamics simulations. Materials 17, 3252. https://doi.org/10.3390/ma17133252.
Grasland-Mongrain, P., Zorgani, A., Nakagawa, S., Bernard, S., Paim, L.G., Fitzharris, G., Catheline, S., Cloutier, G., 2018. Ultrafast imaging of cell elasticity with optical microelastography. Proc. Natl. Acad. Sci. 115, 861–866. https://doi.org/10.1073/pnas.1713395115.
Griffin, M., Premakumar, Y., Seifalian, A., Butler, P.E., Szarko, M., 2016. Biomechanical characterization of human soft tissues using indentation and tensile testing. JoVE J. https://doi.org/10.3791/54872.
Guertler, C.A., Okamoto, R.J., Schmidt, J.L., Badachhape, A.A., Johnson, C.L., Bayly, P. V., 2018. Mechanical properties of porcine brain tissue in vivo and ex vivo estimated by MR elastography. J. Biomech. 69, 10–18. https://doi.org/10.1016/j.jbiomech.2018.01.016.
Guertler, C.A., Okamoto, R.J., Ireland, J.A., Pacia, C.P., Garbow, J.R., Chen, H., Bayly, P. V., 2020. Estimation of anisotropic material properties of soft tissue by MRI of ultrasound-induced shear waves. J. Biomech. Eng. 142. https://doi.org/10.1115/1.4046127.
Guo, Y., Mofrad, M.R.K., Tepole, A.B., 2022. On modeling the multiscale mechanobiology of soft tissues: challenges and progress. Biophys. Rev. 3. https://doi.org/10.1063/5.0085025.
Guz, N., Dokukin, M., Kalaparthi, V., Sokolov, I., 2014. If cell mechanics can be described by elastic modulus: study of different models and probes used in indentation experiments. Biophys. J. 107, 564–575. https://doi.org/10.1016/j.bpj.2014.06.033.
Hao, Y., Cheng, S., Tanaka, Y., Hosokawa, Y., Yalikun, Y., Li, M., 2020. Mechanical properties of single cells: measurement methods and applications. Biotechnol. Adv. 45, 107648. https://doi.org/10.1016/j.biotechadv.2020.107648.
He, Z., Zhang, K., Lin, Y., Yuan, S., 2020. An accurate determination method for constitutive model of anisotropic tubular materials with DIC-Based controlled biaxial tensile test. Int. J. Mech. Sci. 181, 105715. https://doi.org/10.1016/j.ijmecsci.2020.105715.
He, D., Malu, D., Hu, Y., 2024. A comprehensive review of indentation of gels and soft biological materials. Appl. Mech. Rev. 76. https://doi.org/10.1115/1.4065434.
Herbert, E.G., Oliver, W.C., Pharr, G.M., 2008. Nanoindentation and the dynamic characterization of viscoelastic solids. J. Phys. D Appl. Phys. 41, 074021. https://doi.org/10.1088/0022-3727/41/7/074021.
Hermanowicz, P., Sarna, M., Burda, K., Gabryś, H., 2014. AtomicJ: an open source software for analysis of force curves. Rev. Sci. Instrum. 85. https://doi.org/10.1063/1.4881683.
Holzapfel, G.A., Ogden, R.W., 2010. Constitutive modelling of arteries. Proc. R. Soc. A 466, 1551–1597. https://doi.org/10.1098/rspa.2010.0058.
Holzapfel, G.A., Ogden, R.W., 2025. Modeling the biomechanical properties of soft biological tissues: constitutive theories. Eur. J. Mech. Solid. 112, 105634. https://doi.org/10.1016/j.euromechsol.2025.105634.
Holzapfel, G.A., Gasser, T.C., Ogden, R.W., 2000. A new constitutive framework for arterial wall mechanics and a comparative study of material models. J. Elast. Phys. Sci. Solids 61, 1–48. https://doi.org/10.1023/A:1010835316564.
Holzapfel, G.A., Humphrey, J.D., Ogden, R.W., 2025. Biomechanics of soft biological tissues and organs, mechanobiology, homeostasis and modelling. J. R. Soc. Interface 22. https://doi.org/10.1098/rsif.2024.0361.
Hou, Y.Y., Kassim, H.O., 2005. Instrument techniques for rheometry. Rev. Sci. Instrum. 76. https://doi.org/10.1063/1.2085048.
Hrapko, M., van Dommelen, J.A.W., Peters, G.W.M., Wismans, J.S.H.M., 2008. The influence of test conditions on characterization of the mechanical properties of brain tissue. J. Biomech. Eng. 130. https://doi.org/10.1115/1.2907746.
Illi, J., Ilic, M., Stark, A.W., Amstutz, C., Burger, J., Zysset, P., Haeberlin, A., Gräni, C., 2023. Mechanical testing and comparison of porcine tissue, silicones and 3D-printed materials for cardiovascular phantoms. Front. Bioeng. Biotechnol. 11. https://www.frontiersin.org/journals/bioengineering-and-biotechnology/articles/10.3389/fbioe.2023.1274673.
Innocenti, B., Larrieu, J.C., Lambert, P., Pianigiani, S., 2018. Automatic characterization of soft tissues material properties during mechanical tests. Muscles Ligaments Tendons J. 7, 529–537.
Ionescu, C., Chirita, M., 2009. Stress-strain properties of natural and biomimetically formed collagen constructs. Technol. Health Care 16, 437–444. https://doi.org/10.3233/THC-2008-16604.
Islam, M.R., Virag, J., Oyen, M.L., 2020. Micromechanical poroelastic and viscoelastic properties of ex-vivo soft tissues. J. Biomech. 113, 110090. https://doi.org/10.1016/j.jbiomech.2020.110090.
ISO 37-2024, 2024. Rubber, Vulcanized or Thermoplastic - Determination of Tensile stress-strain Properties.
ISO/IEC Guide 98-1, 2024. Guide to the Expression of Uncertainty in Measurement - Part 1: Introduction.
Ito, D., Numano, T., Mizuhara, K., Washio, T., Misawa, M., Nitta, N., 2017. Partial volume effect on MR elastography. Open J. Med. Imag. 7, 131–143. https://doi.org/10.4236/ojmi.2017.74013.
Jacobs, N.T., Cortes, D.H., Vresilovic, E.J., Elliott, D.M., 2013. Biaxial tension of fibrous tissue: using finite element methods to address experimental challenges arising from boundary conditions and anisotropy. J. Biomech. Eng. 135. https://doi.org/10.1115/1.4023503.
Jensen, A.S., Baandrup, U., Hasenkam, J.M., Kundu, T., Jørgensen, C.S., 2006. Distribution of the microelastic properties within the human anterior mitral leaflet. Ultrasound Med. Biol. 32, 1943–1948. https://doi.org/10.1016/j.ultrasmedbio.2006.06.011.
Jeong, W.K., Lim, H.K., Lee, H.-K., Jo, J.M., Kim, Y., 2014. Principles and clinical application of ultrasound elastography for diffuse liver disease. Ultrasonography 33, 149–160. https://doi.org/10.14366/usg.14003.
Jiang, M., Lawson, Z.T., Erel, V., Pervere, S., Nan, T., Robbins, A.B., Feed, A.D., Moreno, M.R., 2020. Clamping soft biologic tissues for uniaxial tensile testing: a brief survey of current methods and development of a novel clamping mechanism. J. Mech. Behav. Biomed. Mater. 103, 103503. https://doi.org/10.1016/j.jmbbm.2019.103503.
Jiang, M., Sridhar, R.L., Robbins, A.B., Freed, A.D., Moreno, M.R., 2021. A versatile biaxial testing platform for soft tissues. J. Mech. Behav. Biomed. Mater. 114, 104144. https://doi.org/10.1016/j.jmbbm.2020.104144.
Johnston, A., Callanan, A., 2023. Recent methods for modifying mechanical properties of tissue-engineered scaffolds for clinical applications. Biomimetics 8, 205. https://doi.org/10.3390/biomimetics8020205.
Jokinen, V., 2017. Reliability and Limitations of Compression Testing of Various Biomaterials. Tampere University of Technology. Master Thesis.
Jóźwiak, B., Boncel, S., 2020. Rheology of ionanofluids – a review. J. Mol. Liq. 302, 112568. https://doi.org/10.1016/j.molliq.2020.112568.
Kahle, E., Alberini, R., Ehret, A.E., Mazza, E., Spagnoli, A., 2025. Length scales in the tear resistance of soft tissues and elastomers: a comparative study based on computational models. Int. J. Fract. 249, 27. https://doi.org/10.1007/s10704-025-00842-6.
Kang, J.S., Navindaran, K., Phillips, J., Kenny, K., Moon, K.S., 2023. Characterization of mechanical properties of soft tissues using sub-microscale tensile testing and 3D-Printed sample holder. J. Mech. Behav. Biomed. Mater. 138, 105581. https://doi.org/10.1016/j.jmbbm.2022.105581.
Kennedy, P., Stocker, D., Carbonell, G., Said, D., Bane, O., Hectors, S., Abboud, G., Cuevas, J., Bolster, B.D., Friedman, S.L., Lewis, S., Schiano, T., Bhattacharya, D., Fischman, A., Thung, S., Taouli, B., 2022. MR elastography outperforms shear wave elastography for the diagnosis of clinically significant portal hypertension. Eur. Radiol. 32, 8339–8349. https://doi.org/10.1007/s00330-022-08935-9.
Kim, J.-Y., Lee, J.-J., Lee, Y.-H., Jang, J., Kwon, D., 2006. Surface roughness effect in instrumented indentation: a simple contact depth model and its verification. J. Mater. Res. 21, 2975–2978. https://doi.org/10.1557/jmr.2006.0370.
Kim, E., Ramos Figueroa, A.L., Schrock, M., Zhang, E., Newcomb, C.J., Bao, Z., Michalek, L., 2025. A guide for nanomechanical characterization of soft matter via AFM: from mode selection to data reporting. STAR Protoc. 6, 103809. https://doi.org/10.1016/j.xpro.2025.103809.
Kimondo, J.J., Hu, Y., Xue, J., Luo, B., Feng, Z., Wu, J., Wu, Z., 2025. Establishing an elastography calibration standard: validation of a shear wave TOF device for measuring elasticity and viscosity in tissue-mimicking phantoms using rheometry. PLoS One 20, e0335645. https://doi.org/10.1371/journal.pone.0335645.
Kirby, M.A., Pelivanov, I., Song, S., Ambrozinski, Ł., Yoon, S.J., Gao, L., Li, D., Shen, T.T., Wang, R.K., O'Donnell, M., 2017. Optical coherence elastography in ophthalmology. J. Biomed. Opt. 22, 1. https://doi.org/10.1117/1.JBO.22.12.121720.
Klatt, D., Friedrich, C., Korth, Y., Vogt, R., Braun, J., Sack, I., 2010. Viscoelastic properties of liver measured by oscillatory rheometry and multifrequency magnetic resonance elastography. Biorheology 47, 133–141. https://doi.org/10.3233/BIR-2010-0565.
Klemuk, S.A., Titze, I.R., 2009. Determining motor inertia of a stress-controlled rheometer. J. Rheol. (N Y. N. Y). 53, 765–780. https://doi.org/10.1122/1.3119056.
Kontomaris, S.V., Georgakopoulos, A., Malamou, A., Stylianou, A., 2021. The average Young's modulus as a physical quantity for describing the depth-dependent mechanical properties of cells. Mech. Mater. 158, 103846. https://doi.org/10.1016/j.mechmat.2021.103846.
Kontomaris, S.V., Malamou, A., Stylianou, A., 2022. The Hertzian theory in AFM nanoindentation experiments regarding biological samples: overcoming limitations in data processing. Micron 155, 103228. https://doi.org/10.1016/j.micron.2022.103228.
Kontomaris, S.V., Stylianou, A., Chliveros, G., Malamou, A., 2023a. Determining spatial variability of elastic properties for biological samples using AFM. Micromachines 14, 182. https://doi.org/10.3390/mi14010182.
Kontomaris, S.V., Stylianou, A., Georgakopoulos, A., Malamou, A., 2023b. 3D AFM nanomechanical characterization of biological materials. Nanomaterials 13, 395. https://doi.org/10.3390/nano13030395.
Kontomaris, S.V., Malamou, A., Stylianou, A., 2024. Accurate modelling of AFM force-indentation curves with blunted indenters at small indentation depths. Micromachines 15, 1209. https://doi.org/10.3390/mi15101209.
Koruk, H., 2014. Quantification and minimization of sensor effects on modal parameters of lightweight structures. J. Vibroeng. 16.
Koruk, H., 2021. Modelling small and large displacements of a sphere on an elastic half-space exposed to a dynamic force. Eur. J. Phys. 52, 055006. https://doi.org/10.1088/1361-6404/ac0e42.
Koruk, H., 2022. Development of an improved mathematical model for the dynamic response of a sphere located at a viscoelastic medium interface. Eur. J. Phys. 43, 25002. https://doi.org/10.1088/1361-6404/ac4647.
Koruk, H., Choi, J.J., 2018. Displacement of a bubble by acoustic radiation force into a fluid-tissue interface. J. Acoust. Soc. Am. 143, 2535–2540. https://doi.org/10.1121/1.5034175.
Koruk, H., Choi, J.J., 2019. Displacement of a bubble located at a fluid-viscoelastic medium interface. J. Acoust. Soc. Am. 145, EL410–EL416. https://doi.org/10.1121/1.5108678.
Koruk, H., Pouliopoulos, A.N., 2023. Elasticity and viscoelasticity imaging based on small particles exposed to external forces. Processes 11, 3402. https://doi.org/10.3390/pr11123402.
Koruk, H., Pouliopoulos, A.N., 2024. Investigation of the motion of a spherical object located at soft elastic and viscoelastic material interface for identification of material properties. Appl. Sci. Eng. Prog. 17, 7277. https://doi.org/10.14416/j.asep.2023.12.002.

Koruk, H., Rajagopal, S., 2024. A comprehensive review on the viscoelastic parameters used for engineering materials, including soft materials, and the relationships between different damping parameters. Sensors 24, 6137. https://doi.org/10.3390/s24186137.

Koruk, H., Sanliturk, K.Y., 2012. Identification and removal of adverse effects of non-contact electromagnetic excitation in oberst beam test method. Mech. Syst. Signal Process. 30. https://doi.org/10.1016/j.ymssp.2012.02.003.

Koruk, H., El Ghamrawy, A., Pouliopoulos, A.N., Choi, J.J., 2015. Acoustic particle palpation for measuring tissue elasticity. Appl. Phys. Lett. 107. https://doi.org/10.1063/1.4936345.

Koruk, H., Koc, H.O., Yurdaer, S.B., Besli, A., Pouliopoulos, A.N., 2024. A new approach for measuring viscoelastic properties of soft materials using the dynamic response of a spherical object placed at the sample interface. Exp. Mech. 64, 21–32. https://doi.org/10.1007/s11340-023-01004-2.

Krieg, M., Fläschner, G., Alsteens, D., Gaub, B.M., Roos, W.H., Wuite, G.J.L., Gaub, H.E., Gerber, C., Dufrêne, Y.F., Müller, D.J., 2018. Atomic force microscopy-based mechanobiology. Nat. Rev. Phys. 1, 41–57. https://doi.org/10.1038/s42254-018-0001-7.

Kriener, K., Lala, R., Homes, R.A.P., Finley, H., Sinclair, K., Williams, M.K., Midwinter, M.J., 2023. Mechanical characterization of the human abdominal wall using uniaxial tensile testing. Bioengineering 10. https://doi.org/10.3390/bioengineering10101213.

Krishnan, P., 2017. Rheology of epoxy/rubber blends. In: Parameswaranpillai, J., Hameed, N., Pionteck, J., Woo, E.M. (Eds.), Handbook of Epoxy Blends. Springer International Publishing, Cham, pp. 185–210. https://doi.org/10.1007/978-3-319-40043-3_7.

Krivega, E.S., Kotova, S.L., Timashev, P.S., Efremov, Y.M., 2024. Mechanical characterization of soft biomaterials: which time and spatial scale to choose? Soft Matter 20, 5095–5104. https://doi.org/10.1039/D4SM00530A.

Kuznetsova, T.G., Starodubtseva, M.N., Yegorenkov, N.I., Chizhik, S.A., Zhdanov, R.I., 2007. Atomic force microscopy probing of cell elasticity. Micron 38, 824–833. https://doi.org/10.1016/j.micron.2007.06.011.

Lam, C.-D., Park, S., 2025. Nanomechanical characterization of soft nanomaterial using atomic force microscopy. Mater. Today Bio 31, 101506. https://doi.org/10.1016/j.mtbio.2025.101506.

Lam, A.C.L., Pang, S.W.A., Ahuja, A.T., Bhatia, K.S.S., 2016. The influence of precompression on elasticity of thyroid nodules estimated by ultrasound shear wave elastography. Eur. Radiol. 26, 2845–2852. https://doi.org/10.1007/s00330-015-4108-2.

Lamers, E., van Kempen, T.H.S., Baaijens, F.P.T., Peters, G.W.M., Oomens, C.W.J., 2013. Large amplitude oscillatory shear properties of human skin. J. Mech. Behav. Biomed. Mater. 28, 462–470. https://doi.org/10.1016/j.jmbbm.2013.01.024.

Laun, M., Auhl, D., Brummer, R., Dijkstra, D.J., Gabriel, C., Mangnus, M.A., Rüllmann, M., Zoetelief, W., Handge, U.A., 2014. Guidelines for checking performance and verifying accuracy of rotational rheometers: viscosity measurements in steady and oscillatory shear (IUPAC technical report). Chem. Int. 86, 1945–1968. https://doi.org/10.1515/pac-2013-0601.

Laurence, D.W., Wang, S., Xiao, R., Qian, J., Mir, A., Burkhart, H.M., Holzapfel, G.A., Lee, C.-H., 2023. An investigation of how specimen dimensions affect biaxial mechanical characterizations with CellScale BioTester and constitutive modeling of porcine tricuspid valve leaflets. J. Biomech. 160, 111829. https://doi.org/10.1016/j.jbiomech.2023.111829.

Laurent, V.M., Hénon, S., Planus, E., Fodil, R., Balland, M., Isabey, D., Gallet, F., 2002. Assessment of mechanical properties of adherent living cells by bead micromanipulation: Comparison of magnetic twisting cytometry vs optical tweezers. J. Biomech. Eng. 124, 408–421. https://doi.org/10.1115/1.1485285.

Laville, C., Pradille, C., Tillier, Y., 2020. Mechanical characterization and identification of material parameters of porcine aortic valve leaflets. J. Mech. Behav. Biomed. Mater. 112, 104036. https://doi.org/10.1016/j.jmbbm.2020.104036.

Ledoux, W.R., Blevins, J.J., 2007. The compressive material properties of the plantar soft tissue. J. Biomech. 40, 2975–2981. https://doi.org/10.1016/j.jbiomech.2007.02.009.

Lekka, M., Laidler, P., Gil, D., Lekki, J., Stachura, Z., Hrynkiewicz, A.Z., 1999. Elasticity of normal and cancerous human bladder cells studied by scanning force microscopy. Eur. Biophys. J. 28, 312–316. https://doi.org/10.1007/s002490050213.

Lemine, A.S., Ahmad, Z., Al-Thani, N.J., Hasan, A., Bhadra, J., 2024. Mechanical properties of human hepatic tissues to develop liver-mimicking phantoms for medical applications. Biomech. Model. Mechanobiol. 23, 373–396. https://doi.org/10.1007/s10237-023-01785-4.

Levy, B.E., Oldenburg, A.L., 2021. Single magnetic particle motion in magnetomotive ultrasound: an analytical model and experimental validation. IEEE Trans. Ultrason. Ferroelectrics Freq. Control 68, 2635–2644. https://doi.org/10.1109/TUFFC.2021.3072867.

Li, Y., Xu, G.-K., 2023. Editorial: mechanobiology at multiple scales. Front. Bioeng. Biotechnol. 11. https://doi.org/10.3389/fbioe.2023.1226198.

Li, P., Yang, Z., Jiang, S., 2018. Tissue mimicking materials in image-guided needle-based interventions: a review. Mater. Sci. Eng. C 93, 1116–1131. https://doi.org/10.1016/j.msec.2018.09.028.

Li, W., Shepherd, D.E.T., Espino, D.M., 2020. Frequency dependent viscoelastic properties of porcine brain tissue. J. Mech. Behav. Biomed. Mater. 102, 103460. https://doi.org/10.1016/j.jmbbm.2019.103460.

Li, H., Flé, G., Bhatt, M., Qu, Z., Ghazavi, S., Yazdani, L., Bosio, G., Rafati, I., Cloutier, G., 2021a. Viscoelasticity imaging of biological tissues and single cells using shear wave propagation. Front. Phys. 9. https://www.frontiersin.org/articles/10.3389/fphy.2021.666192.

Li, H., Flé, G., Bhatt, M., Qu, Z., Ghazavi, S., Yazdani, L., Bosio, G., Rafati, I., Cloutier, G., 2021b. Viscoelasticity imaging of biological tissues and single cells using shear wave propagation. Front. Phys. 9. https://doi.org/10.3389/fphy.2021.666192.

Li, Y., Gao, Q., Chen, N., Zhang, Y., Wang, J., Li, C., He, X., Jiao, Y., Zhang, Z., 2022. Clinical studies of magnetic resonance elastography from 1995 to 2021: scientometric and visualization analysis based on CiteSpace. Quant. Imag. Med. Surg. 12, 5080–5100. https://doi.org/10.21037/qims-22-207.

Liang, X., Crecea, V., Boppart, S.A., 2010. Dynamic optical coherence elastography: a review. J. Innov. Opt. Health Sci. 3, 221–233. https://doi.org/10.1142/S1793545810001180.

Lim, J., Hong, J., Chen, W.W., Weerasooriya, T., 2011. Mechanical response of pig skin under dynamic tensile loading. Int. J. Impact Eng. 38, 130–135. https://doi.org/10.1016/j.ijimpeng.2010.09.003.

Lin, D.C., Shreiber, D.I., Dimitriadis, E.K., Horkay, F., 2009. Spherical indentation of soft matter beyond the Hertzian regime: numerical and experimental validation of hyperelastic models. Biomech. Model. Mechanobiol. 8, 345–358. https://doi.org/10.1007/s10237-008-0139-9.

Lin, H., Shen, Y., Chen, X., Zhu, Y., Zheng, Y., Zhang, X., Guo, Y., Wang, T., Chen, S., 2017. Viscoelastic properties of normal rat liver measured by ultrasound elastography: comparison with oscillatory rheometry. Biorheology 53, 193–207. https://doi.org/10.3233/BIR-16091.

Lin, C.-Y., Mathur, M., Malinowski, M., Timek, T.A., Rausch, M.K., 2023. The impact of thickness heterogeneity on soft tissue biomechanics: a novel measurement technique and a demonstration on heart valve tissue. Biomech. Model. Mechanobiol. 22, 1487–1498. https://doi.org/10.1007/s10237-022-01640-y.

Liu, F., Tschumperlin, D.J., 2011. Micro-mechanical characterization of lung tissue using atomic force microscopy. JoVE J. https://doi.org/10.3791/2911.

Liu, J., Zheng, H., Poh, P., Machens, H.-G., Schilling, A., 2015. Hydrogels for engineering of perfusable vascular networks. Int. J. Mol. Sci. 16, 15997–16016. https://doi.org/10.3390/ijms160715997.

Liu, Y., Sokolov, I., Dokukin, M.E., Xiong, Y., Peng, P., 2020. Can AFM be used to measure absolute values of Young's modulus of nanocomposite materials Down to the nanoscale? Nanoscale 12, 12432–12443. https://doi.org/10.1039/D0NR02314K.

Liu, H.-C., Gaihre, B., Kijanka, P., Lu, L., Urban, M.W., 2023. Acoustic force elastography microscopy. IEEE Trans. Biomed. Eng. 70, 841–852. https://doi.org/10.1109/TBME.2022.3203435.

Liu, Y., Deng, Q., Wang, Y., Zhang, C., Chen, M., Hu, Z., Miao, Y., 2024. Dynamic mechanical response and functional mechanisms in rabbit pulmonary tissue. Mech. Time-Dependent Mater. https://doi.org/10.1007/s11043-024-09697-1.

Lohr, M.J., Sugerman, G.P., Kakaletsis, S., Lejeune, E., Rausch, M.K., 2022. An introduction to the ogden model in biomechanics: benefits, implementation tools and limitations. Philos. Trans. R. Soc. A Math. Phys. Eng. Sci. 380. https://doi.org/10.1098/rsta.2021.0365.

Low, G., Owen, N.E., Joubert, I., Patterson, A.J., Graves, M.J., Glaser, K.J., Alexander, G. J.M., Lomas, D.J., 2015. Reliability of magnetic resonance elastography using multislice two-dimensional spin-echo echo-planar imaging (SE-EPI) and three-dimensional inversion reconstruction for assessing renal stiffness. J. Magn. Reson. Imag. 42, 844–850. https://doi.org/10.1002/jmri.24826.

Lyashenko, I., Borysiuk, V., 2022. Stick-slip motion in the contact between soft elastomer and spherical hard steel indenter: model explanation of superplasticity mode in metal samples with grain boundary defects. Procedia Struct. Integr. 36, 24–29. https://doi.org/10.1016/j.prostr.2021.12.078.

Lyashenko, I.A., Pham, T.H., Popov, V.L., 2024. Effect of indentation depth on friction coefficient in adhesive contacts: experiment and simulation. Biomimetics 9, 52. https://doi.org/10.3390/biomimetics9010052.

Lyshchik, A., Higashi, T., Asato, R., Tanaka, S., Ito, J., Hiraoka, M., Brill, A.B., Saga, T., Togashi, K., 2005. Elastic moduli of thyroid tissues under compression. Ultrason. Imag. 27, 101–110. https://doi.org/10.1177/016173460502700204.

Ma, S., Wang, R., Qiu, S., Li, R., Yue, Q., Sun, Q., Chen, L., Yan, F., Yang, G.-Z., Feng, Y., 2023. MR elastography with optimization-based phase unwrapping and traveling wave expansion-based neural network (TWENN). IEEE Trans. Med. Imag. 42, 2631–2642. https://doi.org/10.1109/TMI.2023.3261346.

Ma, S., He, Z., Wang, R., Zhang, A., Sun, Q., Liu, J., Yan, F., Sacks, M.S., Feng, X.-Q., Yang, G.-Z., Feng, Y., 2025. Measurement of biomechanical properties of transversely isotropic biological tissue using traveling wave expansion. Med. Image Anal. 101, 103457. https://doi.org/10.1016/j.media.2025.103457.

Magazzù, A., Marcuello, C., 2023. Investigation of soft matter nanomechanics by atomic force microscopy and optical tweezers: a comprehensive review. Nanomaterials 13, 963. https://doi.org/10.3390/nano13060963.

Maghsoudy-Louyeh, S., Kropf, M., Tittmann, B.R., 2018. Review of progress in atomic force microscopy. Open Neuroimaging J. 12, 86–104. https://doi.org/10.2174/1874440001812010086.

Maghzinajafabadi, M., Lamprecht, R., Semmler, M., Sutor, A., 2019. Acoustic pressure pipette aspiration method combined with finite element analysis for isotropic materials. Appl. Sci. 9, 3875. https://doi.org/10.3390/app9183875.

Majumdar, S., Klatt, D., 2021. Longitudinal study of sub-regional cerebral viscoelastic properties of 5XFAD Alzheimer's disease mice using multifrequency MR elastography. Magn. Reson. Med. 86, 405–414. https://doi.org/10.1002/mrm.28709.

Manduca, A., Bayly, P.V., Ehman, R.L., Kolipaka, A., Royston, T.J., Sack, I., Sinkus, R., Van Beers, B.E., 2021. MR elastography: principles, guidelines, and terminology. Magn. Reson. Med. 85, 2377–2390. https://doi.org/10.1002/mrm.28627.

Marieswaran, M., Jain, I., Garg, B., Sharma, V., Kalyanasundaram, D., 2018. A review on biomechanics of anterior cruciate ligament and materials for reconstruction. Appl. Bionics Biomech. 2018, 1–14. https://doi.org/10.1155/2018/4657824.

Marinopoulos, T., Zani, L., Li, S., V Silberschmidt, V., 2023. Modelling indentation of human lower-limb soft tissue: simulation parameters and their effects. Continuum Mech. Therm. 35, 939–955. https://doi.org/10.1007/s00161-020-00933-w.

Marrese, M., Guarino, V., Ambrosio, L., 2017. Atomic force microscopy: a powerful tool to address scaffold design in tissue engineering. J. Funct. Biomater. 8, 7. https://doi.org/10.3390/jfb8010007.

Matei, G.A., Thoreson, E.J., Pratt, J.R., Newell, D.B., Burnham, N.A., 2006. Precision and accuracy of thermal calibration of atomic force microscopy cantilevers. Rev. Sci. Instrum. 77. https://doi.org/10.1063/1.2336115.

McKee, C.T., Last, J.A., Russell, P., Murphy, C.J., 2011. Indentation versus tensile measurements of Young's modulus for soft biological tissues. Tissue Eng., Part B 17, 155–164. https://doi.org/10.1089/ten.TEB.2010.0520.

Mijailovic, A.S., Qing, B., Fortunato, D., Van Vliet, K.J., 2018. Characterizing viscoelastic mechanical properties of highly compliant polymers and biological tissues using impact indentation. Acta Biomater. 71, 388–397. https://doi.org/10.1016/j.actbio.2018.02.017.

Mishra, A., Cleveland, R.O., 2024. Rheological properties of porcine organs: measurements and fractional viscoelastic model. Front. Bioeng. Biotechnol. 12. https://www.frontiersin.org/journals/bioengineering-and-biotechnology/articles/10.3389/fbioe.2024.1386955.

Mulk, Md, Islam, K.N., Biswas, MdH.A., 2023. Modeling and numerical analysis for mechanical characterization of soft tissue mechanism applying inverse finite element technique. Front. Appl. Math. Stat 9. https://doi.org/10.3389/fams.2023.1064130.

Nakaoka, K., Hashimoto, S., Miyahara, R., Kawashima, H., Ohno, E., Ishikawa, T., Kuwahara, T., Tanaka, H., Hirooka, Y., 2022. Current status of the diagnosis of chronic pancreatitis by ultrasonographic elastography. Korean J. Intern. Med. 37, 27–36. https://doi.org/10.3904/kjim.2021.252.

Nasseri, S., Bilston, L.E., Phan-Thien, N., 2002. Viscoelastic properties of pig kidney in shear, experimental results and modelling. Rheol. Acta 41, 180–192. https://doi.org/10.1007/s003970200017.

Navarro-Lozoya, M., Kennedy, M.S., Dean, D., Rodriguez-Devora, J.I., 2019. Development of phantom material that resembles compression properties of human brain tissue for training models. Materialia 8, 100438. https://doi.org/10.1016/j.mtla.2019.100438.

Navindaran, K., Kang, J.S., Moon, K., 2023. Techniques for characterizing mechanical properties of soft tissues. J. Mech. Behav. Biomed. Mater. 138, 105575. https://doi.org/10.1016/j.jmbbm.2022.105575.

Nayar, V.T., Weiland, J.D., Hodge, A.M., 2012. Macrocompression and nanoindentation of soft viscoelastic biological materials. Tissue Eng. C Methods 18, 968–975. https://doi.org/10.1089/ten.tec.2012.0034.

Nguyen, M.M., Zhou, S., Robert, J., Shamdasani, V., Xie, H., 2014. Development of oil-in-gelatin phantoms for viscoelasticity measurement in ultrasound shear wave elastography. Ultrasound Med. Biol. 40, 168–176. https://doi.org/10.1016/j.ultrasmedbio.2013.08.020.

Nguyen, T.-N., Ho Ba Tho, M.-C., Dao, T.-T., 2020. A systematic review of real-time medical simulations with soft-tissue deformation: computational approaches, interaction devices, system architectures, and clinical validations. Appl. Bionics Biomech. 2020, 1–30. https://doi.org/10.1155/2020/5039329.

Nie, X., Song, B., Ge, Y., Chen, W.W., Weerasooriya, T., 2009. Dynamic tensile testing of soft materials. Exp. Mech. 49, 451–458. https://doi.org/10.1007/s11340-008-9133-5.

Niestrawska, J.A., Viertler, C., Regitnig, P., Cohnert, T.U., Sommer, G., Holzapfel, G.A., 2016. Microstructure and mechanics of healthy and aneurysmatic abdominal aortas: experimental analysis and modelling. J. R. Soc. Interface 13, 20160620. https://doi.org/10.1098/rsif.2016.0620.

Ning, J., Xu, S., Wang, Y., Lessner, S.M., Sutton, M.A., Anderson, K., Bischoff, J.E., 2010. Deformation measurements and material property estimation of mouse carotid artery using a microstructure-based constitutive model. J. Biomech. Eng. 132. https://doi.org/10.1115/1.4002700.

Norman, M.D.A., Ferreira, S.A., Jowett, G.M., Bozec, L., Gentleman, E., 2021. Measuring the elastic modulus of soft culture surfaces and three-dimensional hydrogels using atomic force microscopy. Nat. Protoc. 16, 2418–2449. https://doi.org/10.1038/s41596-021-00495-4.

Oberai, A.A., Gokhale, N.H., Goenezen, S., Barbone, P.E., Hall, T.J., Sommer, A.M., Jiang, J., 2009. Linear and nonlinear elasticity imaging of soft tissue in vivo: demonstration of feasibility. Phys. Med. Biol. 54, 1191–1207. https://doi.org/10.1088/0031-9155/54/5/006.

Oglat, A.A., Abukhalil, T., 2024. Ultrasound elastography: methods, clinical applications, and limitations: a review article. Appl. Sci. 14, 4308. https://doi.org/10.3390/app14104308.

Ohashi, T., Abe, H., Matsumoto, T., Sato, M., 2005. Pipette aspiration technique for the measurement of nonlinear and anisotropic mechanical properties of blood vessel walls under biaxial stretch. J. Biomech. 38, 2248–2256. https://doi.org/10.1016/j.jbiomech.2004.09.019.

Oliver, W.C., Pharr, G.M., 1992. An improved technique for determining hardness and elastic modulus using load and displacement sensing indentation experiments. J. Mater. Res. 7, 1564–1583. https://doi.org/10.1557/JMR.1992.1564.

Ormachea, J., Parker, K.J., 2020. Comprehensive viscoelastic characterization of tissues and the inter-relationship of shear wave (group and phase) velocity, attenuation and dispersion. Ultrasound Med. Biol. 46, 3448–3459. https://doi.org/10.1016/j.ultrasmedbio.2020.08.023.

Oroszlany, A., Nagy, P., Kovacs, J., 2015. Compressive properties of commercially available PVC foams intended for use as mechanical models for human cancellous bone. Acta Polytechnica Hungarica 12, 89–98. https://doi.org/10.12700/APH.12.2.2015.2.6.

Ottensmeyer, M.P., Kerdok, A.E., Howe, R.D., Dawson, S.L., 2004. The effects of testing environment on the viscoelastic properties of soft tissues. https://doi.org/10.1007/978-3-540-25968-8_2.

Oudry, J., Chen, J., Glaser, K.J., Miette, V., Sandrin, L., Ehman, R.L., 2009. Cross-validation of magnetic resonance elastography and ultrasound-based transient elastography: a preliminary phantom study. J. Magn. Reson. Imag. 30, 1145–1150. https://doi.org/10.1002/jmri.21929.

Owen, D.S., 2023. Toward a better modulus at shallow indentations—Enhanced tip and sample characterization for quantitative atomic force microscopy. Microsc. Res. Tech. 86, 84–96. https://doi.org/10.1002/jemt.24261.

Oyen, M.L., 2014. Mechanical characterisation of hydrogel materials. Int. Mater. Rev. 59, 44–59. https://doi.org/10.1179/1743280413Y.0000000022.

O'Leary, S.A., Doyle, B.J., McGloughlin, T.M., 2013a. Comparison of methods used to measure the thickness of soft tissues and their influence on the evaluation of tensile stress. J. Biomech. 46, 1955–1960. https://doi.org/10.1016/j.jbiomech.2013.05.003.

O'Leary, S.A., Doyle, B.J., McGloughlin, T.M., 2013b. Comparison of methods used to measure the thickness of soft tissues and their influence on the evaluation of tensile stress. J. Biomech. 46, 1955–1960. https://doi.org/10.1016/j.jbiomech.2013.05.003.

Palmeri, M.L., Nightingale, K.R., 2011. Acoustic radiation force-based elasticity imaging methods. Interface Focus 1, 553–564. https://doi.org/10.1098/rsfs.2011.0023.

Palmeri, M.L., Milkowski, A., Barr, R., Carson, P., Couade, M., Chen, J., Chen, S., Dhyani, M., Ehman, R., Garra, B., Gee, A., Guenette, G., Hah, Z., Lynch, T., Macdonald, M., Managuli, R., Miette, V., Nightingale, K.R., Obuchowski, N., Rouze, N.C., Morris, D.C., Fielding, S., Deng, Y., Chan, D., Choudhury, K., Yang, S., Samir, A.E., Shamdasani, V., Urban, M., Wear, K., Xie, H., Ozturk, A., Qiang, B., Song, P., McAleavey, S., Rosenzweig, S., Wang, M., Okamura, Y., McLaughlin, G., Chen, Y., Napolitano, D., Carlson, L., Erpelding, T., Hall, T.J., 2021. Radiological society of north america/quantitative imaging biomarker alliance shear wave speed bias quantification in elastic and viscoelastic phantoms. J. Ultrasound Med. 40, 569–581. https://doi.org/10.1002/jum.15609.

Panda, S.K., Buist, M.L., 2018. A finite nonlinear hyper-viscoelastic model for soft biological tissues. J. Biomech. 69, 121–128. https://doi.org/10.1016/j.jbiomech.2018.01.025.

Patel, J.M., Wise, B.C., Bonnevie, E.D., Mauck, R.L., 2019. A systematic review and guide to mechanical testing for articular cartilage tissue engineering. Tissue Eng. C Methods 25, 593–608. https://doi.org/10.1089/ten.tec.2019.0116.

Patra, S., Grover, S.B., 2022. Physical principles of elastography: a primer for radiologists. Indographics 01. https://doi.org/10.1055/s-0042-1742575, 027–040.

Patteson, A.E., Janmey, P.A., 2024. Rheology in the biological sciences. Rheol. Bull. 93, 20–27.

Pei, M., Zou, D., Gao, Y., Zhang, J., Huang, P., Wang, J., Huang, J., Li, Z., Chen, Y., 2021. The influence of sample geometry and size on porcine aortic material properties from uniaxial tensile tests using custom-designed tissue cutters, clamps and molds. PLoS One 16, e0244390. https://doi.org/10.1371/journal.pone.0244390.

Persch, G., Born, Ch, Utesch, B., 1994. Nano-hardness investigations of thin films by an atomic force microscope. Microelectron. Eng. 24, 113–121. https://doi.org/10.1016/0167-9317(94)90061-2.

Pirri, C., Pirri, N., Guidolin, D., De Rose, E., Macchi, V., Porzionato, A., De Caro, R., Stecco, C., 2025. The (Proteus) Anisotropy Effect in Deep Fascia Ultrasonography: the Impact of Probe Angulation on Echogenicity and Thickness Assessments, vol. 15, p. 822. https://doi.org/10.3390/life15050822.

Plodinec, M., Loparic, M., Monnier, C.A., Obermann, E.C., Zanetti-Dallenbach, R., Oertle, P., Hyotyla, J.T., Aebi, U., Bentires-Alj, M., Lim, R.Y.H., Schoenenberger, C.-A., 2012. The nanomechanical signature of breast cancer. Nat. Nanotechnol. 7, 757–765. https://doi.org/10.1038/nnano.2012.167.

Pogoda, K., Jaczewska, J., Wiltowska-Zuber, J., Klymenko, O., Zuber, K., Fornal, M., Lekka, M., 2012. Depth-sensing analysis of cytoskeleton organization based on AFM data. Eur. Biophys. J. 41, 79–87. https://doi.org/10.1007/s00249-011-0761-9.

Polio, S.R., Kundu, A.N., Dougan, C.E., Birch, N.P., Aurian-Blajeni, D.E., Schiffman, J.D., Crosby, A.J., Peyton, S.R., 2018. Cross-platform mechanical characterization of lung tissue. PLoS One 13, e0204765. https://doi.org/10.1371/journal.pone.0204765.

Qiu, S., Zhao, X., Chen, J., Zeng, J., Chen, S., Chen, L., Meng, Y., Liu, B., Shan, H., Gao, M., Feng, Y., 2018. Characterizing viscoelastic properties of breast cancer tissue in a mouse model using indentation. J. Biomech. 69, 81–89. https://doi.org/10.1016/j.jbiomech.2018.01.007.

Qiu, S., Jiang, W., Alam, M.S., Chen, S., Lai, C., Wang, T., Li, X., Liu, J., Gao, M., Tang, Y., Li, X., Zeng, J., Feng, Y., 2020. Viscoelastic characterization of injured brain tissue after controlled cortical impact (CCI) using a mouse model. J. Neurosci. Methods 330, 108463. https://doi.org/10.1016/j.jneumeth.2019.108463.

Qiu, T., Zhou, R., Li, J., Luo, Y., Ling, W., 2026. Ultrasound shear wave viscoelastic imaging combined with shear wave elastography for characterization of focal liver lesions. J. Biomech. 194, 113073. https://doi.org/10.1016/j.jbiomech.2025.113073.

Racedo, J., Urban, M.W., 2019. Evaluation of reconstruction parameters for 2-D comb-push ultrasound shear wave elastography. IEEE Trans. Ultrason. Ferroelectrics Freq. Control 66, 254–263. https://doi.org/10.1109/TUFFC.2018.2884348.

Radmacher, M., 2007. Studying the mechanics of cellular processes by atomic force microscopy. In: Methods Cell Biol. Academic Press, pp. 347–372. https://doi.org/10.1016/S0091-679X(07)83015-9.

Rashid, B., Destrade, M., Gilchrist, M.D., 2012. Determination of friction coefficient in unconfined compression of brain tissue. J. Mech. Behav. Biomed. Mater. 14, 163–171. https://doi.org/10.1016/j.jmbbm.2012.05.001.

Reiter, R., Shahryari, M., Tzschätzsch, H., Haas, M., Bayerl, C., Siegmund, B., Hamm, B., Asbach, P., Braun, J., Sack, I., 2021. Influence of fibrosis progression on the viscous

properties of in vivo liver tissue elucidated by shear wave dispersion in multifrequency MR elastography. J. Mech. Behav. Biomed. Mater. 121, 104645. https://doi.org/10.1016/j.jmbbm.2021.104645.
Richbourg, N.R., Rausch, M.K., Peppas, N.A., 2022. Cross-evaluation of stiffness measurement methods for hydrogels. Polymer (Guildf). 258, 125316. https://doi.org/10.1016/j.polymer.2022.125316.
Rico, F., Roca-Cusachs, P., Gavara, N., Farré, R., Rotger, M., Navajas, D., 2005. Probing mechanical properties of living cells by atomic force microscopy with blunted pyramidal cantilever tips. Phys. Rev. E 72, 021914. https://doi.org/10.1103/PhysRevE.72.021914.
Rosicka, K., Mierzejewska-Krzyżowska, B., Mrówczyński, W., 2021. Skin biomechanical and viscoelastic properties measured with MyotonPRO in different areas of human body. Skin Res. Technol. 1–10. https://doi.org/10.1111/srt.13116.
Ross, Z., Hirst, G., Rose, A., Graff, N., Dillon, C.R., Terry, B., 2026. Comparative analysis of shear wave elastography and biaxial testing for accurate soft tissue mechanical assessment. J. Mech. Behav. Biomed. Mater. 173, 107204. https://doi.org/10.1016/j.jmbbm.2025.107204.
Rubiano, A., Galitz, C., Simmons, C.S., 2019. Mechanical characterization by mesoscale indentation: advantages and pitfalls for tissue and scaffolds. Tissue Eng. C Methods 25, 619–629. https://doi.org/10.1089/ten.tec.2018.0372.
Saccomandi, G., Vergori, L., Zanetti, E.M., 2022. Linear, weakly nonlinear and fully nonlinear models for soft tissues: which ones provide the Most reliable estimations of the stiffness? Philos. Trans. R. Soc. A Math. Phys. Eng. Sci. 380. https://doi.org/10.1098/rsta.2021.0321.
Sacks, M.S., Sun, W., 2003. Multiaxial mechanical behavior of biological materials. Annu. Rev. Biomed. Eng. 5, 251–284. https://doi.org/10.1146/annurev.bioeng.5.011303.120714.
Sadeghinia, M.J., Skallerud, B., Holzapfel, G.A., Prot, V., 2022. Biomechanics of mitral valve leaflets: second harmonic generation microscopy, biaxial mechanical tests and tissue modeling. Acta Biomater. 141, 244–254. https://doi.org/10.1016/j.actbio.2022.01.003.
Sahebjavaher, R.S., Frew, S., Bylinskii, A., ter Beek, L., Garteiser, P., Honarvar, M., Sinkus, R., Salcudean, S., 2014. Prostate MR elastography with transperineal electromagnetic actuation and a fast fractionally encoded steady-state gradient echo sequence. NMR Biomed. 27, 784–794. https://doi.org/10.1002/nbm.3118.
Saint-Michel, B., Gibaud, T., Manneville, S., 2017. Predicting and assessing rupture in protein gels under oscillatory shear. Soft Matter 13, 2643–2653. https://doi.org/10.1039/C7SM00064B.
Sander, M., Dobicki, H., Ott, A., 2017. Large amplitude oscillatory shear rheology of living fibroblasts: path-dependent steady states. Biophys. J. 113, 1561–1573. https://doi.org/10.1016/j.bpj.2017.07.032.
Santos, J.A.C., Rebêlo, L.M., Araujo, A.C., Barros, E.B., de Sousa, J.S., 2012. Thickness-corrected model for nanoindentation of thin films with conical indenters. Soft Matter 8, 4441. https://doi.org/10.1039/c2sm07062f.
Santos, A.Z., Rocha, S., Carneiro, B., Fernandes, N.A., Padrão, J., Carvalho, Ó., 2025. Current state of elastography research in multiple anatomical structures and respective phantoms. Phys. Med. 138, 105192. https://doi.org/10.1016/j.ejmp.2025.105192.
Sanz-Herrera, J.A., Apolinar-Fernandez, A., Jimenez-Aires, A., Perez-Alcantara, P., Dominguez, J., Reina-Romo, E., 2025. Multiscale characterization of the mechanics of curved fibered structures with application to biological and engineered materials. Comput. Struct. 310, 107690. https://doi.org/10.1016/j.compstruc.2025.107690.
Sarvazyan, A.P., Urban, M.W., Greenleaf, J.F., 2013. Acoustic waves in medical imaging and diagnostics. Ultrasound Med. Biol. 39, 1133–1146. https://doi.org/10.1016/j.ultrasmedbio.2013.02.006.
Schillers, H., Rianna, C., Schäpe, J., Luque, T., Doschke, H., Wälte, M., Uriarte, J.J., Campillo, N., Michanetzis, G.P.A., Bobrowska, J., Dumitru, A., Herruzo, E.T., Bovio, S., Parot, P., Galluzzi, M., Podestà, A., Puricelli, L., Scheuring, S., Missirlis, Y., Garcia, R., Odorico, M., Teulon, J.-M., Lafont, F., Lekka, M., Rico, F., Rigato, A., Pellequer, J.-L., Oberleithner, H., Navajas, D., Radmacher, M., 2017. Standardized nanomechanical atomic force microscopy procedure (SNAP) for measuring soft and biological samples. Sci. Rep. 7, 5117. https://doi.org/10.1038/s41598-017-05383-0.
Schmitt, J.M., 1998. OCT elastography: imaging microscopic deformation and strain of tissue. Opt. Express 3, 199. https://doi.org/10.1364/OE.3.000199.
Scholze, M., Singh, A., Lozano, P.F., Ondruschka, B., Ramezani, M., Werner, M., Hammer, N., 2018. Utilization of 3D printing technology to facilitate and standardize soft tissue testing. Sci. Rep. 8, 11340. https://doi.org/10.1038/s41598-018-29583-4.
Scholze, M., Safavi, S., Li, K.C., Ondruschka, B., Werner, M., Zwirner, J., Hammer, N., 2020. Standardized tensile testing of soft tissue using a 3D printed clamping system. HardwareX 8. https://doi.org/10.1016/j.ohx.2020.e00159.
Schrenk, F., Uhrik, P., Uhrikova, Z., 2020. Ultrasound elastography: review of techniques, clinical application, technical limitations, and safety considerations in neonatology. Acta Med. Martiniana 20, 72–79. https://doi.org/10.2478/acm-2020-0009.
Schwarz, D., Fleisman, J., Vitasek, R., Polzer, S., 2023. Methodology for estimation of undeformed thickness of arterial tissues. Sci. Rep. 13, 2816. https://doi.org/10.1038/s41598-023-28871-y.
Shahmirzadi, D., Hsieh, A.H., 2010. An efficient technique for adjusting and maintaining specific hydration levels in soft biological tissues in vitro. Med. Eng. Phys. 32, 795–801. https://doi.org/10.1016/j.medengphy.2010.04.021.
Shigemura, K., Kuribayashi-Shigetomi, K., Tanaka, R., Yamasaki, H., Okajima, T., 2023. Mechanical properties of epithelial cells in domes investigated using atomic force microscopy. Front. Cell Dev. Biol. 11. https://www.frontiersin.org/journals/cell-and-developmental-biology/articles/10.3389/fcell.2023.1245296.
Sigrist, R.M.S., Liau, J., El Kaffas, A., Chammas, M.C., Willmann, J.K., 2017. Ultrasound elastography: review of techniques and clinical applications. Theranostics 7, 1303–1329. https://doi.org/10.7150/thno.18650.
Singh, G., Chanda, A., 2021. Mechanical properties of whole-body soft human tissues: a review. Biomed. Mater. 16, 062004. https://doi.org/10.1088/1748-605X/ac2b7a.
Singh, P.K., Soulages, J.M., Ewoldt, R.H., 2018. Frequency-sweep medium-amplitude oscillatory shear (MAOS). J. Rheol. (N Y. N. Y). 62, 277–293. https://doi.org/10.1122/1.4999795.
Singh, M., Hepburn, M.S., Kennedy, B.F., Larin, K.V., 2025. Optical coherence elastography. Nat. Rev. Methods Primers 5, 39. https://doi.org/10.1038/s43586-025-00406-x.
Sitters, G., Kamsma, D., Thalhammer, G., Ritsch-Marte, M., Peterman, E.J.G., Wuite, G.J.L., 2015. Acoustic force spectroscopy. Nat. Methods 12, 47–50. https://doi.org/10.1038/nmeth.3183.
Slazansky, M., Polzer, S., Man, V., Bursa, J., 2016. Analysis of accuracy of biaxial tests based on their computational simulations. Strain 52, 424–435. https://doi.org/10.1111/str.12205.
Slouf, M., Strachota, B., Strachota, A., Gajdosova, V., Bertschova, V., Nohava, J., 2020. Macro-, Micro- and nanomechanical characterization of crosslinked polymers with very broad range of mechanical properties. Polymers 12, 2951. https://doi.org/10.3390/polym12122951.
Smolyakov, G., Formosa-Dague, C., Severac, C., Duval, R.E., Dague, E., 2016. High speed indentation measures by FV, QI and QNM introduce a new understanding of bionanomechanical experiments. Micron 85, 8–14. https://doi.org/10.1016/j.micron.2016.03.002.
Sneddon, I.N., 1965. The relation between load and penetration in the axisymmetric boussinesq problem for a punch of arbitrary profile. Int. J. Eng. Sci. 3, 47–57. https://doi.org/10.1016/0020-7225(65)90019-4.
Song, B., Chen, W., Ge, Y., Weerasooriya, T., 2007. Dynamic and quasi-static compressive response of porcine muscle. J. Biomech. 40, 2999–3005. https://doi.org/10.1016/j.jbiomech.2007.02.001.
Song, P., Zhao, H., Manduca, A., Urban, M.W., Greenleaf, J.F., Chen, S., 2012. Comb-push ultrasound shear elastography (CUSE): a novel method for two-dimensional shear elasticity imaging of soft tissues. IEEE Trans. Med. Imag. 31, 1821–1832. https://doi.org/10.1109/TMI.2012.2205586.
Song, P., Urban, M.W., Manduca, A., Zhao, H., Greenleaf, J.F., Chen, S., 2013. Comb-push ultrasound shear elastography (CUSE) with various ultrasound push beams. IEEE Trans. Med. Imag. 32, 1435–1447. https://doi.org/10.1109/TMI.2013.2257831.
Song, H.Y., Salehiyan, R., Li, X., Lee, S.H., Hyun, K., 2017. A comparative study of the effects of cone-plate and parallel-plate geometries on rheological properties under oscillatory shear flow. Korea Aust. Rheol. J. 29, 281–294. https://doi.org/10.1007/s13367-017-0028-9.
Stojkov, G., Niyazov, Z., Picchioni, F., Bose, R.K., 2021. Relationship between structure and rheology of hydrogels for various applications. Gels 7, 255. https://doi.org/10.3390/gels7040255.
Stolz, M., Raiteri, R., Daniels, A.U., VanLandingham, M.R., Baschong, W., Aebi, U., 2004. Dynamic elastic modulus of porcine articular cartilage determined at two different levels of tissue organization by indentation-type atomic force microscopy. Biophys. J. 86, 3269–3283. https://doi.org/10.1016/S0006-3495(04)74375-1.
Su, P., Yue, C., Cui, L., Zhang, Q., Liu, B., Liu, T., 2022. Quasi-static mechanical properties and continuum constitutive model of the thyroid gland. J. Funct. Biomater. 13, 283. https://doi.org/10.3390/jfb13040283.
Sudres, P., Evin, M., Wagnac, E., Bailly, N., Diotalevi, L., Melot, A., Arnoux, P.-J., Petit, Y., 2021. Tensile mechanical properties of the cervical, thoracic and lumbar porcine spinal meninges. J. Mech. Behav. Biomed. Mater. 115, 104280. https://doi.org/10.1016/j.jmbbm.2020.104280.
Sun, C., Standish, B., Yang, V.X.D., 2011. Optical coherence elastography: current status and future applications. J. Biomed. Opt. 16, 043001. https://doi.org/10.1117/1.3560294.
Swan, K.Z., Nielsen, V.E., Bonnema, S.J., 2021. Evaluation of thyroid nodules by shear wave elastography: a review of current knowledge. J. Endocrinol. Investig. 44, 2043–2056. https://doi.org/10.1007/s40618-021-01570-z.
Symons, H.E., Galanti, A., Surmon, J.C., Trask, R.S., Rochat, S., Gobbo, P., 2022. Automated analysis of soft material microindentation. Soft Matter 18, 8302–8314. https://doi.org/10.1039/D2SM00857B.
Takada, J., Hamada, K., Zhu, X., Tsuboko, Y., Iwasaki, K., 2023. Biaxial tensile testing system for measuring mechanical properties of both sides of biological tissues. J. Mech. Behav. Biomed. Mater. 146, 106028. https://doi.org/10.1016/j.jmbbm.2023.106028.
Tecse, A., Romero, S.E., Naemi, R., Castaneda, B., 2023. Characterisation of the soft tissue viscous and elastic properties using ultrasound elastography and rheological models: validation and applications in plantar soft tissue assessment. Phys. Med. Biol. 68, 105005. https://doi.org/10.1088/1361-6560/acc923.
Toohey, K.S., Kalyanam, S., Palaniappan, J., Insana, M.F., 2016. Indentation analysis of biphasic viscoelastic hydrogels. Mech. Mater. 92, 175–184. https://doi.org/10.1016/j.mechmat.2015.09.010.
Torres, F.G., Troncoso, O.P., Diaz, J., Arce, D., 2014. Failure analysis of porcupine quills under axial compression reveals their mechanical response during buckling. J. Mech. Behav. Biomed. Mater. 39, 111–118. https://doi.org/10.1016/j.jmbbm.2014.07.017.
Tunick, M.H., 2011. Small-strain dynamic rheology of food protein networks. J. Agric. Food Chem. 59, 1481–1486. https://doi.org/10.1021/jf1016237.
Urban, M.W., Chen, S., Fatemi, M., 2012. A review of shearwave dispersion ultrasound vibrometry (SDUV) and its applications. Curr. Med. Imag. Rev. 8, 27–36. https://doi.org/10.2174/157340512799220625.

V Kontomaris, S., Malamou, A., 2021. A novel approximate method to calculate the force applied on an elastic half space by a rigid sphere. Eur. J. Phys. 42, 25010. https://doi.org/10.1088/1361-6404/abccfb.

van Hoorn, H., Kurniawan, N.A., Koenderink, G.H., Iannuzzi, D., 2016. Local dynamic mechanical analysis for heterogeneous soft matter using ferrule-top indentation. Soft Matter 12, 3066–3073. https://doi.org/10.1039/C6SM00300A.

VanLandingham, M.R., 2003. Review of instrumented indentation. J. Res. Natl. Inst. Stand. Technol. 108, 249. https://doi.org/10.6028/jres.108.024.

Variola, F., 2015. Atomic force microscopy in biomaterials surface science. Phys. Chem. Chem. Phys. 17, 2950–2959. https://doi.org/10.1039/C4CP04427D.

Venkatesh, S.K., Yin, M., Ehman, R.L., 2013. Magnetic resonance elastography of liver: technique, analysis, and clinical applications. J. Magn. Reson. Imag. 37, 544–555. https://doi.org/10.1002/jmri.23731.

Walsh, M.T., Cunnane, E.M., Mulvihill, J.J., Akyildiz, A.C., Gijsen, F.J.H., Holzapfel, G. A., 2014. Uniaxial tensile testing approaches for characterisation of atherosclerotic plaques. J. Biomech. 47, 793–804. https://doi.org/10.1016/j.jbiomech.2014.01.017.

Walter, B.L., Pelteret, J.-P., Kaschta, J., Schubert, D.W., Steinmann, P., 2017. On the wall slip phenomenon of elastomers in oscillatory shear measurements using parallel-plate rotational rheometry: I. Detecting wall slip. Polym. Test. 61, 430–440. https://doi.org/10.1016/j.polymertesting.2017.05.035.

Wang, L., Liu, X., 2014. Characterization of viscoelastic materials by quasi-static and dynamic indentation. Meas. Sci. Technol. 25, 064017. https://doi.org/10.1088/0957-0233/25/6/064017.

Wang, B., Moura, A.G., Chen, J., Erturk, A., Hu, Y., 2020. Characterization of hydrogel structural damping. Extreme Mech. Lett. 40, 100841. https://doi.org/10.1016/j.eml.2020.100841.

Wang, Y., Jacobson, D.S., Urban, M.W., 2022. A non-invasive method to estimate the stress–strain curve of soft tissue using ultrasound elastography. Ultrasound Med. Biol. 48, 786–807. https://doi.org/10.1016/j.ultrasmedbio.2021.12.016.

Wang, C., Zhu, J., Ma, J., Meng, X., Ma, Z., Fan, F., 2023a. Optical coherence elastography and its applications for the biomechanical characterization of tissues. J. Biophot. 16. https://doi.org/10.1002/jbio.202300292.

Wang, Y., Du, Y., Xu, F., 2023b. Strain stiffening retards growth instability in residually stressed biological tissues. J. Mech. Phys. Solid. 178, 105360. https://doi.org/10.1016/j.jmps.2023.105360.

Wang, Y., Zhou, J., Lin, H., Wang, H., Sack, I., Guo, J., Yan, F., Li, R., 2024. Viscoelastic parameters derived from multifrequency MR elastography for depicting hepatic fibrosis and inflammation in chronic viral hepatitis. Insights Imaging 15, 91. https://doi.org/10.1186/s13244-024-01652-5.

Wenger, M.P.E., Bozec, L., Horton, M.A., Mesquida, P., 2007. Mechanical properties of collagen fibrils. Biophys. J. 93, 1255–1263. https://doi.org/10.1529/biophysj.106.103192.

Wong, C.A., Fraticelli Guzmán, N.S., Read, A.T., Hedberg-Buenz, A., Anderson, M.G., Feola, A.J., Sulchek, T., Ethier, C.R., 2023. A method for analyzing AFM force mapping data obtained from soft tissue cryosections. https://doi.org/10.1101/2023.11.08.566263.

Wu, J.Z., Dong, R.G., Schopper, A.W., 2004. Analysis of effects of friction on the deformation behavior of soft tissues in unconfined compression tests. J. Biomech. 37, 147–155. https://doi.org/10.1016/S0021-9290(03)00240-9.

Wu, C.-E., Lin, K.-H., Juang, J.-Y., 2016. Hertzian load–displacement relation holds for spherical indentation on soft elastic solids undergoing large deformations. Tribol. Int. 97, 71–76. https://doi.org/10.1016/j.triboint.2015.12.034.

Wu, P.H., Ben Aroush, D.R., Asnacios, A., Chen, W.C., Dokukin, M.E., Doss, B.L., Durand-Smet, P., Ekpenyong, A., Guck, J., Guz, N.V., Janmey, P.A., Lee, J.S.H., Moore, N.M., Ott, A., Poh, Y.C., Ros, R., Sander, M., Sokolov, I., Staunton, J.R., Wang, N., Whyte, G., Wirtz, D., 2018. A comparison of methods to assess cell mechanical properties. Nat. Methods 15, 491–498. https://doi.org/10.1038/s41592-018-0015-1.

Wu, G., Gotthardt, M., Gollasch, M., 2020. Assessment of nanoindentation in stiffness measurement of soft biomaterials: kidney, liver, spleen and uterus. Sci. Rep. 10, 18784. https://doi.org/10.1038/s41598-020-75738-7.

Yakovenko, A.A., Lai, Y.-X., Goryacheva, I.G., Ju, M.-S., Dosaev, M.Z., Selyutskiy, Y.D., 2021. Modeling and experimental study of the needle indentation into a brain phantom. Int. J. Non Lin. Mech. 137, 103832. https://doi.org/10.1016/j.ijnonlinmec.2021.103832.

Yang, N., Wong, K.K.H., de Bruyn, J.R., Hutter, J.L., 2009. Frequency-dependent viscoelasticity measurement by atomic force microscopy. Meas. Sci. Technol. 20, 025703. https://doi.org/10.1088/0957-0233/20/2/025703.

Yang, W., Sherman, V.R., Gludovatz, B., Schaible, E., Stewart, P., Ritchie, R.O., Meyers, M.A., 2015. On the tear resistance of skin. Nat. Commun. 6, 6649. https://doi.org/10.1038/ncomms7649.

Yang, J., Yu, L., Wang, L., Wang, W., Cui, J., 2018. The estimation method of friction in unconfined compression tests of liver tissue. Proc. Inst. Mech. Eng. H 232, 573–587. https://doi.org/10.1177/0954411918774377.

Yengul, S.S., Barbone, P.E., Madore, B., 2019. Dispersion in tissue-mimicking gels measured with shear wave elastography and torsional vibration rheometry. Ultrasound Med. Biol. 45, 586–604. https://doi.org/10.1016/j.ultrasmedbio.2018.07.002.

Yohsuke, B., Urayama, K., Takigawa, T., Ito, K., 2011. Biaxial strain testing of extremely soft polymer gels. Soft Matter 7, 2632–2638. https://doi.org/10.1039/C0SM00955E.

Yoo, L., Reed, J., Shin, A., Kung, J., Gimzewski, J.K., Poukens, V., Goldberg, R.A., Mancini, R., Taban, M., Moy, R., Demer, J.L., 2011. Characterization of ocular tissues using microindentation and Hertzian viscoelastic models. Investig. Ophthalmol. Vis. Sci. 52, 3475–3482. https://doi.org/10.1167/iovs.10-6867.

Yu, J., Manouchehri, N., Yamamoto, S., Kwon, B.K., Oxland, T.R., 2020. Mechanical properties of spinal cord grey matter and white matter in confined compression. J. Mech. Behav. Biomed. Mater. 112, 104044. https://doi.org/10.1016/j.jmbbm.2020.104044.

Yurtsever, A., Yoshida, T., Badami Behjat, A., Araki, Y., Hanayama, R., Fukuma, T., 2021. Structural and mechanical characteristics of exosomes from osteosarcoma cells explored by 3D-atomic force microscopy. Nanoscale 13, 6661–6677. https://doi.org/10.1039/D0NR09178B.

Zelesco, M., Abbott, S., O'Hara, S., 2018. Pitfalls and sources of variability in two dimensional shear wave elastography of the liver: an overview. Sonography 5, 20–28. https://doi.org/10.1002/sono.12132.

Zhang, G., 2005. Evaluating the viscoelastic properties of biological tissues in a new way. J. Musculoskelet. Neuronal Interact. 5, 85–90.

Zhang, M., Zheng, Y.P., Mak, A.F.T., 1997. Estimating the effective Young's modulus of soft tissues from indentation Tests—nonlinear finite element analysis of effects of friction and large deformation. Med. Eng. Phys. 19, 512–517. https://doi.org/10.1016/S1350-4533(97)00017-9.

Zhang, Y., Murphy, K.D., 2010. Static and dynamic structural modeling analysis of atomic force microscope. In: Bhushan, B. (Ed.), Scanning Probe Microscopy in Nanoscience and Nanotechnology. Springer Berlin Heidelberg, Berlin, Heidelberg, pp. 225–257. https://doi.org/10.1007/978-3-642-03535-7_8.

Zhang, Y., Wei, F., Poh, Y.-C., Jia, Q., Chen, J., Chen, J., Luo, J., Yao, W., Zhou, W., Huang, W., Yang, F., Zhang, Y., Wang, N., 2017. Interfacing 3D magnetic twisting cytometry with confocal fluorescence microscopy to image force responses in living cells. Nat. Protoc. 12, 1437–1450. https://doi.org/10.1038/nprot.2017.042.

Zhang, Y.N., Fowler, K.J., Ozturk, A., Potu, C.K., Louie, A.L., Montes, V., Henderson, W. C., Wang, K., Andre, M.P., Samir, A.E., Sirlin, C.B., 2020. Liver fibrosis imaging: a clinical review of ultrasound and magnetic resonance elastography. J. Magn. Reson. Imag. 51, 25–42. https://doi.org/10.1002/jmri.26716.

Zhang, K., Zhu, M., Thomas, E., Hopyan, S., Sun, Y., 2021. Existing and potential applications of elastography for measuring the viscoelasticity of biological tissues in vivo. Front. Phys. 9. https://doi.org/10.3389/fphy.2021.670571.

Zhang, X.-Y., Wei, Q., Wu, G.-G., Tang, Q., Pan, X.-F., Chen, G.-Q., Zhang, D., Dietrich, C. F., Cui, X.-W., 2023. Artificial intelligence - based ultrasound elastography for disease evaluation - a narrative review. Front. Oncol. 13. https://doi.org/10.3389/fonc.2023.1197447.

Zhao, H., Chen, J., Meixner, D.D., Xie, H., Shamdasani, V., Zhou, S., Robert, J.-L., Urban, M.W., Sanchez, W., Callstrom, M.R., Ehman, R.L., Greenleaf, J.F., Chen, S., 2014. Noninvasive assessment of liver fibrosis using ultrasound-based shear wave measurement and comparison to magnetic resonance elastography. J. Ultrasound Med. 33, 1597–1604. https://doi.org/10.7863/ultra.33.9.1597.

Zhu, Y., Dong, C., Yin, Y., Chen, X., Guo, Y., Zheng, Y., Shen, Y., Wang, T., Zhang, X., Chen, S., 2015. The role of viscosity estimation for oil-in-gelatin phantom in shear wave based ultrasound elastography. Ultrasound Med. Biol. 41, 601–609. https://doi.org/10.1016/j.ultrasmedbio.2014.09.028.

Zhu, W., Han, X., Deng, L., Wang, X., 2025. Mechanical behavior and indentation-induced injury of soft microtissues with different densification levels. ACS Omega 10, 19675–19681. https://doi.org/10.1021/acsomega.5c00639.

Żmudzińska, M., Inglot, M., Zaleska-Dorobisz, U., Jankowski, L., Świątek-Najwer, E., 2018. The assessment of the applicability of shear wave elastography in modelling of the mechanical parameters of the liver. Acta Bioeng. Biomech. 20, 59–64. https://doi.org/10.5277/ABB-01228-2018-02.

Zvietcovich, F., V Larin, K., 2022. Wave-based optical coherence elastography: the 10-year perspective. Prog. Biomed. Eng. 4, 012007. https://doi.org/10.1088/2516-1091/ac4512.